ABSTRACT

ANOMALOUS ε/β^+ DECAY BRANCHING RATIOS

By

Richard Brian Firestone

ε/β^+ decay branching ratios were measured for decays from ^{143}Eu, ^{143g}Sm, and ^{143g}Gd. $\gamma^{\pm}$-γ triple coincidence experiments were performed to get relative positron feedings to respective daughter levels. X-γ coincidence measurements were done for ^{145g}Gd decay to obtain relative electron capture feedings and these feedings were inferred from singles intensities for ^{143}Eu and ^{143g}Sm decay.

The decay schemes of ^{143}Eu and ^{143g}Sm were also studied, and 12 levels were reported in ^{143}Pm as well as 16 levels in ^{143}Sm. Data were also gathered relevant to ^{140m}Pm decay and a β^+ endpoint for ^{66}Ga decay is reported.

β decay theory is discussed in some detail, especially concerning the implications of ε/β^+ decay branching ratios. It is shown that anomalous ratios can only occur for higher order terms in allowed transitions or if a pseudoscalar force is present. Neither possibilities were hitherto eliminated experimentally.

Among 15 measured ε/β^+ branching ratios, two were significantly anomalous. The transition to the 808.5 keV level in ^{145}Eu was anomalous by a factor of 24 and the transition to the 1173.1 keV level in ^{143}Pm was anomalous by a factor of 4.9. Each case involved a similar hindered

allowed transition and it was suggested that the higher order allowed terms might be dominant in those instances.

ANOMALOUS ε/β^+ DECAY BRANCHING RATIOS

By

Richard Brian Firestone

A DISSERTATION

Submitted to

Michigan State University

in partial fulfillment of the requirements

for the degree of

DOCTOR OF PHILOSOPHY

Department of Chemistry

1974

To Chuang Tzu

ACKNOWLEDGMENTS

I wish to thank Dr. Wm. C. McHarris for suggesting this very interesting and fruitful project, and for his valuable help and friendship during its completion. I would also like to thank Dr. W. H. Kelly and Dr. F. M. Bernthal for their willing assistance throughout this work.

Very special thanks are extended to Dr. R. A. Warner for his invaluable experimental assistance and to Mr. C. B. Morgan for his extensive aid in the preparation of many of the figures.

To all the other members of the nuclear spectroscopy research group I offer my thanks not only for the innumerable times you assisted me in my work, but especially for the great kindness you showed me during my illness.

I gratefully acknowledge the aid of the cyclotron staff in the completion of this work, and the financial assistance of the National Science Foundation, U.S. Atomic Energy Commission, and Michigan State University.

Finally, a special thanks goes to my wife, Mary, who married me for better or worse and got a little of both, and to my parents without whom this work could not have been possible.

TABLE OF CONTENTS

Chapter

Page

Chapter

Page

LIST OF TABLES

Table

Page

LIST OF FIGURES

CHAPTER I

INTRODUCTION

A major purpose of this thesis is to investigate the anomalous ε/β^+ decay branching ratios first reported by Eppley and McHarris (Ep71). These ratios are an important test of allowed $\beta-$ decay theory, and large discrepancies, such as those Eppley saw in ^{145}gGd decay, are not easily explained. It was shown for pure Fermi ($0^+ \rightarrow 0^+$) decay (Ar53) and for ^{22}Na Gamow-Teller decay (Sh53) that the interference terms were small or zero, and many measurements of allowed decay have since confirmed this. Unique forbidden decays were shown to yield much larger ratios than allowed decays, but this seemed adequately explained by $C_V C_A$ interference terms (Pe58). Thus, instances of small deviations (<50%) in certain allowed ratios were explained in terms of higher order affects not considered in the calculation or by experimental problems. Eppley's anomaly was a factor of 30, so this could not be explained away so easily. It was, therefore, the first goal of this work to establish the validity of Eppley's measurement.

Chapters 2 and 3 cover the experimental techniques adopted to study the problem. When it became apparent that the anomaly would not go away, the feasibility of looking at the β spectrum was investigated. Both Si(Li) and Pilot B plastic $\beta-$ detection systems were studied with mixed results as to their applicability to these problems. A plastic detector β spectrum, in which the β^+ endpoint of ^{62}Ga was measured is discussed in Chapter 7 and a fast means of calibrating Si(Li) detectors at high energies is given in Chapter 3.

Resolution and backscattering problems prevented these techniques from being applied to the study of the anomalies.

Having confirmed the $^{145}g_{Gd}$ anomaly, it was determined to look for similar anomalies elsewhere. In conjunction with previous work, the decays of ^{143}Eu and $^{143}g_{Sm}$ were investigated for ε/β^+ ratio anomalies. The development of the ^{143}Eu decay scheme is given in Chapter 4, and the $^{143}g_{Sm}$ decay scheme is presented in Chapter 5. ^{140m}Pm decay was inadvertently studied as an impurity in both these decays and the data relevant to it are presented in Chapter 6. A second large anomaly was seen in the $^{143}g_{Sm}$ decay and similarities between this anomaly and the $^{145}g_{Gd}$ anomaly led to a theoretical study of the possible implications.

In Chapter 8, β-decay theory is developed without the usual assumptions of a *V-A* interaction. It is shown that the anomalies can be explained in terms of interference affects of the traditional Fierz form or of higher order contributions. The ε/β^+ ratio results are presented in Chapter 8 and it is suggested that the fact that the anomalies involve hindered transitions is significant. Such large anomalies can indicate a gross failure of the allowed assumption and, possibly, suggest that *V-A* theory is only an approximation with Pseudo-scalar and even small degrees of Scalar and Tensor also present. Such a discovery would indicate a failure of two-component neutrino theory and suggest an exciting reopening of β decay theory in general. Finally, further experiments to elucidate the cause of the anomalies are proposed in the last section of Chapter 8.

CHAPTER II

EXPERIMENTAL APPARATUS AND METHODS

2.1 γ-Ray Spectrometer Systems

2.1.1 Ge(Li) Singles Spectrometer

Numerous state of the art Ge(Li) detectors have been used during the course of these experiments. Starting with small, locally made detectors of less than 1% efficiency, relative to 3×3 in. NaI(Tl), we progressed to large detectors of over 10% efficiency. A list of the detectors used in this work is presented in Table 2-1.

Although some of the early work was done with 3 keV resolution FWHM (at 1332 keV), virtually all of the data presented here were acquired with commercial detectors rated at about 2 keV. It is important to point out that the warranted resolutions of these detectors were never actually realized under experimental conditions. Frequently, such effects as high count rates or electronic noise forced the obtainable resolution to be 2.5 keV or worse. In general this was not a grave problem because the spectra described here were simple enough to provide only few cases of unresolvable multiplets.

The vast majority of data were collected with the large volume detectors due to their inherently large peak to Compton ratios. This was particularly necessary because of the large amount of higher energy γ rays present in our spectra. Even with our largest detector, considerable counting times were required to get sufficient statistics at high energies.

In general, the electronics used in obtaining singles spectra

Table 2-1

Ge(Li) Detector Specifications

Efficiency[a]	Resolution	Peak to Compton Ratio	Shape	Manufacturer
≈1.0%	3.2 keV[b]	6 to 1	Trapezoidal	MSU Cyclotron Lab.
3.6%	2.0 keV[b]	22 to 1	True Coaxial	Ortec
4.6%	1.9 keV[b]	24 to 1	True Coaxial	Ortec
7.0%	1.9 keV[b]	31 to 1	True Coaxial	Canberra
10.4%	2.1 keV[b]	38 to 1	True Coaxial	Nuclear Diodes
<1 %	570 eV[c]	-----	Planar (LEPS)	Ortec

[a]With respect to the 1332 keV peak of ^{60}Co at 25 cm from a 3×3-in. NaI(Tl) detector.

[b]FWHM for the 1332 keV peak of ^{60}Co.

[c]FWHM for the 122 keV peak of ^{57}Co.

were not especially elaborate. The FET preamps were all supplied by the detector manufacturers, and the most commonly used amplifiers were the ORTEC 451, 452, and 453 spectroscopy amplifiers. Those spectra involving large count rates (≥5000/sec) were taken with a Canberra 1464 Restorer/Rejector following the amplifier. This module included a high quality base line restorer as well as pile-up rejection. The pile-up rejection system eliminated counts that would create false "Compton" background below a peak and thus maintained good peak-to-Compton ratios at high count rates. Table 2-2 shows typical performance of the Restorer/Rejector with the 4.6% detector.

Data were collected with three separate multichannel analyzer systems depending on the experimental convenience and the "up" status of the system in question. Some data were acquired with a Nuclear Data 2200 ADC with a hard wired 4096 channel memory and a 16 MHz digitizing rate. This system had the advantage of being quite portable but the only means of output at the times it was used was a Tally punch. This output was quite slow, and the means of interpreting the ensuant IBM-format tape was very tedious. A second system which was employed was a Northern Scientific 625 ADC interfaced to a DEC PDP-9 computer and with a digitizing rate of 40 MHz. The ADC was capable of taking two 4096 channel spectra but our use was limited to only a single spectra. The disadvantages of taking data at the PDP-9 were the distance from the cyclotron which made counting short-lived activities into a foot race, and also some output slowdowns because of the fact that an interface to the Sigma-7 cyclotron computer was not yet completed. Nevertheless, the PDP-9 was usually our most reliable system and its isolation from many sources of electronic

Table 2-2

CANBERRA 1464 Restorer-Rejector Performance

Count Rate (cps)	Singles[a] Peak to Compton	Singles[a] Resolution[b]	Restorer Only Peak to Compton	Restorer Only Resolution[b]	Restorer and Rejector Peak to Compton	Restorer and Rejector Resolution[b]
2000	19.6:1	2.5 keV	18.1:1	2.6 keV	21.3:1	2.6 keV
10000	20.2:1	2.5 keV	18.4:1	2.6 keV	21.7:1	2.6 keV
20000	16.8:1	2.6 keV	16.8:1	2.6 keV	21.6:1	2.6 keV
40000	13.9:1	3.0 keV	13.9:1	2.9 keV	18.9:1	2.8 keV

[a] 4.5% detector rated at Peak to Compton = 22:1; Resolution (1332 keV) = 2.0 keV FWHM.

[b] Measured at 1332 keV.

noise (cycloton RF, etc.) made it often possible to obtain fine quality resolution. The third, and most heavily used, system was the Northern Scientific 629 ADC's which allowed up to four 8192 channel spectra to be sent simultaneously to the XDS Sigma-7 computer. This system has the very fast digitizing rate of 50 MHz. The proximity of the cyclotron and the availability of extensive input and output capabilities made this system very convenient. Additionally, most coincidence experiments were performed here, and frequently a singles spectra was taken parasitically to the main experiment. Although optimum resolution was not generally obtained at the Sigma-7, the advantages of this location were evident.

2.1.2 Ge(Li)-Ge(Li) Coincidence Spectrometer

The detectors used in these experiments are the same as those described in the previous section. The largest detectors available were always used in order to gain maximum efficiency for the experiment. A block diagram of the fast-slow coincidence electronics is shown in Figure 2-1.

The detectors are placed at an angle of 90° to reduce positron annihilation as $\gamma^{\pm}$-coincidences would otherwise comprise over 90% of all coincidences (for the activities studied in this thesis). This arrangement also avoids scattering processes between detectors and it was possible to introduce a lead wedge between detectors to further reduce scattering.

The timing pulses were picked off by an ORTEC 454 Timing Filter Amplifier which was followed by an ORTEC 453 Constant Fraction Timing Discriminator which provided fast pulses to stop or start an ORTEC 437A

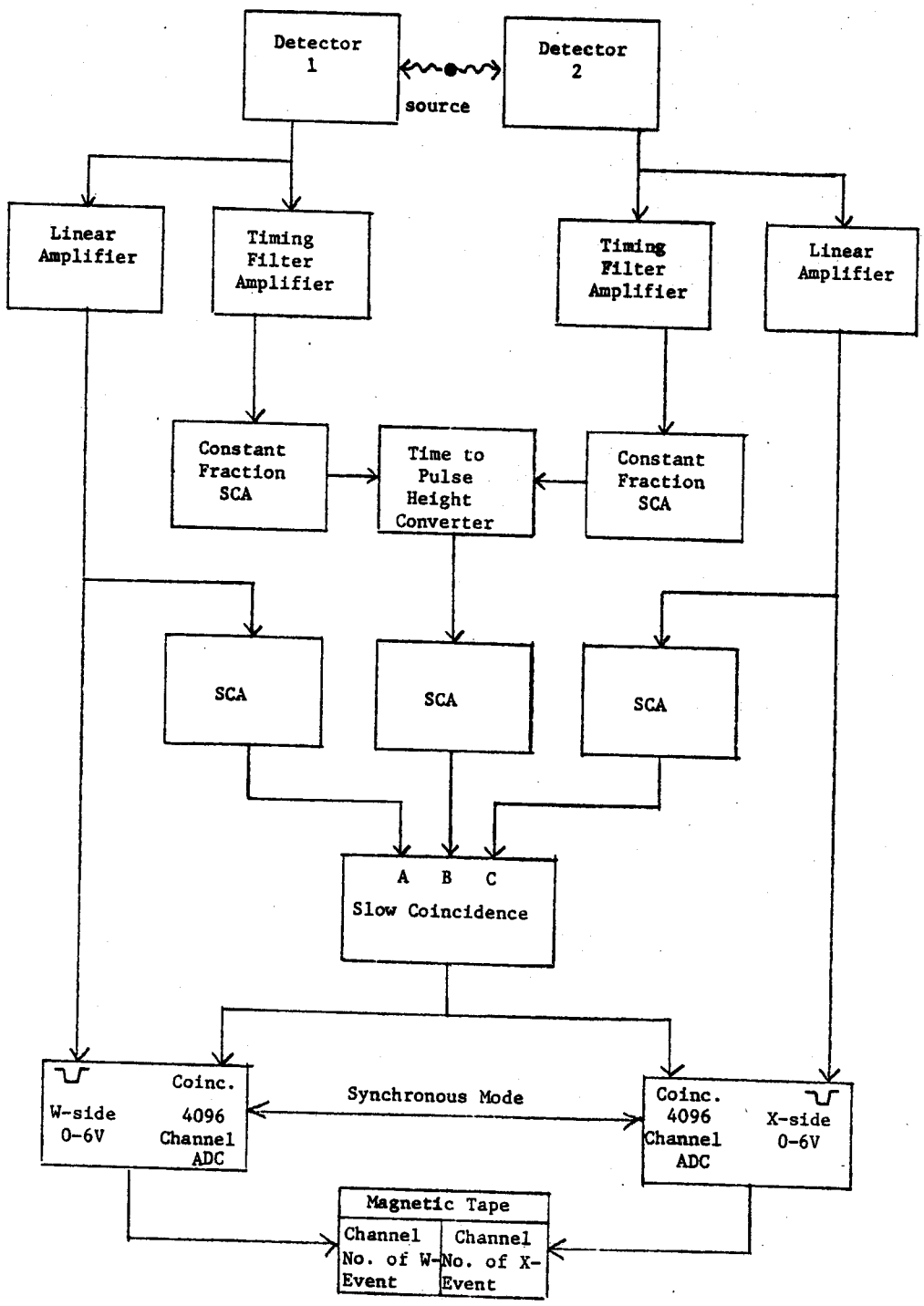

Figure 2-1. γ-γ "FAST-SLOW" coincidence block diagram.

Time to Pulse Height Converter. An identical system was established for both detectors to start and stop the TAC whose output was sent through an ORTEC 418 Slow Coincidence box along with the output from ORTEC 451 Spectroscopy Amplifiers corresponding to the energy signals from each detector. The three signals in the slow coincidence were gated by ORTEC 455 Single Channel Analyzers to allow choice in the dynamic energy range observed as well as the ability to restrict the time range accepted. The slow coincidence output guaranteed pairs of real coincident events so noise triggering was mostly eliminated. This output was used to gate the ADC's which operated in synchronous mode to collect both gated energy legs under program EVENT or IIEVENT where data were written in pairs on magnetic tape. A description of EVENT follows later in this chapter.

Timing obtainable using this system was better than 20 nsec FWHM for a TAC peak, but at high count rates (~10,000/sec) and large dynamic range the realized timing was sometimes as low as 80 nsec. This meant that at worst a count rate of ≈5000/sec in each detector would allow 2 chance events per second; yet real rates were generally ≳100 coincidences per second. The problem of chance coincidences is further reduced by background subtraction in the data recovery which is discussed in a later chapter.

2.1.3 Ge(Li) vs 8×8-in. NaI(Tl) Split-Annulus Pair Spectrometer

A large split-annulus with optically isolated halves was used in these experiments. The energy resolution of each half of this annulus was nearly 10% for ^{137}Cs (662 keV), which was sufficient for gating annihilation $\gamma^{\pm}$ radiation. The absolute singles efficiency

for a central source in the annulus was about 60%, allowing reasonable efficiency for coincidence spectrometry. The annulus was open at both ends allowing the snout of a Ge(Li) detector cryostat to project to the center of the annulus.

In positron-feedings experiments the annulus was used to verify positron events. The source was enveloped in a teflon absorber such that all β^+'s annihilated near the source. Coincidences between the $\gamma^{\pm}$ annihilation photons in the two halves of the annulus signified a positron event. Having established a positron event, a third γ-ray coincidence in the Ge(Li) detector was sought to label the level which was positron fed. The spectrum obtained in the Ge(Li) detector then corresponded strictly to the positron decay of the source and provided relative feedings to all levels of the daughter nucleus with the exception of the ground state, which, of course, doesn't deexcite.

An electronics block diagram for this spectrometer is shown in Figure 2-2. Each half of the annulus' phototube outputs was sent through a cathode follower to a Canberra 1411 DDL Spectroscopy Amplifier where the DDL output was sent to an ORTEC 455 Timing Single Channel Analyzer gated on the 511-keV $\gamma^{\pm}$ annihilation radiation. The crossover timing TSCA output was then sent to an ORTEC 414A Fast Coincidence box. Timing signals from the Ge(Li) detector were sent through an ORTEC 454 Timing Filter Amplifier and an ORTEC 453 Constant Fraction Discriminator, where the constant fraction timing output was also sent to the fast coincidence box. Requiring coincidences from both halves of the annulus as well as the Ge(Li) detector within a preset time of up to 110 nsec, the resultant logic signals

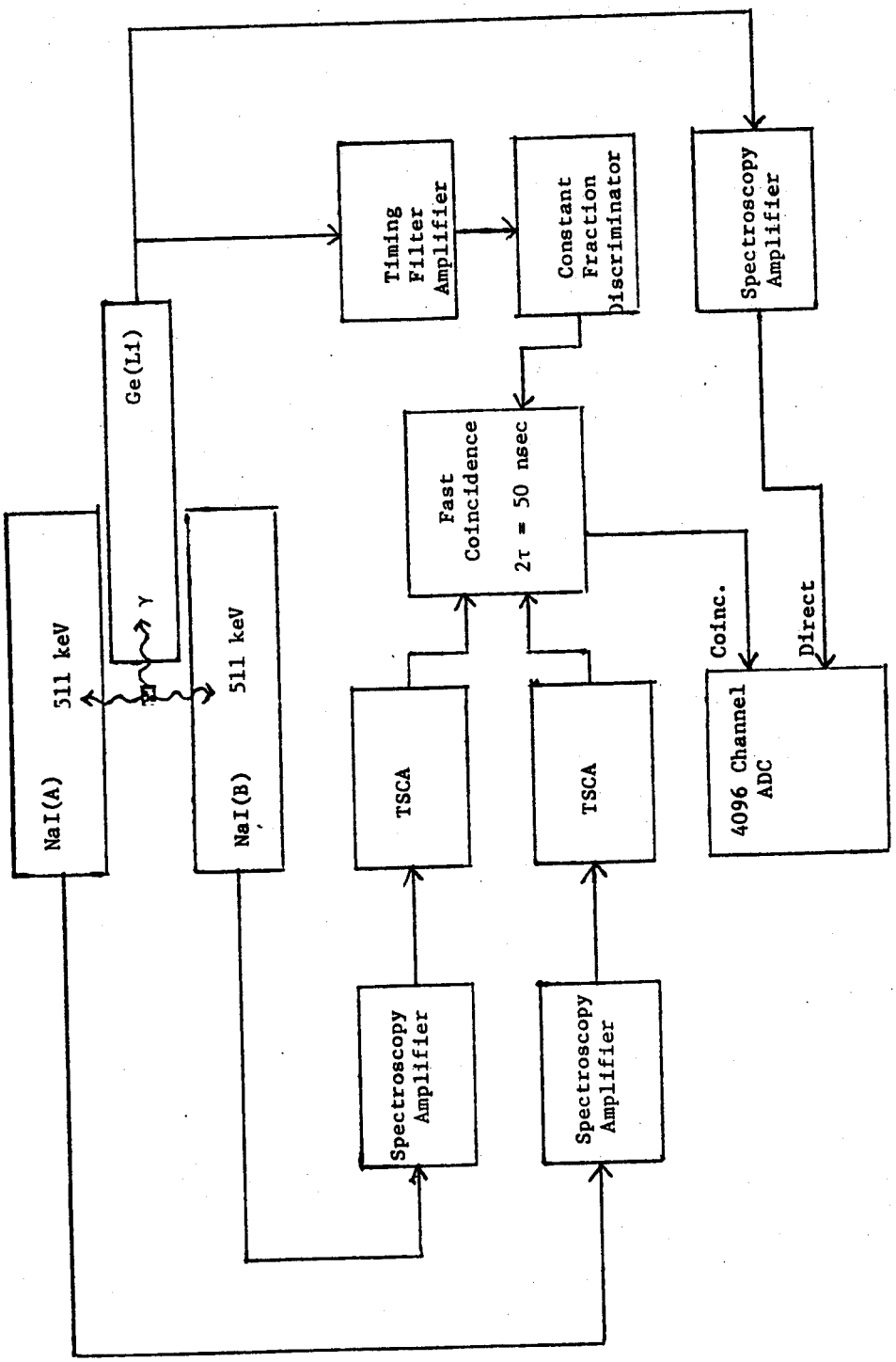

Figure 2-2. 511-511-γ Triple coincidence apparatus block diagram.

were used to gate the energy leg of the Ge(Li) detector at the ADC. The high resolution energy spectra were taken with an ORTEC 451 amplifier and Canberra 1464 Restorer/Rejector to allow high count rates. These spectra were all taken at the PDP-9 computer.

Calibration spectra were obtained for this spectrometer using a ^{22}Na source. In Figure 2-3 are self-gated singles spectra of each axis of the spectrometer where C is Ge(Li) and A,B are NaI(Tl). Figure 2-4 shows TAC spectra for combinations AB, AC and BC indicating the timing spread between the designated coincidences. We could get 20 nsec FWHM between the NaI(Tl) halves of the annulus and 23 nsec between either half of the annulus and Ge(Li). The total timing obtainable for the triple coincidence was 25 nsec FWHM. Figure 2-5 shows spectra with the fast coincidence box set at 50 nsec. The first spectrum is a ^{22}Na gated spectrum and the second is the singles spectrum. A third spectrum is shown indicating the chance for an identical counting time. The triple coincidence requirement is quite stringent and thus a very low count rate is expected (0.02/sec) in a chance spectrum. Thus, it is clear that the appearance of the annihilation peak in the coincidence spectrum is a result of real coincidences. This can be explained by events where one half of the annulus sees not a positron event but a compton event and the other half of the annulus sees annihilation while the Ge(Li) sees annihilation. If one observes the relative intensities of the two annihilation peaks, one sees that this is quite a small effect.

An interesting sidelight to this experiment is the effect of transitions to levels deexciting by means of more than one coincident γ ray. In such a case, in addition to annihilation $\gamma^{\pm}$ in the annulus,

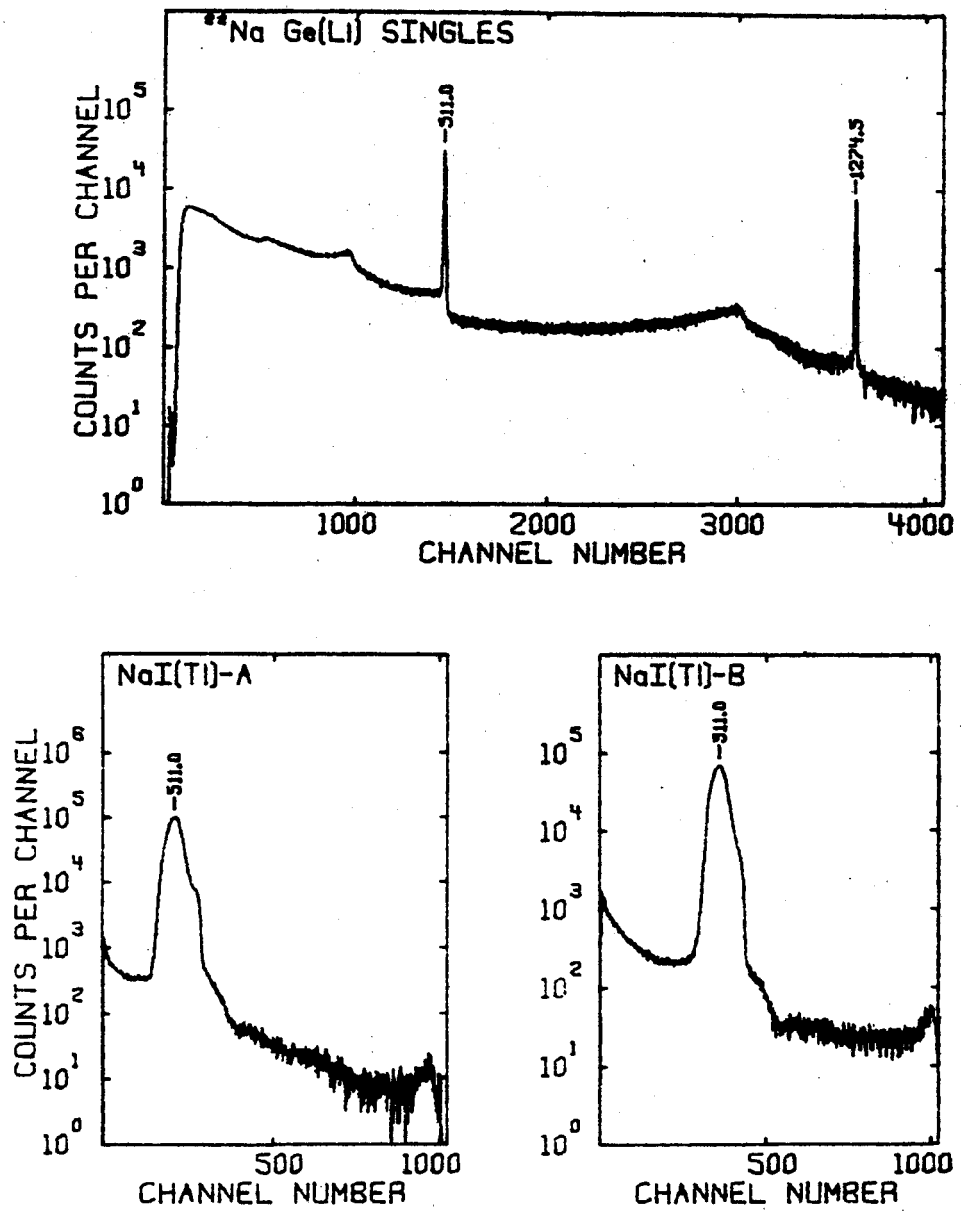

Figure 2-3. NaI(Tl)-A, NaI(Tl)-B, and Ge(Li) singles spectra of ^{22}Na.

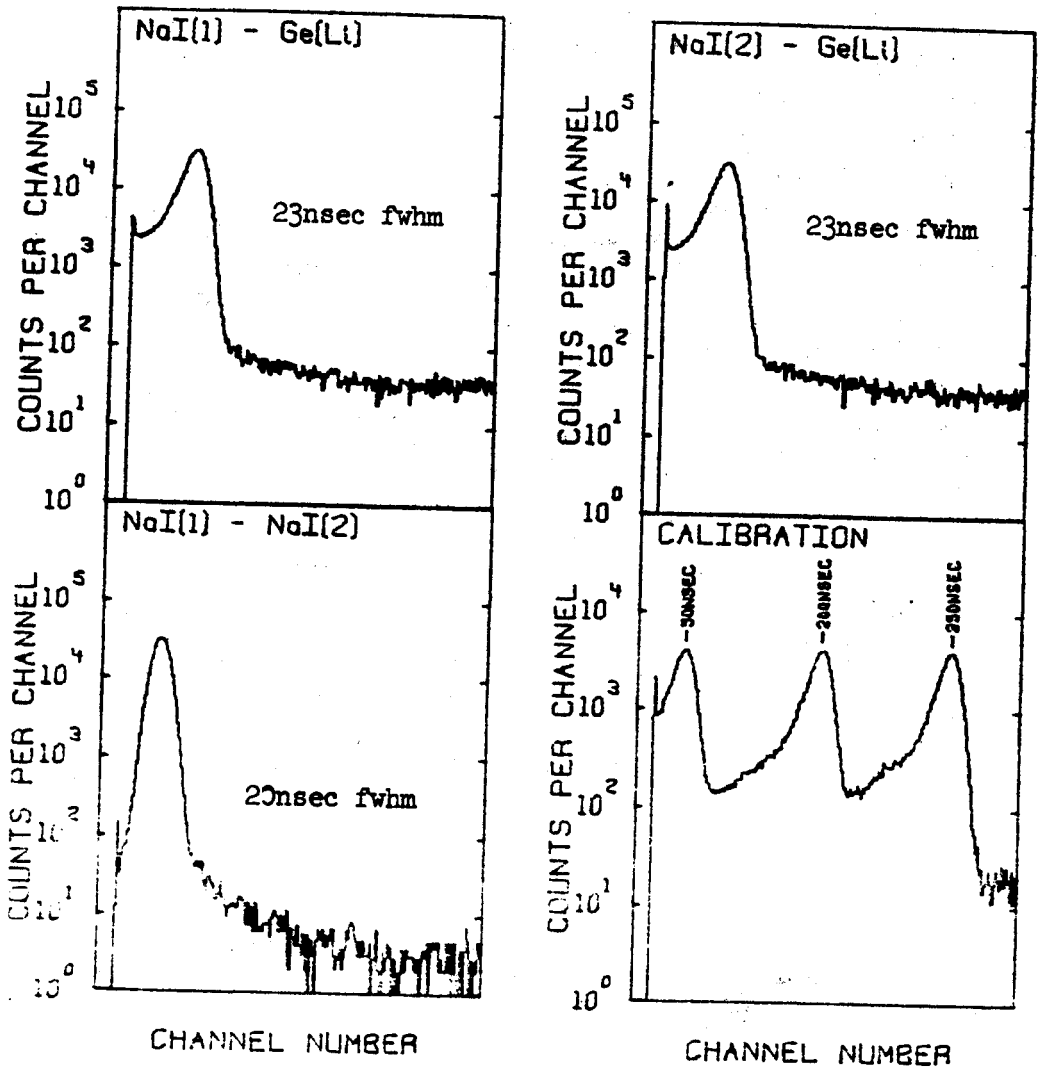

Figure 2-4. $\gamma^{\pm}$-γ TAC spectra for ^{22}Na decay.

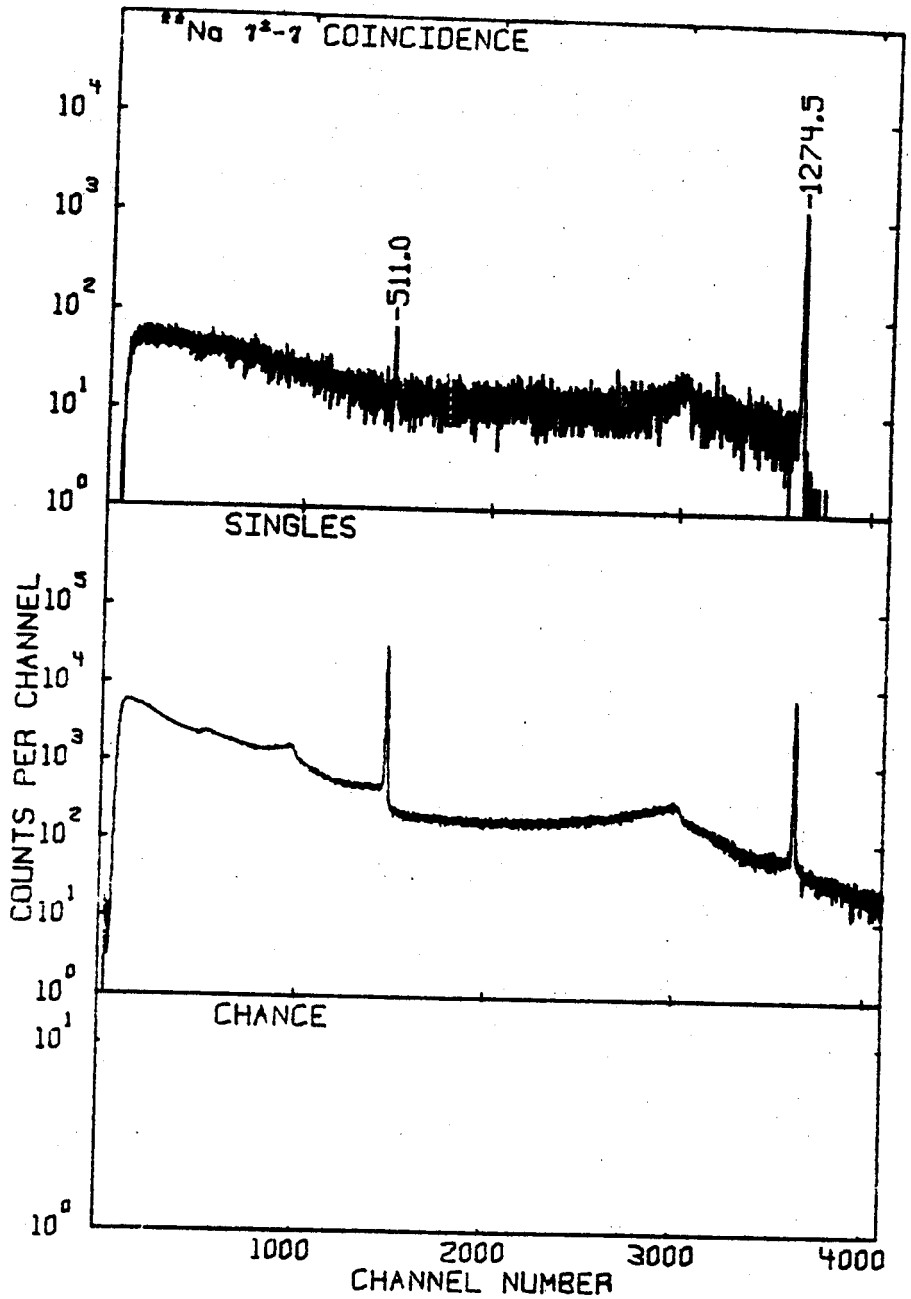

Figure 2-5. Triple coincidence, singles and chance spectra for ^{22}Na decay.

one can get coincident summing with one or the other of the coincident γ rays. This occurrence will throw the event out of the 511-keV gate and so decrease the intensity of the corresponding γ rays in the gated spectrum. As the annulus as a whole is nearly 60% efficient, these transitions are expected to lose about 60% of their intensity. Such an effect is observed experimentally. Fortunately, the transitions studied all concerned direct ground state transitions so this was not a problem, but in general great care would be necessary to analyze such transitions. This property is valuable, however, in identifyingy the ground state transitions and was used in the elucidation of several decay schemes presented in this thesis.

2.1.4. Ge(Li) vs LEPS Electron Capture-Feedings Spectrometer

In addition to the relative positron feedings, it was desirable to elucidate electron capture feedings in order to better determine the ε/β^+ ratios. To this end the standard coincidence experiment described previously was employed with the exception that one coincidence leg involved an ORTEC LEPS (Low Energy Photon Spectrometer) designed specifically for high resolution at low energy (570 eV @127 keV). We easily resolved the K_α and K_β lines which we gated on (indicating an electron capture type transition), and looked for coincidences from γ rays deexciting the fed levels. Chance events were very rare as we obtained ≈20 nsec FWHM timing and could obtain excellent statistics with count rates of about 5000/sec. Background subtraction was possible on either axis of this experiment through the data analysis routine II EVENT RECOVERY, which is discussed later. For this reason, a gated TAC spectrum was collected on a third axis

with a wide SCA gate leaving the option of which counts to accept to an off-line decision.

2.2 Beta Spectrometer Systems

In order to obtain both beta energy endpoints and beta spectrum shapes, several beta spectrometers of varying resolution were constructed.

2.2.1 Pilot B Plastic Beta Spectrometer

For measurement of high energy beta spectra a Pilot B plastic scintillator was mounted on an EMI 9536B phototube. The cylindrical detector was 4 inches long (able to stop 20 MeV betas) and 1.5 inches in diameter. It was coated with a MgO powder reflector and additionally wrapped with aluminized mylar (0.25 mil). Conversion electron resolution at ^{137}Cs (662 keV) was ≈20% as shown in Figure 2-6. As in all spectra taken with this detector it was necessary to take two spectra, one with and one without an absorber, so that corrections for Compton electrons could be made.

Only a primitive collimation system was employed in using this detector, involving a lead ring to avoid grazing electrons at the detector edge and sufficient distance to insure detection of only electrons normal to the detector surface. Poor resolution and systematic difficulties lead to only minimal use of this detector and no attempt to get spectral shapes was made.

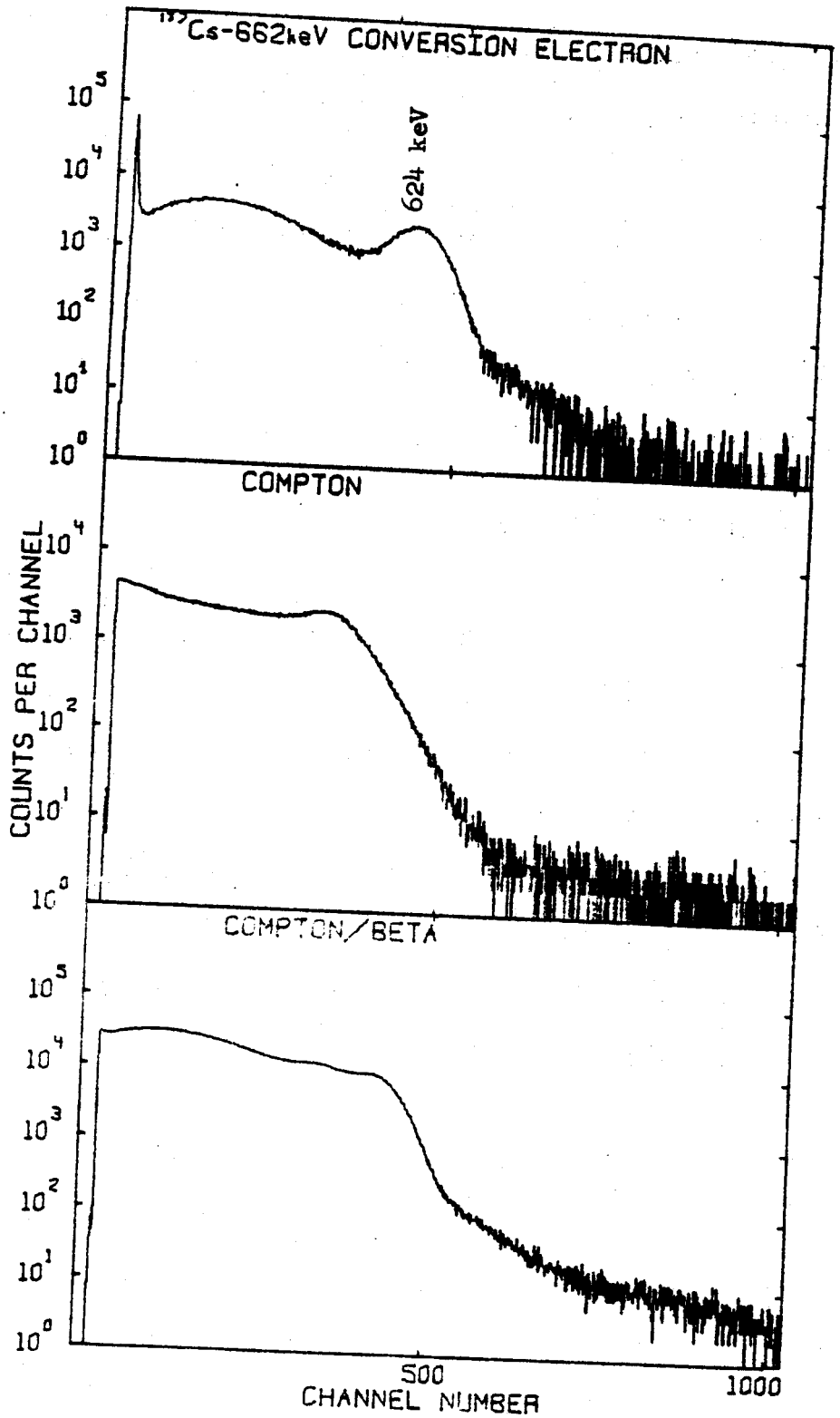

Figure 2-6. ^{137}Cs β-spectra taken with a Pilot-B plastic detector; without absorber (bottom), with absorber (middle), and the difference between the bottom two spectra (top).

2.2.2 Si(Li) Spectrometer

In an attempt to accurately measure large β endpoints, a 1 cm active depth Si(Li) detector was obtained from Simtec, Inc. This detector should suffice for electrons greater than 4.0 MeV in energy. The problem of energy calibration for this detector was puzzling at first because conversion electrons and Compton edges were not readily available at higher energies. This problem was overcome through the novel approach of using double escape peaks from ^{66}Ga.

^{66}Ga is a well known γ ray standard (Ph70,Ca71) with numerous high-energy lines up to 4806.60 keV. Consequently, a large Si(Li) detector can see double escape events up to 3784.6 keV and a Compton edge as high as 4564.0 keV. The detector is nearly transparent to the high energy γ rays, but the double-escape events give sharp, easily analyzed peaks while the Compton edges are quite steep. A list of the usable transitions are given in Table 2-3. Figure 2-7 shows a typical ^{66}Ga double-escape spectrum. The counting time for this spectrum was two hours. A criterion of a good spectrometer is not only that it can be rapidly calibrated, but that its output is linear with respect to energy. Figure 2-8 shows a plot of energy versus channel number and the fit is very linear with a standard deviation of only 2.6 keV. This indicates that interpolation and extrapolation to higher energies are both allowable.

While the energy calibration of the spectrometer proved quite straightforward, its use in measuring β endpoints is very limited. The Fermi-Kurie plot obtained was quite nonlinearity because of the response function of the detector. Many events deposited less than full energy in the detector, skewing the spectrum towards lower

Table 2-3

Calibration Energies From ^{66}Ga

Energy[a] (keV)	Event
511.0	Positron annihilation
1168.2	2190.2-keV D.E.
1730.3	2752.3-keV D.E.
2518.5	2752.3-keV Compton
2745.3	3767.3-keV D.E.
2784.3	3806.3-keV D.E.
3064.5	4086.5-keV D.E.
3273.5	4295.5-keV D.E.
3440.1	4462.1-keV D.E.
3784.6	4806.6-keV D.E.
4564.0	4806.6-keV Compton

[a]Values from reference (Ca71).

Figure 2-7. ^{66}Ga Double-escape spectrum taken with 1 cm Si(Li) detector.

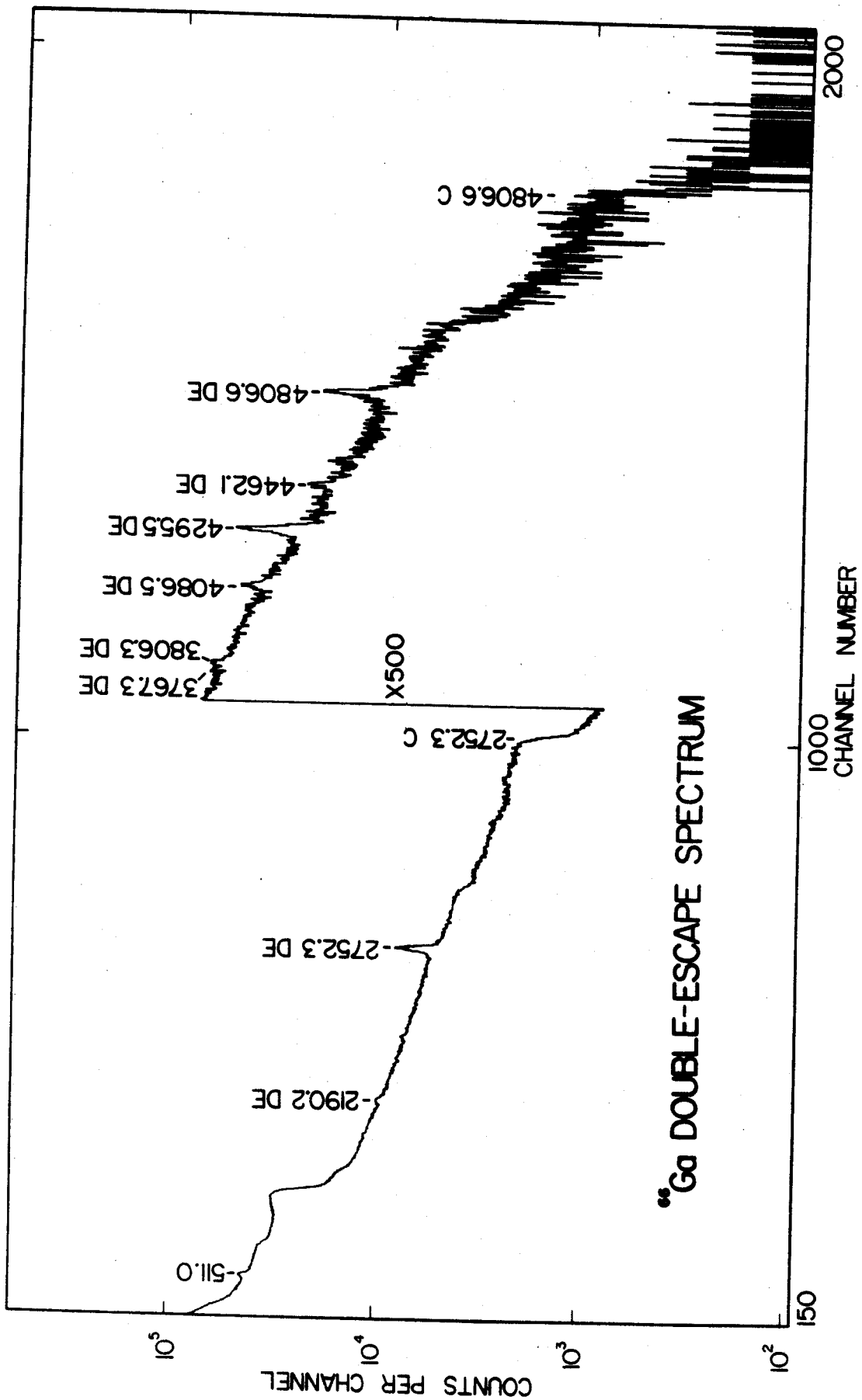
^{66}Ga DOUBLE-ESCAPE SPECTRUM
COUNTS PER CHANNEL
CHANNEL NUMBER
150
1000
2000
10^2
10^3
10^4
10^5
511.0
2190.2 DE
2752.3 DE
2752.3 C
X500
3767.3 DE
3806.3 DE
4086.5 DE
4295.5 DE
4462.1 DE
4806.6 DE
4806.6 C

Figure 2-8. Si(Li) Energy calibration curve. Standard deviation of the linear, least squares fit is 2.6 keV.

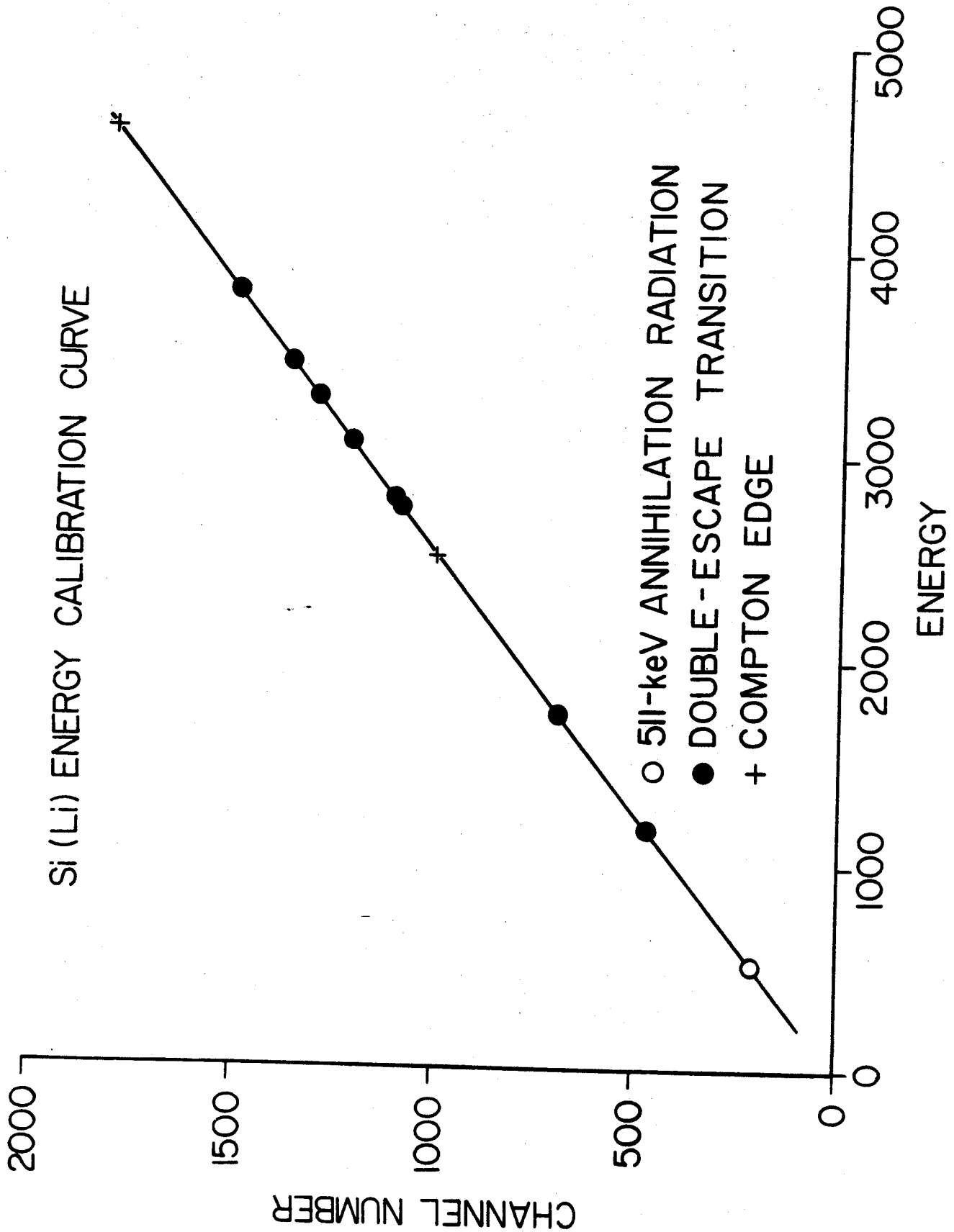
Si (Li) ENERGY CALIBRATION CURVE
CHANNEL NUMBER
ENERGY
2000
1500
1000
500
0
0
1000
2000
3000
4000
5000
○ 511-keV ANNIHILATION RADIATION
● DOUBLE-ESCAPE TRANSITION
+ COMPTON EDGE

energies. Collimation was difficult, and many of the lost events involved scattering from the detector. The response problem is well known in the literature (Gr66,Wi67,Be68), and, although complex correction functions are given, it would be difficult or impossible to obtain good Fermi-Kurie plots. With these problems in mind, the measurement of β endpoints was abandoned for the present.

2.3 Target Preparation

2.3.1 MSU Sector Focused Cyclotron

All of the activities discussed in this thesis were prepared at the Michigan State University Sector Focused Cyclotron. This machine allowed a variable energy proton beam to over 50 MeV deuteron beams to 28 MeV, ^{3}He beams to over 70 MeV, and ^{4}He beams to over 50 MeV. Generally activations with currents considerably above 1 μA were possible, and during long experiments the machine could be expected to operate quite reliably.

2.3.2 The Rabbit System

In order to facilitate the handling of short lived activities, a rabbit system was constructed to transport samples to the bombardment area. Transport time was typically about 3 seconds, and the system was fully automated to allow efficient operation.

Most irradiation samples were in powder form so that it was necessary to use aluminum foil packets to contain the material. Separation of the activity from the packet, after bombardment, took about 30 seconds additional time. Those samples which were foils could be counted more quickly, but, in general, it was desirable to allow

several seconds for short activities to die away.

Whenever possible, bombardments were done at the energy desired and no degraders were needed. When necessary, aluminum degraders were placed in front of the target to obtain required energies.

2.3.3 The He-Jet Thermalizer

In order to study very short activities (≥50 msec) a gas transport system was developed (Kos73). This involved thermalizing nuclear recoils from the target, transporting them by He-gas flow through a narrow capillary at near-sonic velocities, and collecting them on a tape-transport system. It was possible to collect the recoils directly in front of a detector or elsewhere on a movable tape which could be stepped in any desired fashion.

Generally, metal foil targets were preferred although the use of fragile rare earth targets, prepared in this laboratory, was unsuccessful because of the short (≈1 hour) usable life of such targets in intense beams. Attempts were made with powder-epoxy emulsions with some promising results.

2.4 Data Acquisition Programs

The cyclotron computer staff provided a number of valuable data-taking programs to ease our experiments considerably. These programs utilized NS629 ADC's, routing electronics, storage scopes, and their associated switches. Input was by means of teletype or scope switches, and output was available through line printer, plotter, or card punch as well as live display on the scopes.

Data taking programs for the PDP-9 were provided by DEC and altered

by Giesler, Bradford, Howard, and others (PDP73). These were all essentially singles routines and are explained later. Display at the PDP-9 was limited to an oscilloscope for all but one program which used a storage scope. Input was generally through the teletype, and output was via teletype, paper tape, DECTAPE, or magnetic tape.

A brief discussion of each of the major programs used follows. No attempt will be made to explain the inner workings of these programs.

2.4.1 POLYPHEMUS

POLYPHEMUS (Au70) is a program which allows the use of up to four 8192-channel ADC's independently. This program was most useful for taking singles spectra and setting up for coincidence experiments.

2.4.2 TOOTSIE

TOOTSIE (Ba71) is a program designed for multiparameter data acquisition. A variety of options are available to perform various calculations on the data before they are stored. This program operates in two modes, SETUP and RUN. In SETUP mode the data are stored in two-dimensional arrays of dimension (64,64), (64,256), 128,128), or (256,64). The data are displayed on a scope as a series of bands across the screen. Polynomial fits to a set of points obtained by accepting the coordinates of a movable cross define the lower and upper bound for each band.

Up to eight independent detector systems may be used at one time with three routing bits supplying detector identification. In SETUP mode data from one detector are stored, all others being discarded, permitting bands for each detector to be set.

Having set all bands, the program is switched to RUN. Tables of 256 points per fit are generated and stored for each detector. Events are then checked against the tables corresponding to the detector indicated by the routing bits and the aypropriate channel of the spectrum in which the match was found is incremented.

2.4.3 EVENT and IIEVENT

EVENT (Ba70) is a program for taking up to four parameter coincidence data. Each multiplet of coincidence data is written on magnetic tape for off-line analysis. In the instance of data appearing in only some of the ADC's, a channel zero conversion is given for the barren ADC's and recorded on tape.

IIEVENT (Au73) is a more recent version of the program with the ability to monitor the input from each ADC and set one gate for observation simultaneous to the data acquisition. This program runs in two modes, SETUP where no data is recorded on magnetic tape and RUN where data is recorded on tape.

2.4.4 HYDRA

HYDRA (Au69) is a program which can use routing to store up to eight spectra in a given ADC. This is useful for half-life determinations where consecutive spectra from the same ADC are desired. This program is limited to only half-words (65,535 counts) requiring frequent punching of data in some instances.

2.4.5 PDP-9 PHA Programs

A package of Pulse Height Analysis (PHA) programs was available from DEC(PDP73) and modified here. These programs allowed singles

spectra to be taken. A total of 262,143 counts were obtainable for each channel upon which data taking was either disabled, or a channel overflow message was printed out and data taking resumed with the overflowed channel reset to zero.

CHAPTER III

DATA ANALYSIS

3.1 γ-Ray Energy and Intensity Analysis

3.1.1 γ-Ray Intensity Calibration

The Ge(Li) detectors used in these experiments were calibrated for relative efficiency by myself and others using standards listed in Table 3-1. As these standards varied in their energy ranges, their relative intensities were normalized and fit by least squares analysis to give an efficiency function. This function was usually fitted in two parts, a lower energy region where efficiency dropped off rapidly from its maximum and a higher energy region.

Generally, efficiency curves were measured at contact, 2 inches, and 10 inches from the detector. The differences in these curves were generally minor until one looked at lower energies, but, in general, data were taken at sufficient distance to justify using the calibration for 10 inches. While most standards were internally consistent, deviations between different standards were often considerable. It was general practice to weed out all "bad" points and take the best fit of the remaining points. It is this experimenter's opinion that an efficiency curve cannot be trusted to better than 5-10% below 300 keV. Below this energy detector efficiency is changing very rapidly and source thickness and geometry become increasingly important. It is doubtful if efficiencies in the low energy range can be believed to better than 20% and some very low values may not be believed at all.

Table 3-1

γ Ray Energy and Intensity Standards

E	I	E	I	E	I
^{24}Na(Led68)		^{137}Cs(Led68)		^{180m}Hf(Led68)	
1368.53	100.	32.1	6.85	93.3	16.8
2753.92	100.	36.5	1.54	215.3	80.6
		661.6	100.	332.5	94.8
^{56}Co(Ca71)				444.	83.0
846.79	100,000	^{152}Eu(Mow70)		501.	14.2
1037.91	14302±170	186.18	8.20±0.12		
1175.13	2302±25	242.00	16.1 ±0.21	^{182}Ta(Gu69)	
1238.30	67638±680	295.20	41.45±0.56	100.10	0.119
1360.22	4340±45	351.76	79.7 ±1.1	152.44	0.071
1771.41	15778±160	609.19	100.	156.39	0.0272
2015.36	3095±31	1120.4	34.9 ±0.7	179.39	0.0317
2598.58	16851±170			222.11	0.0798
3202.30	3030±30	^{160}Tb(Gu69)		229.32	0.038
3253.62	7392±74	86.79	0.209	264.07	0.0376
3273.26	1756±18	197.04	0.065	1121.28	0.370
3451.56	875±9	215.62	0.050	1189.03	0.171
		298.54	0.350	1221.28	0.289
^{57}Co(Lin71)		309.49	0.011	1230.93	0.121
14.41	11410±500	337.30	0.0054		
122.06	100000	392.43	0.019	^{192}Ir(Geh73)	
136.47	13000±400	765.20	0.017	205.77	3.86±0.08
^{60}Co(Led68)		879.31	0.40	295.95	34.64±0.35
1173.23	100.	962.46	0.14	308.45	35.77±0.36
1332.48	100.	966.17	0.344	316.50	100.
		1002.90	0.0163	468.06	58.0 ±0.9
^{88}Y(Led68)		1115.16	0.0216	588.57	5.52±0.10
898.0	93.	1177.98	0.206	604.40	10.04±0.26
1836.1	99.	1199.92	0.033	612.45	6.55±0.13
		1251.30	0.0017		
^{110m}Ag(Lav71)		1271.90	0.103	^{203}Hg(Led68)	
657.70	100.	1312.17	0.040	72.	11.9
677.57	11.93±0.41			82.	3.4
686.71	7.25±0.33	^{177m}Lu(Bern69)		279.2	100.
706.78	17.15±0.85	105.3	100.		
763.81	23.73±0.72	113.0	184.	^{226}Ra(Me70)	
818.25	7.81±0.39	128.5	131.	53.24	0.123
884.22	80.28±4.01	153.3	144.	186.21	0.032
937.31	37.31±1.42	204.1	117.	241.98	0.079
1383.85	28.26±1.42	208.3	512.	295.24	0.202

Table 3-1 (Cont'd.)

E	I	E	I	E	I
1506.65	15.19 0.49	228.4	310.	351.93	0.401
		281.8	118.	609.27	0.484
^{133}Ba(Gu69)		327.7	152.	665.40	0.0165
81.01	0.360	378.5	240.	768.45	0.0532
160.60	0.0076	413.6	135.	785.80	0.0121
276.29	0.075	418.5	172.	806.16	0.0131
302.71	0.196	466.0	20.	934.06	0.0334
355.86	0.670			1120.28	0.160
383.70	0.094			1155.17	0.0182
				1238.13	0.062
				1280.98	0.0156
				1377.64	0.0418
				1509.22	0.0230
				1661.24	0.0121
				1729.55	0.0307
				1764.99	0.166
				1842.44	0.022
				2118.52	0.0123
				2204.14	0.0530
				2293.21	0.0034
				2447.63	0.0165

3.1.2 γ-Ray Energy Calibration

Energy calibration of Ge(Li) detectors could be performed quite precisely although sometimes not with comparable accuracy. This is because the centroids of peaks would tend to shift with count rate or source position.

For accurate energy calibration, γ ray standards were counted simultaneously with the source of interest. A list of energy standards is also presented in Table 3-1. Using the appropriate internal standards, the more prominent transitions of interest could be accurately measured for use as secondary standards for weaker transitions. Additionally, decay scheme information on cascades with crossover transitions allowed further refinement of energy accuracy.

If only a rough energy calibration was desired, external standards were run separately from the source of interest. These calibrations were generally done solely to orient oneself when going over data.

3.1.3 Data-Analysis Programs

A series of analysis programs were available to automate the recovery of spectral energies, intensities, and coincidence information. A brief description of each program is presented with no explanation of the finer workings or input parameters inherent in their use. Such information can be obtained through the references given below.

3.1.3A MOD-7

MOD-7 (Ba70) is a program to generate peak intensities and centroids in an interactive fashion. Raw spectral data are displayed on a storage scope where a set of switches allow the operator to expand portions of his data in any manner. He can then visually make up to a ninth

order polynomial fit of the background under the peaks of interest and then either generate peak areas and centroids or start over with a new background fit. This program was particularly useful for analyzing peaks with unusual backgrounds.

3.1.3B SAMPO

SAMPO (Ro69) is a program to automatically find peaks in a spectra, analyze them for energy and intensity, and tabulate the results. The necessary input included only peak-shape intensity, and energy-calibration information. The program would automatically generate shape calibrations for peaks of the users preference and could search out peaks to analyze automatically if desired. An additional feature of SAMPO is its ability to strip out multiplets of up to six peaks. SAMPO was heavily used for data analysis in this work because of its great speed and consistency in obtaining good fits.

3.1.3C EVENT RECOVERY

EVENT RECOVERY (Mo73) is a program to analyze data taken under EVENT or IIEVENT mentioned earlier. This program allows the setting of gates on up to three ADC's and displaying coincidences in the remaining ADC. In addition to merely gating a region under a transition, background regions near the transition can also be gated and the background under the data of interest effectively subtracted out. Background gates were automatically normalized to the size of the peak gate so that the correct subtraction was made.

3.2 Analysis of Beta-Spectra

3.2.1 Principles of Beta Analysis

The energy distribution of electrons in a beta spectrum is given in general form by

$$N(E)dE = \frac{1}{2\pi^3 c^5 \hbar^7} g^2 |M|^2 pE(E_o-E)^2 dE \qquad (3\text{-}1)$$

where

E_o = total decay energy

E = electron energy

p = electron momentum

$|M|^2$ = matrix element of the interaction

E_o-E = neutrino energy (neglecting recoil energy).

Correcting for Coulomb interaction between the escaping beta and the recoil atom, the term $F(Z,E)$ is incorporated. The Kurie function $K(E)$ can then be written

$$K(E) = \left[\frac{N(E)}{F(Z,E)pE}\right]^{1/2} \approx \text{const.} \quad (E_o-E) \qquad (3\text{-}2)$$

where a plot of $K(E)$ vs E should yield a linear plot intersecting the energy axis at E_o. The function $K(E)$ is available in tables of Wapstra *et al.* (Wa59), Nuclear Data Sheets (Go71) and elsewhere. Additionally, such plots can be prepared through computer program FERMPLOT discussed in the following section.

3.2.2 FERMPLOT

FERMPLOT (Bla72) is a program for calculating the Kurie function K(E) (3-2) and fitting the best possible least squared fit straight line to the data plotting K(E) versus E. The calculation is done as outlined in Wapstra, and output is in the form of binary spectra for direct plotting on the Calcomp plotters.

3.2.3 Preparation of Fermi Plots

Although the calculations outlined in the previous sections are straightforward, actual preparation of Fermi plots were quite difficult. This is because the actual data collected in both scintillation and Si(Li) experiments do not directly correspond to actual beta spectra. An additional efficiency correction must be folded in for detector response as a function of energy. This arises from scattering of betas out of the detector as well as resolution corrections. Such corrections were difficult to do and, as exact beta shapes were not desired, they were dispensed with. The data are thus reasonably analyzable only in the region near the endpoint. In the case of multiple endpoints FERMPLOT was not used and data were compiled by hand. In this case tabulated values of K(E) were used and as many endpoints as practical stripped out by hand.

3.2.4 Energy Calibration of Scintillation Spectra

In the case of scintillation spectra, calibration was done primarily by means of measuring known beta endpoints. As has been seen frequently before, it was observed that such calibrations were quite linear to pulse height over a wide energy range. This meant that two points technically supplied enough information to define a calibration

curve. In actual use several calibration points were chosen for better accuracy. The standards used are given in Table 3-2.

Table 3-2

Calibration Sources for the Energy Calibration of Scintillation Detectors

Source	E (keV)	Transition
^{22}Na	340.7	Compton edge
^{137}Cs	624.2	Conversion electron
^{228}Th	2381.7	Compton edge
^{62}Cu	2930.	Beta endpoint
^{144}Pr	2990.	Beta endpoint
^{64}Ga	6050.	Beta endpoint

CHAPTER IV

THE ε/β^+ DECAY OF ^{143}Eu

4.1 Introduction

This investigation continues our overall studies of the ε/β^+ decay of N=80 odd-Z isotopes. The decays of ^{141}Pm and ^{139}Pr were reported previously (Ya73, Bee69).

Very little has yet been reported on ^{143}Eu decay. Kotajima (Ko65) measured the half-life of ^{143}Eu as 2.3 min and determined a β^+ end-point of 4.0 MeV using a plastic scintillator. Investigation with a NaI(Tl) detector indicated only 511-keV annihilation radiation. Malan (Ma66) measured 1110-keV and 1550-keV γ rays with NaI(Tl) detectors; these were assigned to ^{143}Eu and found to decay with a 2.61 min half-life.

To the best of our knowledge, no conversion-electron studies have been made on ^{143}Eu, although, indeed, its short half-life and preponderance of high energy transitions would make such measurements quite difficult. In addition, no high resolution γ-ray studies have been made. The lack of electron data makes it more difficult to assemble a complete decay scheme, for we have to work without direct information on the multipolarities of the transitions. The spins and parities of a number of states in the daughter ^{143}Sm were determined through analysis of the ^{144}Sm$(p,d)^{143}$Sm reaction studies by Kashy and Jolly (Jo71) and Chaumeaux *et al.* (Ch71) as well as the ^{144}Sm(τ,α)-^{143}Sm reaction study by Woolam *et al.* (Wo71). These reactions tend to favor simple states such as the single particle, low-lying states

predicted in shell model theory. The reaction studies were generally of sufficient energy resolution to compare unambiguously with levels found in γ-ray spectroscopy, and in this manner the spins of a number of levels were placed.

4.2 Source Preparation

^{143}Eu sources were prepared predominantly by the ^{144}Sm(p,2n)^{143}Eu reaction, which has a Q value of -16.5 MeV (Mo71). 28 MeV proton beams (threshold for ^{142}Eu production) furnished by the Michigan State University (MSU) Sector-Focused Cyclotron were used to bombard enriched targets of $^{144}Sm_2O_3$ (95.10% ^{144}Sm, obtained from the Isotopes Division, Oak Ridge National Laboratory). Typically, 25-μg targets were bombarded for 1 min with 0.5 μA of beam current.

It is interesting to note that several competing reactions can accompany (p,xn) reactions. The ^{144}Sm(p,d)^{143m}Sm reaction competed quite well producing 1-min (Ko60) ^{143m}Sm. In addition, the low binding energy of α particles below the N=82 closed shell lead to significant ^{144}Sm(p,αxn) competition. Most noticeably, the ^{144}Sm(p,αn) was seen to produce the 5.8 min (At66) ^{140m}Pm rather abundantly. Other impurities were also produced to a lesser degree.

Our bombardments did produce predominantly ^{143}Eu sources, and whatever impurities were produced could easily be eliminated by half-life comparisons. In addition, most impurities have already been well characterized. A somewhat more difficult problem involved the 8.8 min (Bl68) ^{143}Sm daughter activity. Stronger transitions could be assigned on the basis of half-life, but the weaker transitions were

assigned, in part, on the basis of a detailed study of ^{143}Sm decay at this laboratory (Fi74a).

Each source was retrieved from the bombardment area within several seconds by a rabbit retrieval system (Kos70) and counting was initiated from 1-2 min after the end of the bombardment. Counting continued up to a maximum of 10 min, i.e. approximately four half-lives. The γ rays attributed to ^{143}Eu all retained their constant relative intensities over this period.

4.3 Experimental Data

4.3.1 Singles γ-Ray Spectra

Two separate Ge(Li) detectors were used to obtain the ^{143}Eu γ-ray spectra. One was a 4.5% efficient (relative to 3×3-in NaI(Tl) detector at 25 cm) detector manufactured by ORTEC, Inc., and the other was a 10.4% efficient detector manufactured by Nuclear Diodes, Inc. The best resolution we obtained was 2.1 keV full width at half maximum for the ^{60}Co 1333 keV peak.

The γ-ray energies were determined by counting the spectra simultaneously with ^{56}Co, ^{110m}Ag, ^{152}Eu, and ^{226}Ra standards. The larger peaks, in turn, were used to determine the energies of the weaker peaks in spectra taken without standards. The centroids and net peak areas were determined with the aid of the computer code SAMPO (Ro69). The backgrounds were first subtracted and the centroids were then determined by fitting the peaks to Gaussian functions having exponential tails on both the upper and lower sides of the peaks. The specific peak shapes were determined by comparisons with reference peaks

specified at intervals throughout the spectrum. The energies were then determined by fitting the centroids to a quadratic calibration equation. Peak areas were then converted to γ ray intensities through curves previously determined in this laboratory (Gi71) for each detector. These curves were obtained by using a set of standard γ-ray sources whose relative intensities had been carefully measured with a 3×3-in NaI(Tl) detector.

A caution about the energies of the higher-energy γ rays (E_γ > 1600 keV): Because of the weakness of these peaks, internal energy calibrations could not be run. In these cases, both external standards and linear extrapolation were used to determine the energies of the γ rays. One should be somewhat wary, however, of possible systematic errors in the energies of these γ rays.

After taking spectra and following the decay of at least 6 sets of ^{143}Eu sources at widely varying times, we have identified 33 γ rays as resulting from the ε/β^+ decay of ^{143}Eu. A singles spectrum taken with the 10.4% detector is shown in Fig. 4-1. A list of these γ rays and their relative intensities is given in Table 4-1. All values from our work are averages from many determinations, with the quoted errors reflecting the statistical fluctuations found among the different runs and the quoted errors on the standards used.

4.3.2 Coincidence Spectra

4.3.2A Megachannel Coincidence Spectra

Our two-dimensional "megachannel" coincidence experiment utilized two Ge(Li) detectors, the Nuclear Diodes 10.4% detector and an ORTEC 7.0% detector. A block diagram of the electronics was shown earlier

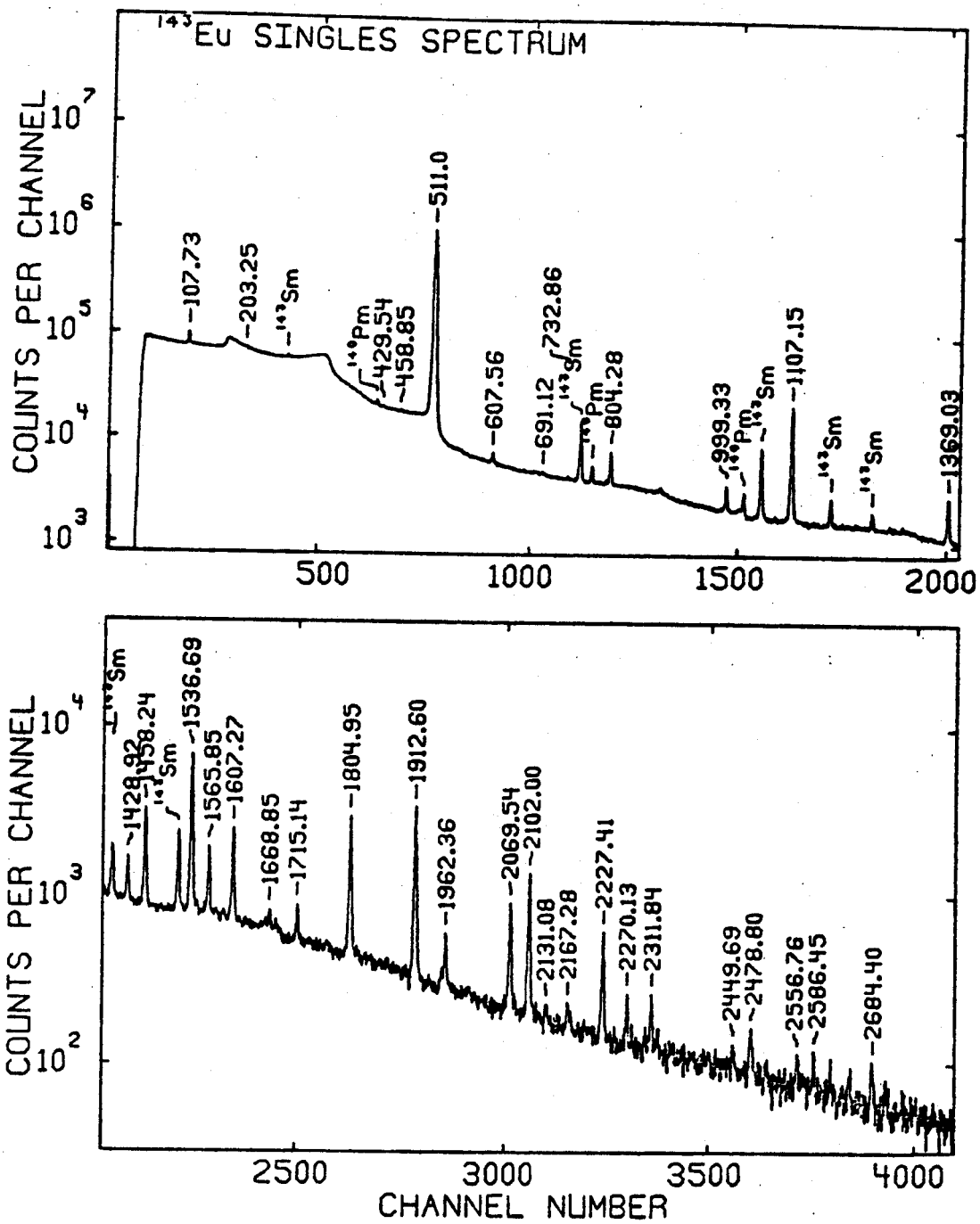

Figure 4-1. ^{143}Eu singles spectrum taken with the 10.4% Ge(Li) detector.

Table 4-1

Energies and Relative Intensities of γ-rays From the Decay of ^{143}Eu

Energy (keV)[a]	Intensity[b]	Energy (keV)[a]	Intensity[b]
107.73±0.05	24.3±1.5	1715.14±0.09	2.4±0.4
203.25±0.07	2.0±0.3	1804.95±0.07	22.7±0.8
429.54±0.07	1.8±0.2	1912.60±0.07	29.7±1.0
458.85±0.12	1.5±0.2	1962.36±0.09	3.2±0.5
607.56±0.05	4.3±0.7	2069.99±0.08	6.9±0.5
691.12±0.10	0.7±0.2	2102.00±0.08	13.0±0.6
732.86±0.10	0.7±0.2	2131.08±0.12	0.6±0.1
805.28±0.07	13.8±0.5	2167.28±0.12	0.8±0.1
999.33±0.07	7.2±0.6	2227.41±0.12	5.6±0.3
1107.15±0.07	≡100	2270.13±0.12	1.7±0.2
1369.03±0.07	12.0±0.6	2311.84±0.12	1.2±0.4
1428.92±0.09	4.9±0.4	2449.69±0.2	0.3±0.1
1458.24±0.07	15.7±0.4	2478.80±0.2	1.1±0.2
1536.69±0.07	44.6±2.0	2556.76±0.2	0.5±0.2
1565.85±0.07	7.8±0.8	2586.45±0.2	0.7±0.2
1607.27±0.07	12.8±0.7	2684.40±0.3	0.6±0.1
1668.85±0.10	1.3±0.3	------	------

[a] The errors given on the energies reflect both statistical scatter over several runs and the means of standardization used.

[b] The errors given on the intensities reflect only the statistical scatter about the average over many runs. The absolute uncertainties will be larger, perhaps ±10% for the stronger peaks and correspondingly greater for less intense or lower energy transitions.

[c] The intensities given are normalized relative to the 1107.15-keV γ≡100.

in Figure 2-1. The experiment was much like a standard fast slow coincidence experiment, except that both the *X* and *Y* events were processed each time a fast coincidence event was detected. The *X* and *Y* addresses were stored in the two halves of a single (32-bit) word in a dedicated buffer in the MSU Cyclotron Laboratory Sigma-7 computer. When the buffer was filled, events were collected in a second, similar buffer while the contents of the first were written on magnetic tape. The spectra were recovered later, off-line, by a program that allowed one to obtain gated "slices" with or without a linearly interpolated background subtraction (Mo73).

Despite the short half-life and low coincidence rate of ^{143}Eu, we used a 90° geometry for the detectors. This reduced the count rate significantly; however, a major reduction in the scattering between detectors was also achieved and in addition, the considerable contribution of the annihilation peak was greatly reduced. Coincidence data for ^{143}Sm were taken simultaneously, but were easily separated by a knowledge of the ^{143}Sm decay scheme. A resolving time of $2\tau = 80$ nsec and a maximum count rate of 6000 counts per second in the larger detector guaranteed a low chance rate. With repeated bombardments during a 12-h period we were able to collect 245,463 coincidence events, which were then analyzed. The integral coincidence spectra for the *X* (10.4%) and *Y* (7.0%) detectors are shown at the top of Figures 4-2 and 4-3, respectively, and the gated spectra including background subtraction are shown in the remainder of these figures. Of the slices taken, these were the only ones that contained substantially useful information. A summary of this data is given in Table 4-2.

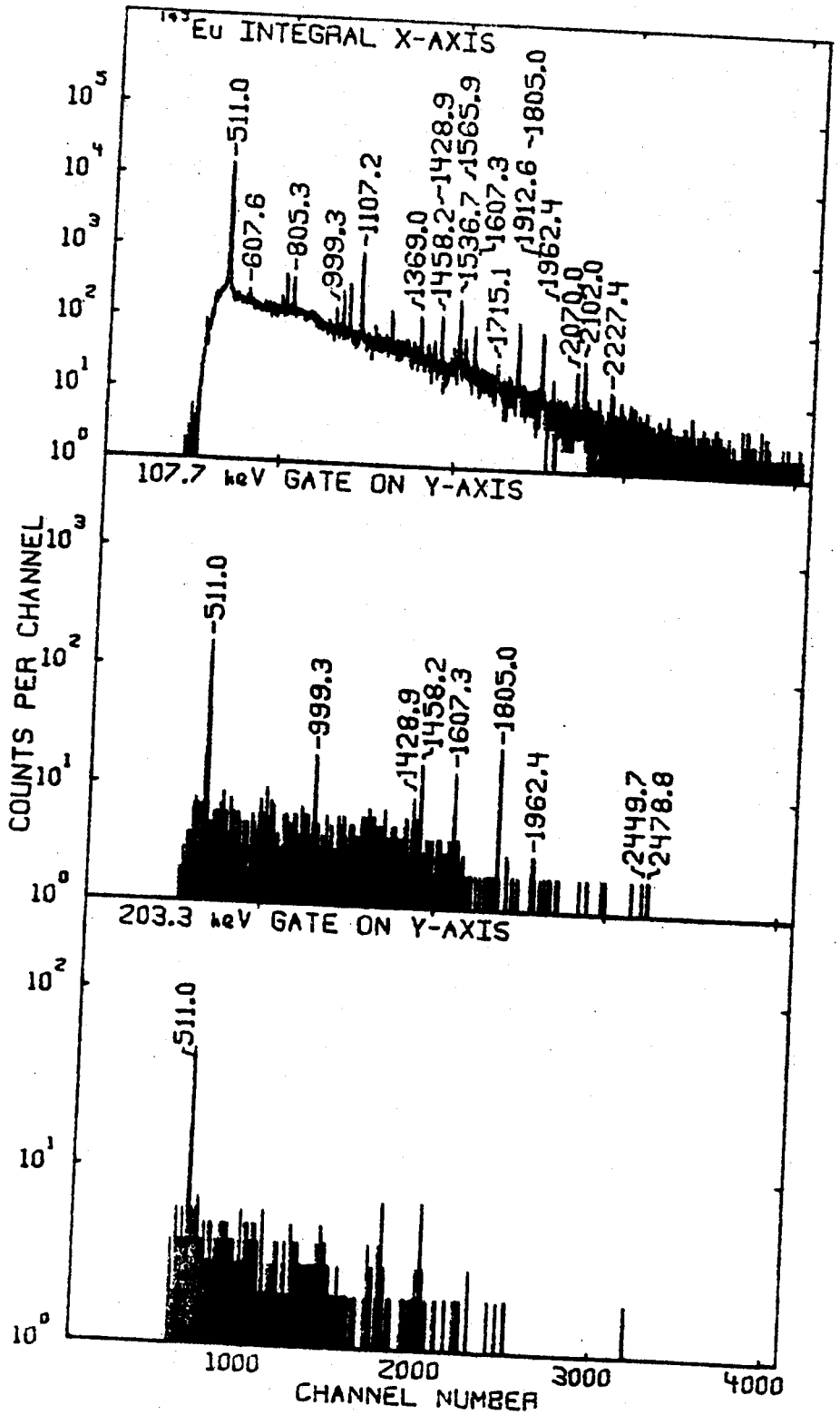

Figure 4-2. ^{143}Eu γ-γ coincidence spectra gating on the *Y* axis and displaying the coincident *X* axis.

Figure 4-2 (cont'd.)

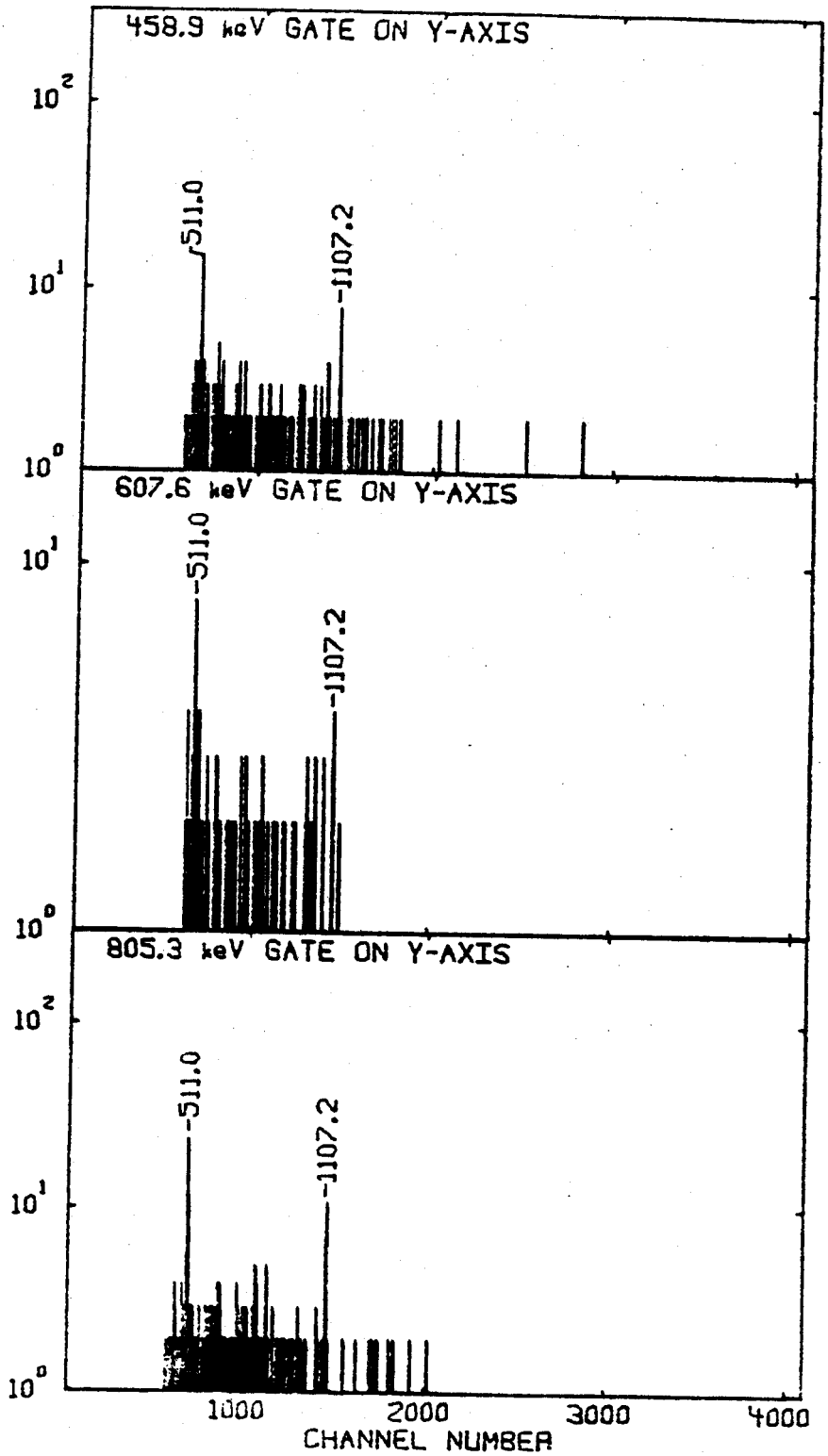

Figure 4-2 (cont'd.)

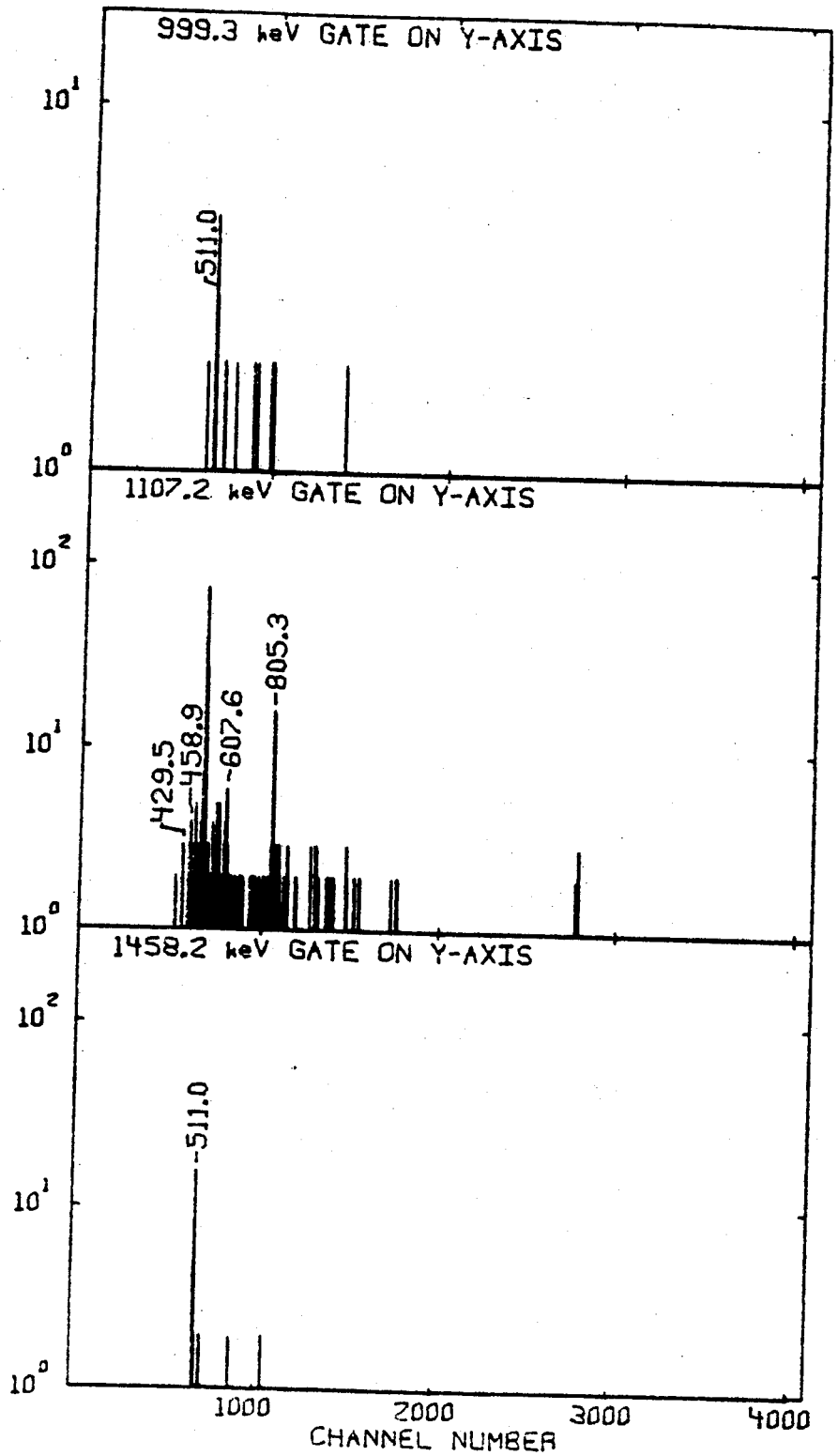

Figure 4-2 (cont'd.)

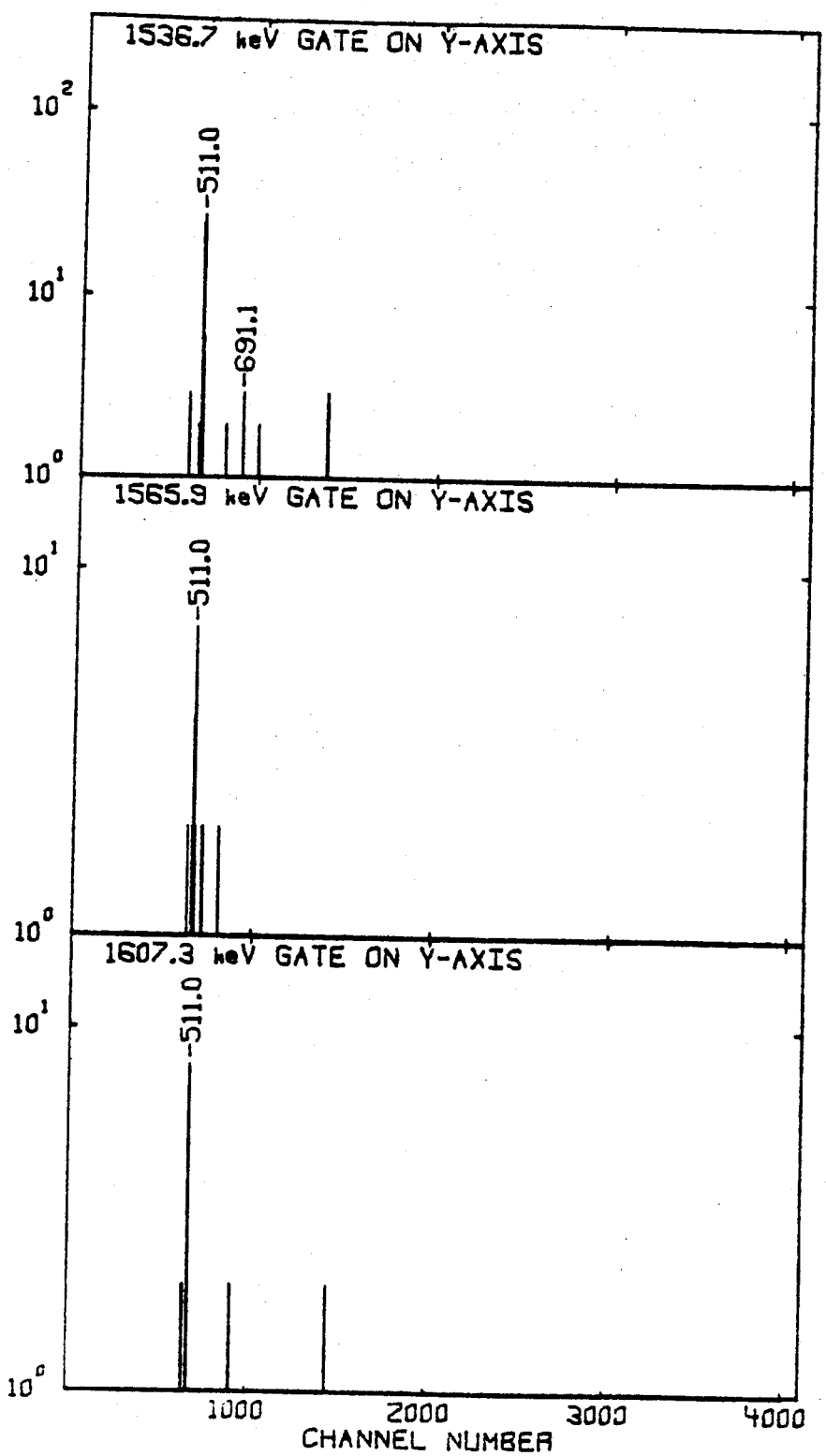

Figure 4-2 (cont'd.)

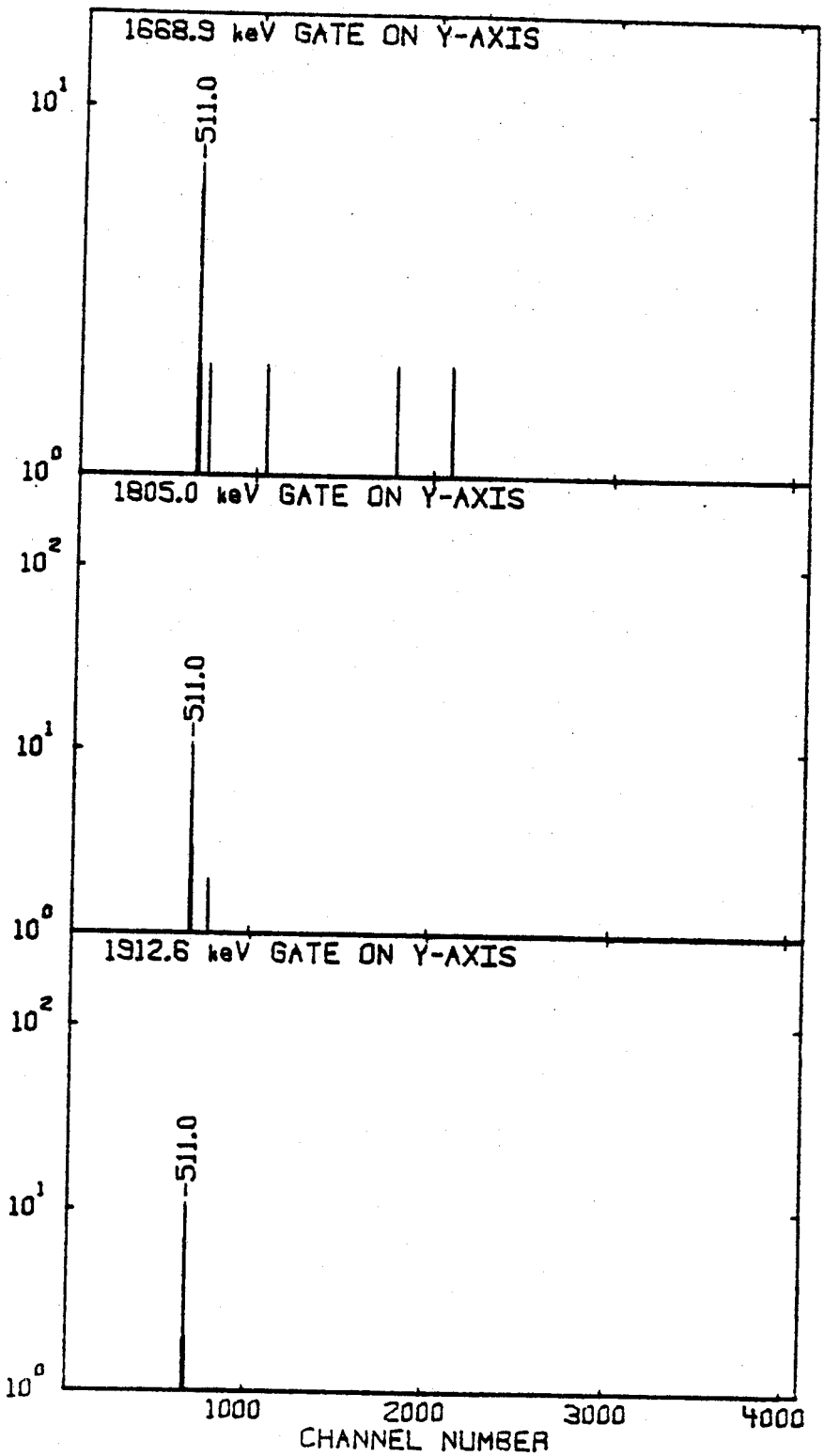

Figure 4-2 (cont'd.)

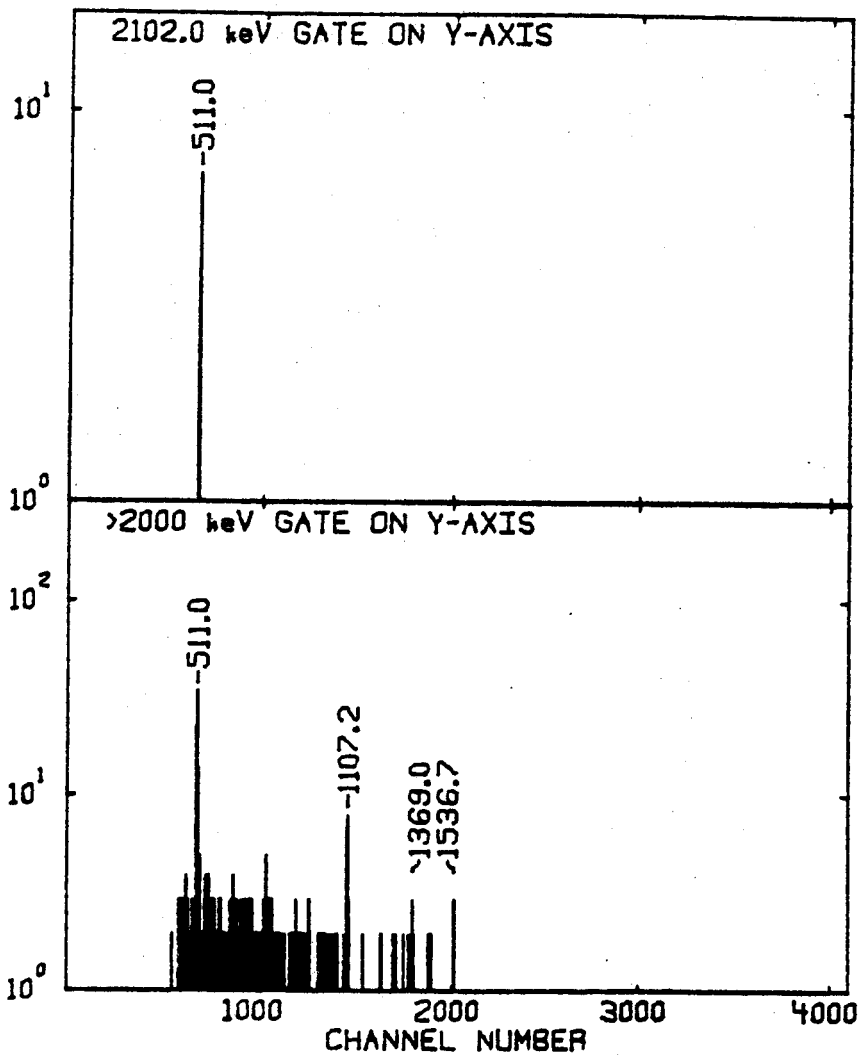

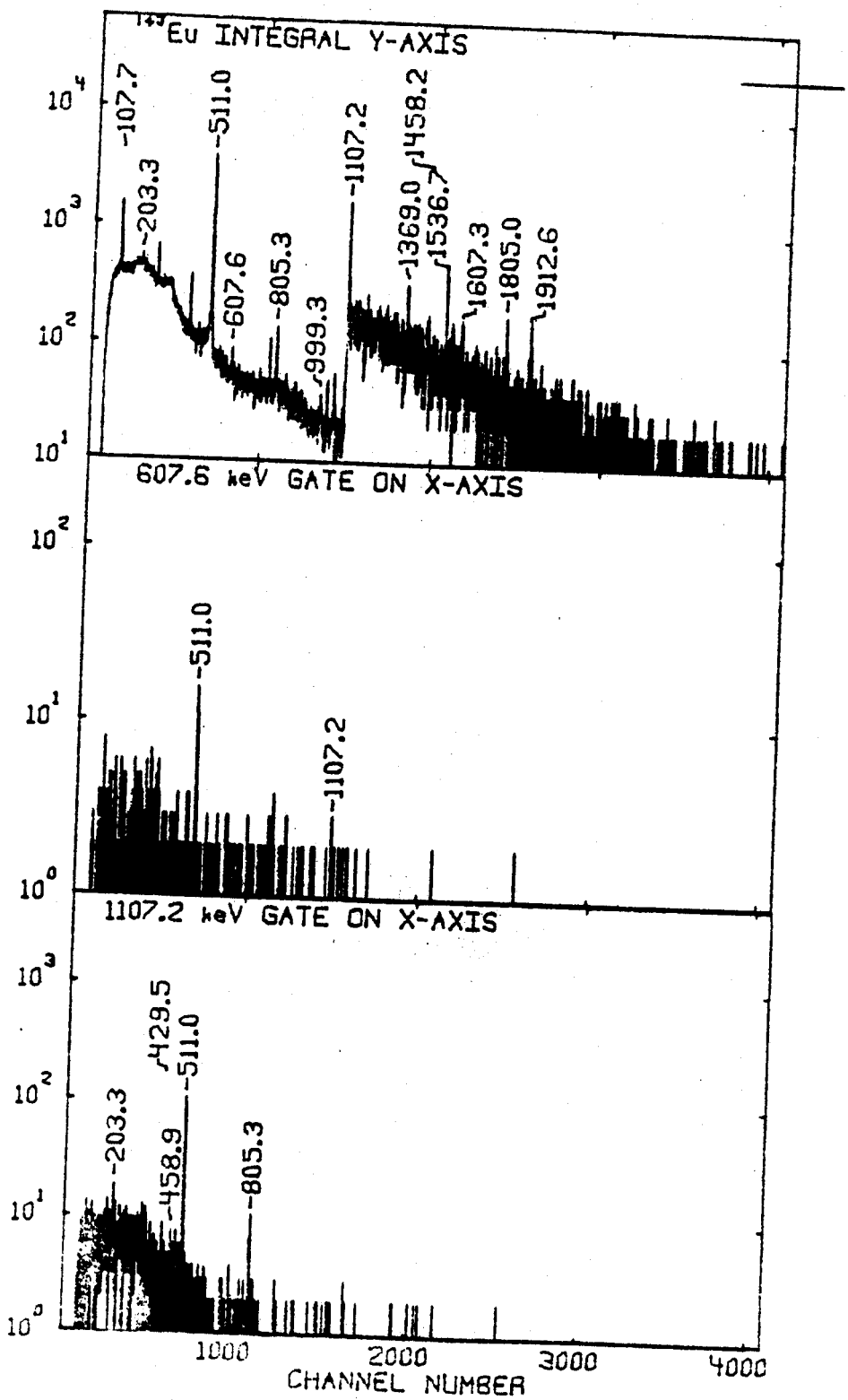

Figure 4-3. ^{143}Eu γ-γ coincidence spectra gating on the *X* axis and displaying the coincident *Y* axis.

Figure 4-3 (cont'd.)

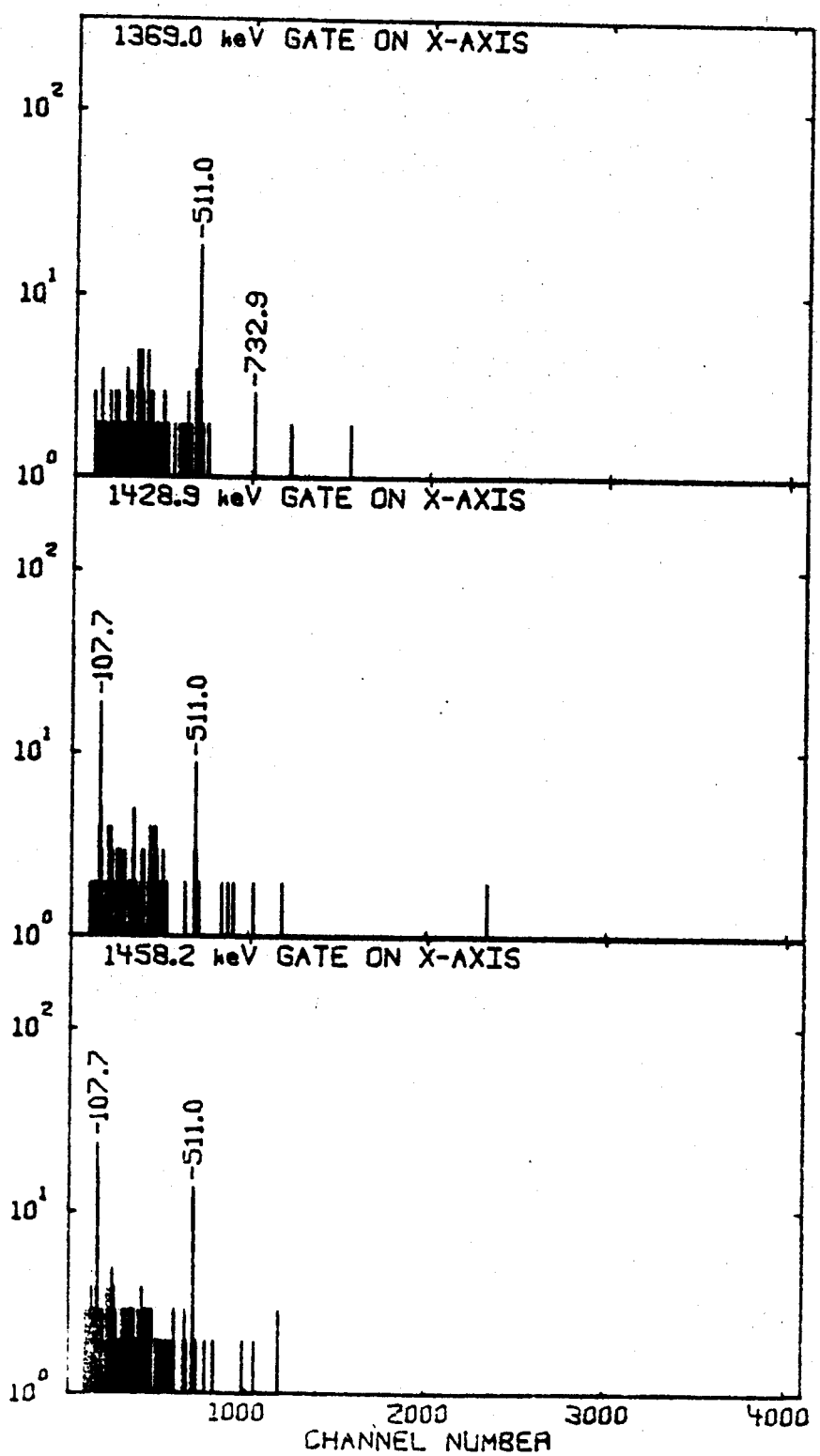

Figure 4-3 (cont'd.)

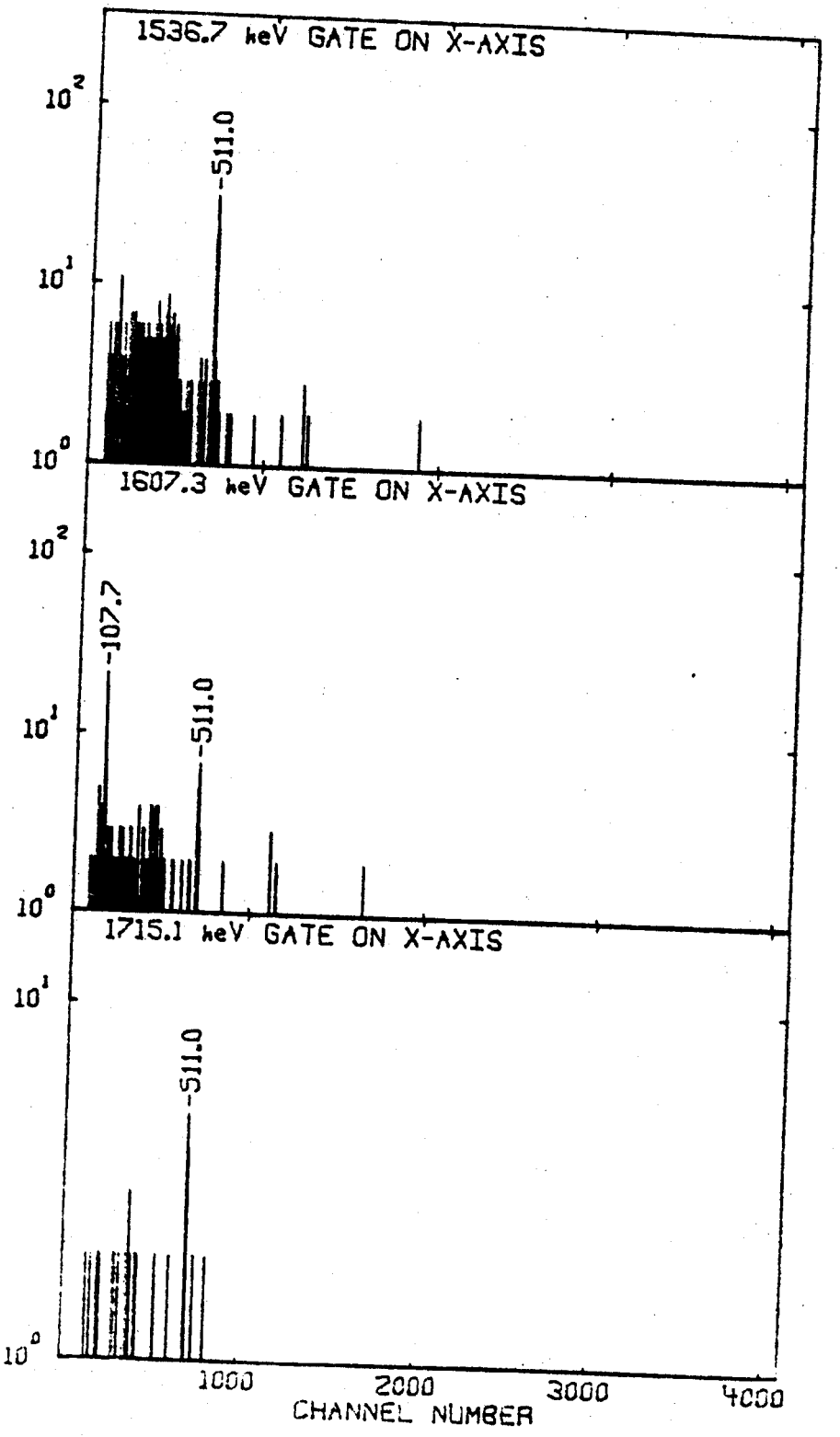

Figure 4-3 (cont'd.)

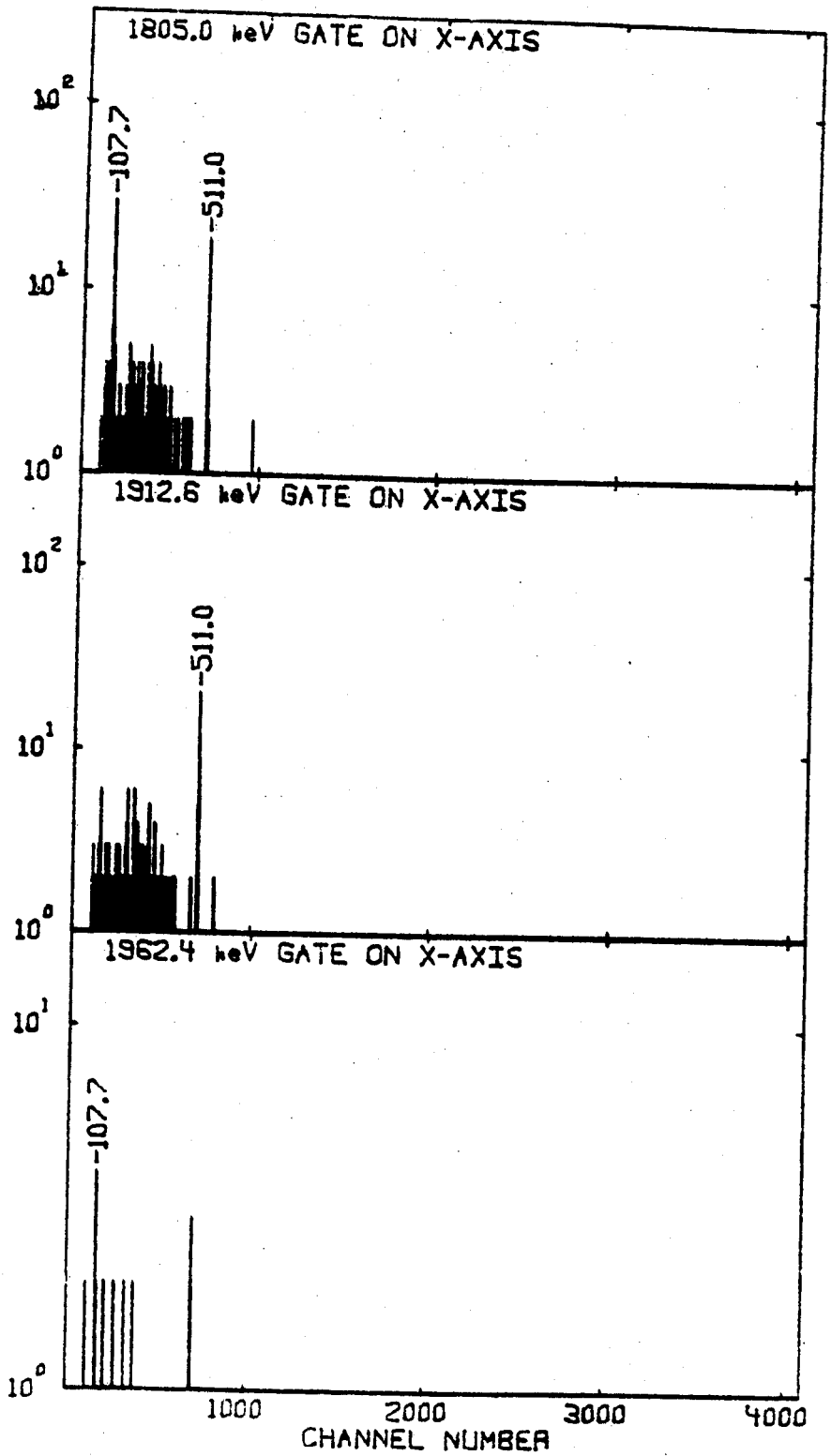

Figure 4-3 (cont'd.)

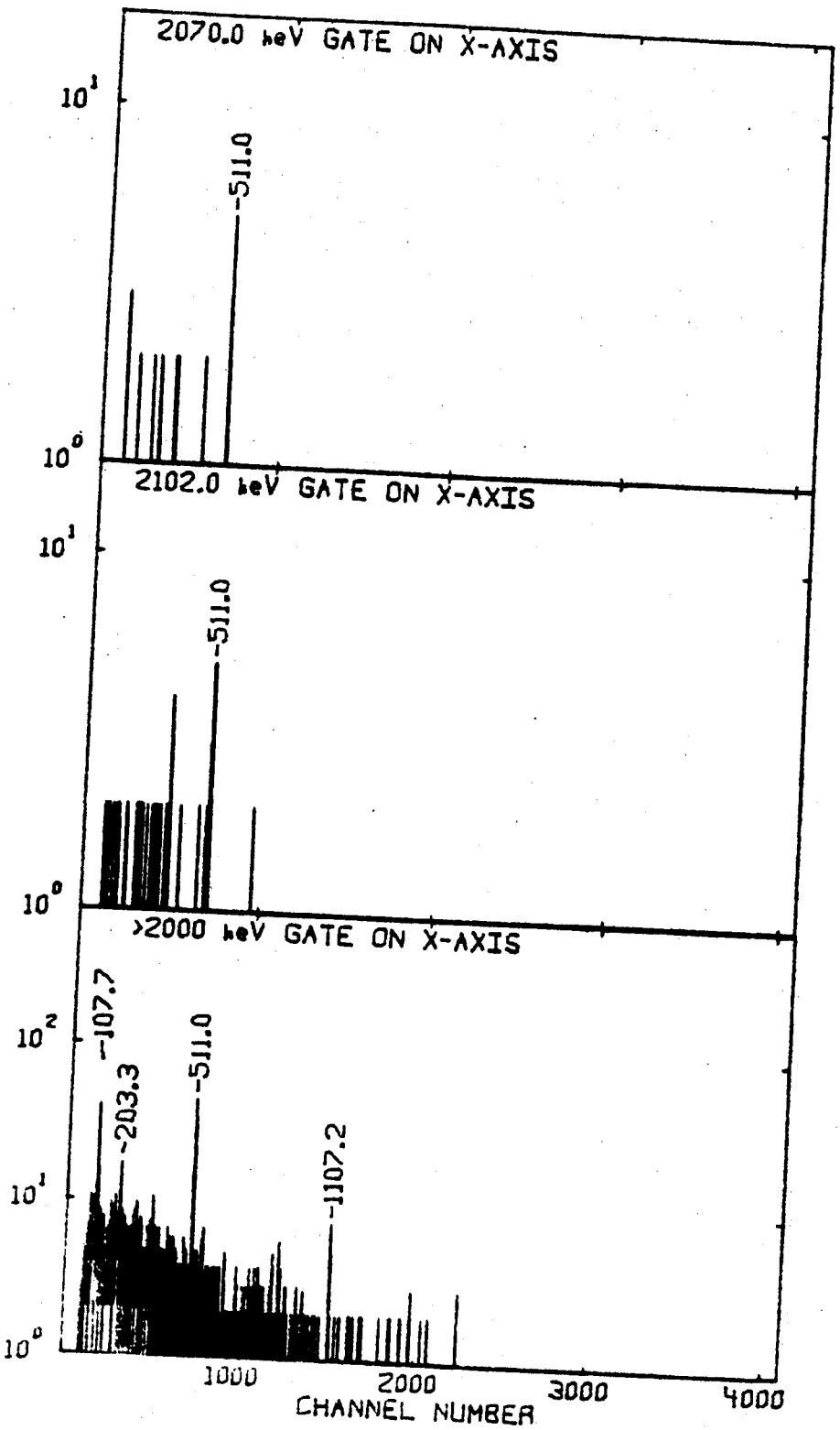

Table 4-2

^{143}Eu Coincidence Summary

Gate (keV)	Coincident γ Rays
107.7(Y)	999.3, 1428.9, 1458.2, 1607.3, 1805.0, 1962.4, 2449.7?, 2478.8?
458.9(Y)	110[illegible].2
607.6(X)	110[illegible].2
805.3(Y)	110[illegible].2
1107.2(X)	203.3, 429.5, 458.9, 805.3
1107.2(Y)	429.5, 458.9, 607.6, 805.3
1369.0(X)	732.9
1428.9(X)	107.7
1458.2(X)	107.7
1536.7(Y)	691.1
1607.3(X)	107.7
1805.0(X)	107.7
1962.4(X)	107.7
> 2000 (X)	107.7, 203.3, 1107.2
> 2000 (Y)	1107.2, 1369.0, 1536.7

4.3.2B Pair Spectra

The two halves of an 8×8-in NaI(Tl) split annulus were used in conjunction with the 10.4% Ge(Li) detector to determine the relative amounts of β^+ feeding to the various levels in ^{143}Sm. Each half of the annulus was gated on the 511-keV $\gamma^{\pm}$ peak and a triple coincidence (resolving time, 2τ = 100 nsec) was required among these and the Ge(Li) detector. The resulting spectrum is shown in Figure 4-4. A discussion of the β^+ feedings extracted from this experiment is deferred until Section 4.5 where they are presented in Table 4-5.

4.4 Proposed Decay Scheme

Our proposed decay scheme for ^{143}Eu is shown in Figure 4-5. Of the 33 γ rays listed in Table 4-1, 29 have been placed in the decay scheme, accounting for over 98% of the total γ ray intensity. It is entirely possible that many of the remaining γ rays proceed from levels that decay via a single transition. These γ rays are all too weak to have been seen in any of our coincidence work, so, with no further evidence for their placement, we have omitted them entirely.

The assigned spins and parities, discussed in Section 4-5, represent a combination of deductions from our work and conclusions from reaction studies. The agreement between our work and reaction studies are quite good. The results of the reaction studies are presented in Table 4-3. We used the total ε-decay energy measured by Kotajima (Ko65) of 5.0 MeV.

The feeding to the ground state of ^{143}Sm was inferred from the intensity of the 511 keV annihilation peak corrected for contribution

Figure 4-4. ^{143}Eu $\gamma^{\pm}$-γ pair coincidence spectrum.

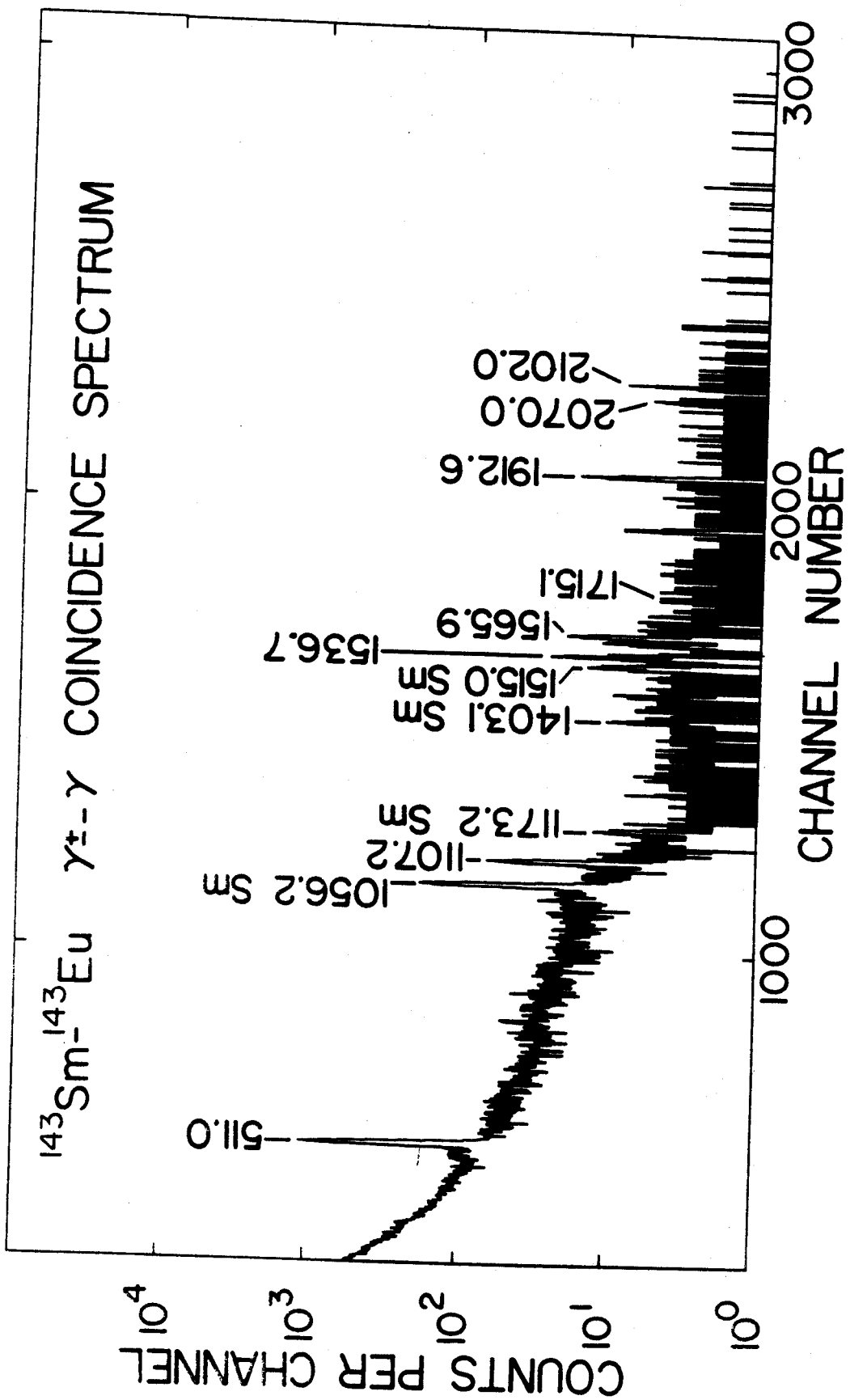
^{143}Sm-^{143}Eu $\gamma^{\pm}$-γ COINCIDENCE SPECTRUM
COUNTS PER CHANNEL
CHANNEL NUMBER
511.0
1056.2 Sm
1107.2
1173.2 Sm
1403.1 Sm
1515.0 Sm
1536.7
1565.9
1715.1
1912.6
2070.0
2102.0
1000
2000
3000

Figure 4-5. ^{143}Eu decay scheme. All energies are given in keV and transition intensities are given in terms of percent per disintegration of the parent. The 107.7-keV transition is corrected for internal conversion. The logft values are calculated from tables by Gove and Martin (Go71).

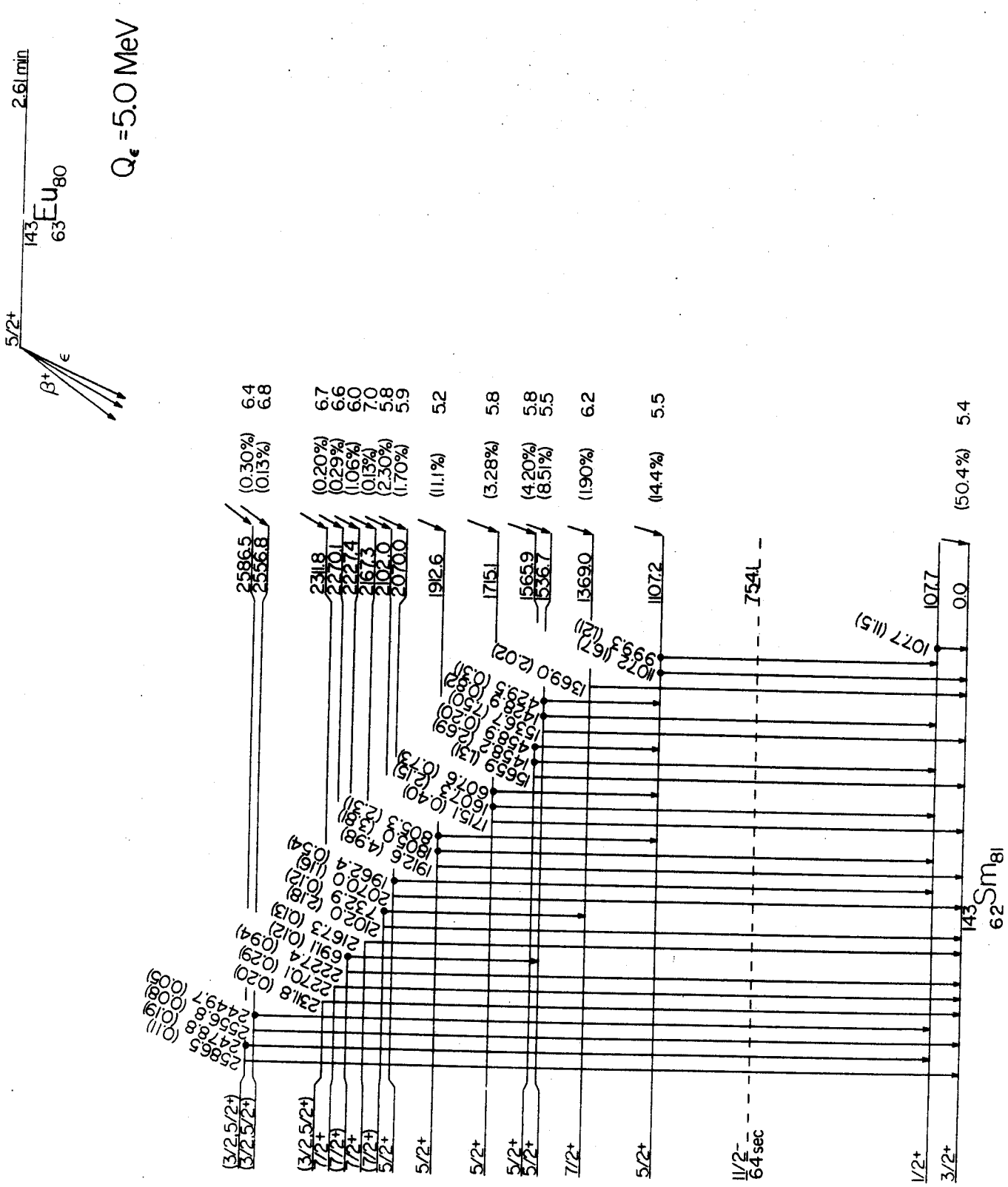
Q$_\epsilon$ = 5.0 MeV
$^{143}_{63}Eu_{80}$
2.61 min
5/2+
β+
ε
$^{143}_{62}Sm_{81}$
(3/2,5/2+)
(3/2,5/2+)
7/2+
(7/2+)
7/2+
(7/2+)
5/2+
5/2+
5/2+
5/2+
5/2+
7/2+
5/2+
11/2−
64 sec
1/2+
3/2+
2586.5
2556.8
2311.8
2270.1
2227.4
2167.3
2102.0
2070.0
1912.6
1715.1
1565.9
1536.7
1369.0
1107.2
754.1
107.7
0.0
(0.30%)
(0.13%)
(0.20%)
(0.29%)
(1.06%)
(0.13%)
(2.30%)
(1.70%)
(11.1%)
(3.28%)
(4.20%)
(8.51%)
(1.90%)
(14.4%)
(50.4%)
6.4
6.8
6.7
6.6
6.0
7.0
5.8
5.9
5.2
5.8
5.8
5.5
6.2
5.5
5.4
1369.0 (2.0)
1072 (16.7)
999.3 (12)
1077 (11.5)

Table 4-3

Levels in ^{143}Sm From Beta Decay and Reaction Studies

This Work		^{144}Sm(p,d) (Jo71)			^{144}Sm(p,d) (Ch71)		
Energy	Assignment	Energy	Assignment	S	Energy	Assignment	S
0.0	$3/2^+$	0.0	$3/2^+$	4.0	0.0	$3/2^+$	4.0
107.7	$1/2^+$	110.	$1/2^+$	1.4	107.	$1/2^+$	1.6
754.1	$11/2^-$	760.	$11/2^-$	7.4	748.	$11/2^-$	9.86
1107.2	$5/2^+$	1110.	$5/2^+$	3.7	1100.	$5/2^+$	2.57
1369.0	$7/2^+$	1360.	$7/2^+$	3.1	1360.	$11/2^-$]	1.04
1536.7	$5/2^+$	1530.	$5/2^+$	0.34	1532.	$5/2^+$	0.1
1565.9	$5/2^+$						
1715.1	$5/2^+$	1720.	$5/2^+$	0.8	1697.	$5/2^+$	----
1912.6	$5/2^+$						
2070.0	$5/2^+$	2060.	$5/2^+$	0.6	2040.	$5/2^+$	----
2102.0	$(7/2^+)$						
2167.3	$7/2^+$	2160.	$7/2^+$	2.7			
2227.4	$(7/2^+)$						
2270.1	$7/2^+$	2290.	$7/2^+$	1.8			
2311.8	$(3/2,5/2^+)$						
		2470.	$11/2^+$	1.4	2440.	$7/2^+$	0.65
2556.8	$(3/2,5/2^+)$						
2586.5	$(3/2,5/2^+)$	2590.	$(11/2^-)$	0.84			
		3040.	$(7/2^+)$	2.1			
		3170.	$(5/2^+)$	0.7			

from ^{143}Sm decay. The contribution of electron capture was calculated yielding the percentage ground state feeding. The intensities in Fig. 4-5 are given as percent of decays of ^{143}Eu.

Specific evidence for the placement of levels and transitions in the decay scheme is given as follows:

Ground, 107.73, 754.06, 1107.15, and 1369.03-keV states. These states were all populated strongly by the ^{144}Sm(p,d) reaction and appear to be essentially single particle states, viz., the $d_{3/2}$, $s_{1/2}$, $h_{11/2}$, $d_{5/2}$, and $g_{7/2}$ in that order. We, too, see specific evidence for all but the 754.06-keV state which is the $h_{11/2}$ metastable state and would not be expected to be populated by low spin ^{143}Eu.

The 107.73 keV transition appears to deexcite the level of the same energy. Coincidence data indicate the 999.33-, 1428.92-, 1458.24-, 1607.27-, 1804.95-, and 1962.36-keV γ-rays in certain coincidence with this transition, and very weakly suggest that the 2449.69- and 2478.80-keV transitions may also be in coincidence with it. Thus, all the transitions shown through the 107.73-keV level are at least weakly indicated in coincidence data. Clearly the unadjusted intensities into the 107.73-keV level greatly exceed the intensity out of this level. This can be accounted for by calculating the γ-ray intensity loss due to internal conversion. The 107.73-keV γ ray should be an $E2$,$M1$ mixture where the calculated conversion coefficients are 1.1 and 1.4, respectively (Ro58). Assuming no β feeding, the conversion coefficient necessary to get an even intensity balance is 1.8±0.4. This is within error for a pure $M1$ transition and if other losses are taken into account might allow some $E2$ mixing. Beta feeding to this level appears quite unlikely in accordance with the chosen spin of

$5/2^+$ for the ground state of ^{143}Eu. Indeed spins $1/2^+$ or $3/2^+$ are very unlikely without significant feeding to the 107.73-keV state in ^{143}Sm. Such low spin states are not expected to lie so low in energy.

The 1107.15-keV γ-ray transition depopulating the level of the same energy is the single most intense transition in the spectrum. γ-rays at 429.54, 458.85, 607.46 and 805.28 keV are seen strongly in coincidence with this transition. The log *ft* of 5.5 is well within the range of allowed transitions and supports the spin $5/2^+$ assigned to ^{143}Eu ground state which is discussed later.

The 1369.03-keV transition is in coincidence with the 732.86 γ ray. This state was assigned as $7/2^+$ by Kashy and Jolly (Jo71) but as $11/2^-$ by Chaumeaux (Ch71). The log *ft* of 6.2 is somewhat high for an allowed transition but still unreasonably low for the third-forbidden transition. This state will be discussed further in Section 4.5.

1536.69-, 1565.85-, 1715.14-, and 1912.60-keV states. These levels are certainly quite similar in that they all deexcite through the ground, first, and second excited states. In addition, the 1536.69-keV γ is in coincidence with a 691.12 keV γ-ray deexciting the higher lying 2227.41-keV state. The other states in this group evidence no corresponding transitions, but such transitions may easily be too weak to be observed. Kashy and Jolly found levels at 1530 and 1720 keV both of spin $5/2^+$. We have thus chosen spin $5/2^+$ for all four levels on the basis of their similarities, although the spin-parity assignments for the 1565.85- and 1912.60-keV levels have no basis in reaction studies. The log *ft* measurements for feeding to these levels are 5.5, 5.8, 5.8, and 5.2 respectively indicative both of their

similarities and that they are allowed transitions. Their nature will further be discussed in Section 4.5.

2069.99-, 2311.84-, 2556.76-, and 2586.45-keV states. These states are all similar in that they deexcite only through the ground and first excited states. The log *ft* values to these levels are 5.9, 6.7, 6.8, and 6.4, respectively, indicative of rather hindered allowed transitions. Angular momentum and β selection rules constrain these levels to spins $3/2^+$ or $5/2^+$. The only level in this group reported in reaction studies is the $5/2^+$ level at 2060 keV. The 2069.99-keV state appears to correspond to this level and is assigned spin $5/2^+$. The other states cannot be interpreted any more unambiguously.

2101.00-, 2167.28-, 2227.41-, and 2270.13-keV states. These states are all alike in that they all feed the ground state but not the first excited state. The log *ft* values to these levels are 5.8, 7.0, 6.0, and 6.6, respectively. These are again indicative of slow allowed transitions. The β selection rules indicate these levels can be $3/2^+$, $5/2^+$, or $7/2^+$, but the lack of feeding to the $1/2^+$ first excited state strongly suggests that all these levels may be $(5/2^+)$ or $7/2^+$. Kashy and Jolly report $7/2^+$ levels at 2160 and 2290 keV so we will make definite assignments of $7/2^+$ to the 2167.78- and 2270.13-keV states. The 2102.00- and 2227.41-keV states will also be assigned spin $7/2^+$ or $(5/2^+)$ but with somewhat lesser certainty.

The ground state spin of the parent ^{143}Eu is now clearly established. Allowed transitions proceed to $3/2^+$, $5/2^+$, and $7/2^+$ states which can only be true if the ground state of ^{143}Eu is $5/2^+$. This is also predictable from the systematics of N=80 nuclei as will be shown in the following section.

4.5 Discussion

Some 16 states have now been placed, with varying degrees of confidence, in ^{143}Sm. All five major neutron orbits between N=50 and 82 lie reasonably close together, resulting in relatively low-lying single particle states which are not terribly fragmented.

4.5.1 Single-Particle States

The five states at 0, 107.73, 454.06, 1107.15 and 1369.03 keV compromise the major components of the single-neutron orbits between N=50 and 82, viz., $d_{3/2}$, $s_{1/2}$, $h_{11/2}$, $d_{5/2}$, and $g_{7/2}$ respectively. The first four states appear to be well documented in reaction studies and confirmed by their decay properties. The $11/2^-$ and $1/2^+$ states are not fed at all by the β decay of ^{143}Eu as would be expected but the $11/2^-$ is made directly. The fifth state 1369.0 keV appears to be wrongly assigned by Chaumeaux (Ch71) as an $11/2^-$ state which is not expected so low in energy. This state is weakly fed in ^{144}Sm(p,d) leading to significant statistical uncertainty. In addition, the cross sections for the ℓ=4 transitions were so much smaller than for ℓ=5 transitions (experimental (Jo71) and DWBA) that Kashy and Jolly et al. claim that this state is definitely the $7/2^+$ single particle state.

The systematics of these single-particle states in the N=81 nuclei ^{139}Ce, ^{141}Nd, and ^{143}Sm is most notable for its monotony. The ordering of states is the same in all cases, and the $1/2^+$ first excited state decreases from 254.7- to 107.73-keV in the interval relative to the $3/2^+$ ground state. Similarly, the $11/2^-$ state stays at virtually the same energy and the $5/2^+$ state decreases only from 1320.0 to 1107.15 keV.

The $7/2^+$ state increases only slightly from 1347.4 to 1369.03 keV in the same interval. Clearly the addition of proton pairs to the N=81 nuclei does little to disturb the single particle neutron states. These systematics are shown in Table 4-4.

4.5.2 Other States

Assuredly, the higher lying states in ^{143}Sm are more complex. Although little quantitatively can be said about these states, it is clear that at least some of these states must arise from couplings of the lowest 2^+ or 3^- core excitations to the single neutron hole states. Indeed, Kashy and Jolly show that the 1536.69-, and 1715.14-keV states probably have an appreciable $(d_{3/2})_\nu^{-1} \times 2^+$ component. In addition, other states of possible multiparticle nature are expected to be present, although little can be said about them at this time except that they should not be expected to be seen in ^{144}Sm(p,d) studies.

4.5.3 The ^{143}Eu Ground State

The decay properties of ^{143}Eu clearly indicate the $5/2^+$ nature of this ground state. This spin is strongly confirmed by the systematics of N=80 nuclei where the $5/2^+$ state first falls below the $7/2^+$ state in ^{139}Pr and continues to drop rapidly at ^{141}Pm. Although no direct measurement of the spin of the ^{143}Eu ground state has been made, we are quite certain of its accuracy.

4.5.4 ε/β^+ Ratios

From our $\gamma^\pm$ gated spectrum (Figure 4-4) the relative β^+ feedings to seven of the ^{143}Sm states were measured. The deduced ε/β^+ ratios for transitions to these states are listed in Table 4-5. We normalized

Table 4-4

Single Particle States of N=81 Nuclei

State	Energy (keV) ^{139}Ce	^{141}Nd	^{143}Sm
$3/2^+$	0.	0.	0.
$1/2^+$	254.7	193.8	107.7
$11/2^-$	628.6	756.7	754.1
$5/2^+$	1320.0	1223.3	1107.2
$7/2^+$	1347.4	1345.8	1369.0

Table 4-5

Comparison of Experimental and Theoretical $\varepsilon(tot)/\beta^+$ Ratios for the Decay to States in ^{143}Sm

Energy[a] (keV)	$\varepsilon(tot)/\beta^+$ Experimental	Theoretical[b]
1107.15	0.51±0.06[c]	0.46
1536.69	0.62±0.06	0.69
1565.85	0.69±0.15	0.72
1715.14	0.75±0.17	0.83
1912.60	1.07±0.11	1.02

[a]These are the only states in ^{143}Sm that are measurably fed by β^+ decay, as determined from that $\gamma^{\pm}$ gated coincidence spectrum.

[b]These values are from Nuclear Data Tables 10 (1971). Q_ε = 5.5 MeV is chosen to get these values.

[c]The experimental ratios were normalized to the theoretical ratios by assuming that the transition to the 1107.15-keV state is allowed and unhindered, presumably yielding the expected ratio.

our experimental values to the theoretical values for the transition to the 1107.15-keV state which we considered to be a fast, straightforward transition with good statistical information. Indeed, the measured values compare quite well with the theoretical values.

Chapter V

ε/β^+ Decay of ^{143}Sm

5.1 Introduction:

This investigation continues our over-all studies of the N=81 isotones. The decay of ^{141}Nd and ^{145}Gd have been presented previously (Bee68,Ep71).

Although several papers have characterized ^{143}Sm decay properties (B168,Bel66,Dew72,DeF68,DeF70), the most definitive work published to date is by D. DeFrenne *et al.* (DeF70). They produced ^{143}Sm by the ^{144}Sm(γ,n) reaction and presented a decay scheme based on very limited coincidence data and energy sums.

To the best of our knowledge, no conversion electron studies have been done on ^{143}Sm decay, so the multipolarities of γ-ray transitions are undetermined. This makes the assignment of spins to levels in ^{143}Pm more difficult, but the problem is partially obviated by the ^{142}Nd(τ,d) and ^{144}Sm(d,τ) reaction studies of Wildenthal *et al.* (Wil71). It is often possible to associate levels found in reaction studies with the same levels seen in decay scheme studies.

The ^{143}Sm decay study presented here was in part an offshoot of the study of ^{143}Eu decay (Fi74d). In order to characterize ^{143}Eu decay, a knowledge of its ^{143}Sm daughter decay was necessary. In addition to that, however, the ^{143}Sm decay offers particularly interesting information in light of our studies of its neighboring isotones. Of particular interest are the apparent β transitions from the $3/2^+$ and $1/2^+$ ground states of ^{141}Nd and ^{145}Gd to the $7/2^+$ first excited

states in their respective daughters, ^{141}Pr and ^{145}Eu. In the first case the second forbidden transition which should proceed with a log ft in the range of 10 to 14 is seen to occur with a logft of ≥8.8. The second case involves a second forbidden unique transition which should proceed with a logft of ≈14. This transition occurs with a logft of ≥7.5. It seems likely that a similarly enhanced, second forbidden transition will exist to ^{143}m. D. DeFrenne (DeF70) indicates a small feeding to the corresponding level and one of the goals of these experiments was to measure this feeding more precisely.

5.2 Source Preparation

^{143}Sm sources were prepared primarily by the ^{144}Sm(p,2n)^{143}Eu (β^+/ε)^{143}Sm reaction which has a Q value of -16.5 MeV (Mo71). 28 MeV proton beams (the threshold for ^{142}Eu production) furnished by the Michigan State University (MSU) Sector-Focused Cyclotron were used to bombard enriched targets of $^{144}Sm_2O_3$(95.10% ^{144}Sm, obtained from the Isotopes Division, Oak Ridge National Laboratory). Typically, 25-μg targets were bombarded for ≈1 min with 0.5 μA of beam current. We also attempted the ^{142}Nd(τ,2n)^{143}Sm reaction (Q = -7.7 MeV) with little success. The major product of this reaction appeared to be ^{140}Pm ($t_{1/2}$ = 6.8 min) although the (τ,αxn) reactions were also evidenced. Clearly the τ reactions are quite complex in this region where protons and alpha particles are rather weakly bound.

The ^{144}Sm(p,2n) reaction was considerably cleaner, although again the major impurity was ^{140}Pm produced presumably by the ^{144}Sm(p,αn) reaction. Other impurities included ^{143m}Sm (63 sec), ^{142}Sm (72.5 min),

and ^{141}Sm (20.9 min) and were of low intensity and easily resolved by half-life from the 8.83 min ^{143}Sm.

The initial ^{143}Eu (2.61 min) quickly decayed to ^{143}Sm and sources were counted starting from 10-15 min following bombardment, for intervals up to a maximum of 40 minutes following bombardment the γ-rays attributed to ^{143}Sm decay all retained their constant relative intensities over that period. Transitions emanating from ^{143}Eu were easily distinguished by the study of ^{143}Eu decay presented in Chapter 4.

5.3 Experimental Data

5.3.1 Singles γ-Ray Spectra

Several separate Ge(Li) detectors of different manufacturer were used at different times to obtain the ^{143}Sm spectra. They were all of coaxial design and varied from 4.5% to 10.4% in efficiency (relative to a 3×3-in. NaI(Tl) detector at 25 cm). The best resolution we obtained was 2.0 keV full width at half maximum for the ^{60}Co 1332-keV γ ray. In most cases these detectors were used with baseline restoration and pileup rejection which decreased resolution slightly but allowed large count rates (upwards of 60,000 counts per second). The γ-ray energies under 1600 keV were determined by counting the spectra simultaneously with ^{56}Co, ^{152}Eu, ^{110m}Ag and ^{226}Ra standards. The larger peaks in the spectrum were calculated using these standards. These calibrated peaks, in turn, were used to determine the energies of the weaker peaks in the spectra taken without standards. The centroids and net peak areas were taken with the aid of the computer code SAMPO (Ro69). The backgrounds were first subtracted and the centroids then

determined by fitting the peaks to Gaussian functions having exponential tails on both the upper and lower sides of the peaks. The peak shapes were determined by comparisons with reference peaks specified at intervals throughout the spectrum. The energies were then determined by fitting the centroids to a quadratic calibration equation. Peak areas were then converted to γ-ray intensities through curves previously determined in this laboratory (Do69) for each detector. These curves were obtained by using a set of standard γ-ray sources whose relative intensities had been carefully measured with a 3×3-in. NaI(Tl) detector.

Transitions above 1600 keV were all too weak to be calibrated in the foregoing manner. In these cases a combination of methods was used to find the centroids. External standards were run before or after the singles spectra to give a fairly close calibration. These are prone to systematic error, so, in addition, well known energy differences for transitions from a state to levels of a better measured energy difference were used in an interactive manner to improve the energy calibrations. It must be emphasized, however, that there may be systematic errors in the energies of the higher transitions.

After taking spectra from and following the decay of at least 6 different sets of ^{143}Sm sources prepared at widely separated times we have identified 23 γ rays resulting from the ε/β^+ decay of ^{143}Sm. A singles spectrum is shown in Figure 5-1. A list of these γ rays and their relative intensities is given in Table 5-1, where they are compared with the results of DeFrenne *et al.* (DeF70). All values from our work are the averages from many determinations, with the quoted errors reflecting the statistical fluctuations found in different runs and the quoted errors on the standards used.

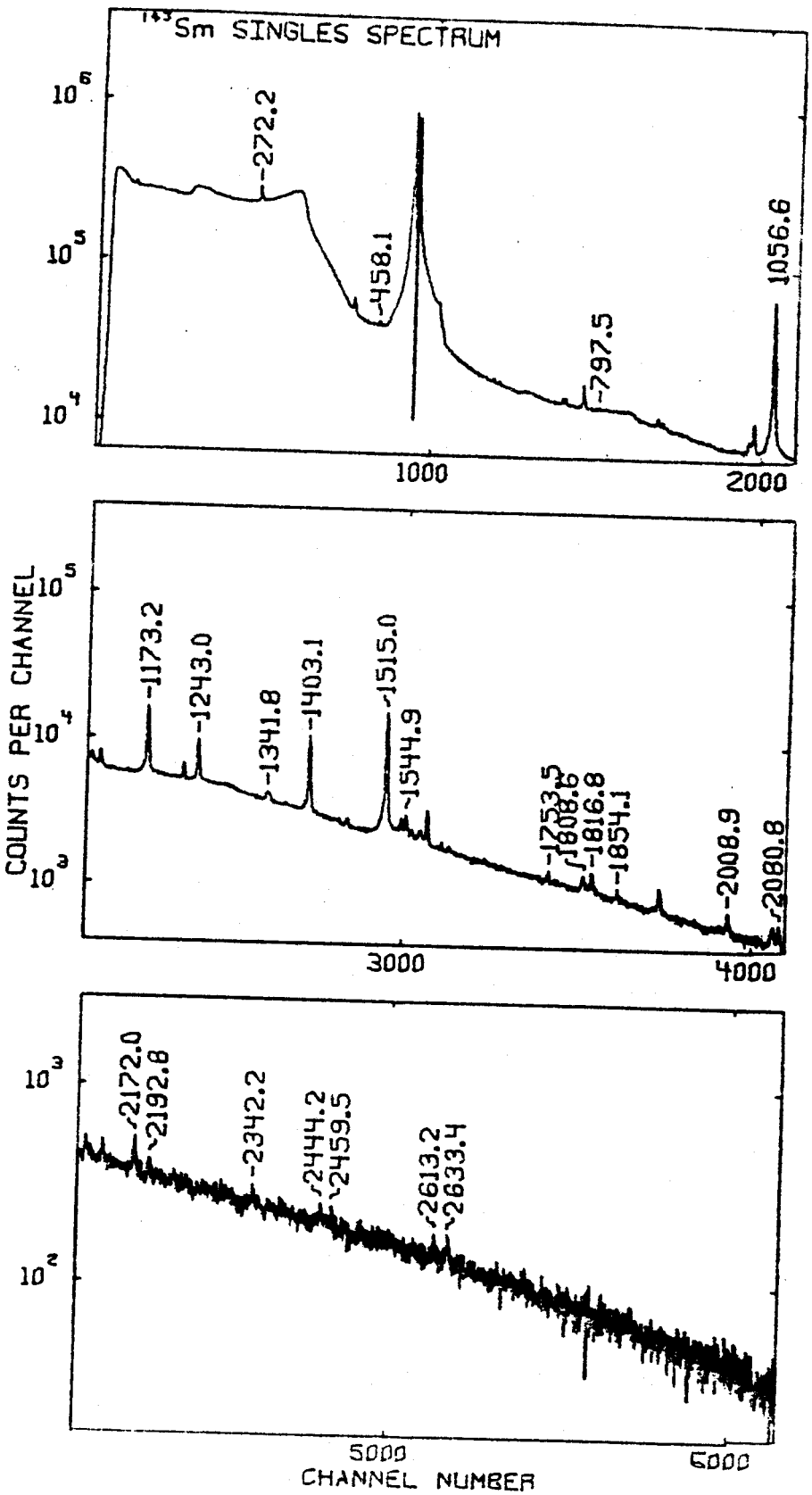

Figure 5-1. ^{143}Sm singles spectrum taken with the 10.4% Ge(Li) detector.

Table 5-1

Energies and Relative Intensities of γ-Rays from the Decay of ^{143}Sm

This Work		D. DeFrenne *et al.*[c]	
Energy (keV)[a]	Intensity[b]	Energy (keV)	Intensity
272.18±0.05	16.0±1.6	271.8	15.9
458.11±0.15	1.9±0.2	458.5	2.6
797.49±0.15	0.8±0.2	797.6	0.6
1056.58±0.07	≡100	1056.5	≡100
1173.18±0.07	21.9±1.7	1173.4	21.9
1242.95±0.07	11.5±0.5	1243.1	11.4
1341.81±0.15	1.5±0.4	1342.1	1.5
1403.06±0.07	18.4±1.0	1403.2	17.2
1514.98±0.07	34.7±1.5	1514.9	34.6
1544.87±0.10	2.7±0.3	1544.3	2.6
1753.45±0.10	0.5±0.1	1752.8	0.6
1808.64±0.25	0.07±0.03	1808.5	0.17
1816.78±0.10	1.3±0.3	1816.6	1.2
1854.08±0.10	0.6±0.1	1853.6	0.28
2008.87±0.10	0.8±0.2	2009.0	0.65
2080.83±0.10	0.7±0.2	2080.7	0.6
2171.95±0.10	0.8±0.1	2171.6	0.85
2192.84±0.10	0.2±0.1	2192	0.18
2342.24±0.30	0.3±0.1	2344	0.20
2444.17±0.40	0.4±0.2	2443	0.12
2459.52±0.60	0.2±0.1	2461	0.08
2613.15±0.20	1.9±0.3		
2633.35±0.50	0.3±0.1	2634.8	0.25

[a] These energies reflect a weighted average over several runs as well as the method of determination employed.

[b] These intensities reflect essentially the statistical fluctuations over several runs. Systematic calibration errors may be much larger, especially in the lower (<100 keV) regions.

[c] Values from D. DeFrenne, E. Jacobs, and J. Demuynck, Z. Phys. 237, 327 (1970).

5.3.2 Coincidence Spectra

5.3.2A Megachannel Coincidence Spectra

Our two-dimensional "megachannel" coincidence experiment utilized 7.0% and 10.4% Ge(Li) detectors. A block diagram of the electronics was shown earlier in Figure 2-1. The experiment was much like a standard fast-slow coincidence experiment, except that both the *X* and *Y* events were processed each time a fast-coincident event was detected. The *X* and *Y* addresses were stored in the two halves of a single (32-bit) word in a dedicated buffer in the MSU Cyclotron Laboratory Sigma-7 computer. When the buffer was filled, events were collected in a second, similar buffer while the contents of the first were written on magnetic tape. The spectra were recovered later off-line by a program that allowed one to obtain gated "slices" with or without a linearly interpolated background subtraction (Mo73).

Data were collected simultaneously for both ^{143}Eu and ^{143}Sm decays. As both spectra were well known, it was simple to separate events in both integral coincidence spectra. In addition the overlap of energies in the two decays was not a problem so it was easy to set the appropriate gates.

The short half-life of ^{143}Sm coupled with the fact that only a small percentage of events were associated with coincidences made the collection of decent statistics virtually impossible. In addition, about 50% of the decay was by β^+ making 180° geometry of the detectors undesirable. For this reason we used 90° geometry, which also lessens the chance of scattering between detectors (Gi73) was used. With repeated bombardments over twelve hours we were able to collect 245,463 events, many of which pertained to ^{143}Eu. The resolving time was 2τ=90

nsec and count rates were always less than 6000/s in the larger detector so the chance rate was indeed quite small.

The integral coincidence spectra for the *X* (10.4%) and *Y* (7.0%) detectors are shown at the top of Figures 5-2 and 5-3, respectively, and gated spectra with background subtraction containing the useful information are shown below in the remainder of Figures 5-2 and 5-3. These coincidence results are summarized in Table 5-2.

5.3.2B Pair Spectra

The two halves of an 8×8-in. NaI(Tl) split annulus were used in conjunction with the 10.4% Ge(Li) detector to determine the relative amounts of β^+ feeding to the various levels in ^{143}Pm. Each half of the annulus was gated on the 511-keV $\gamma^{\pm}$ peak and a triple coincidence (resolving time 2τ = 100 nsec) was required among these and the Ge(Li) detector. A resulting spectrum was shown in Figure 4-4. A discussion of the β^+ feedings extracted from this experiment is deferred until Section 5.5 where they are presented in Table 5-4.

5.4 Proposed Decay Scheme

Our proposed decay scheme for ^{143}Sm is shown in Figure 5-4. It is largely in agreement with the level scheme proposed by D. DeFrenne *et al.* (DeF70) the main difference being our omission of their proposed levels at 1342.1, 1752.8, 2000., 2009.0, 2344, 2463.0 and 2906.0 keV and the addition of levels at 1613.99 and 2613.15 keV. Of the 23 γ rays listed in Table 4-1, 18 have been placed in the decay scheme, accounting for over 99% of the total γ-ray intensity. It is entirely possible that many of the remaining γ rays proceed from levels that

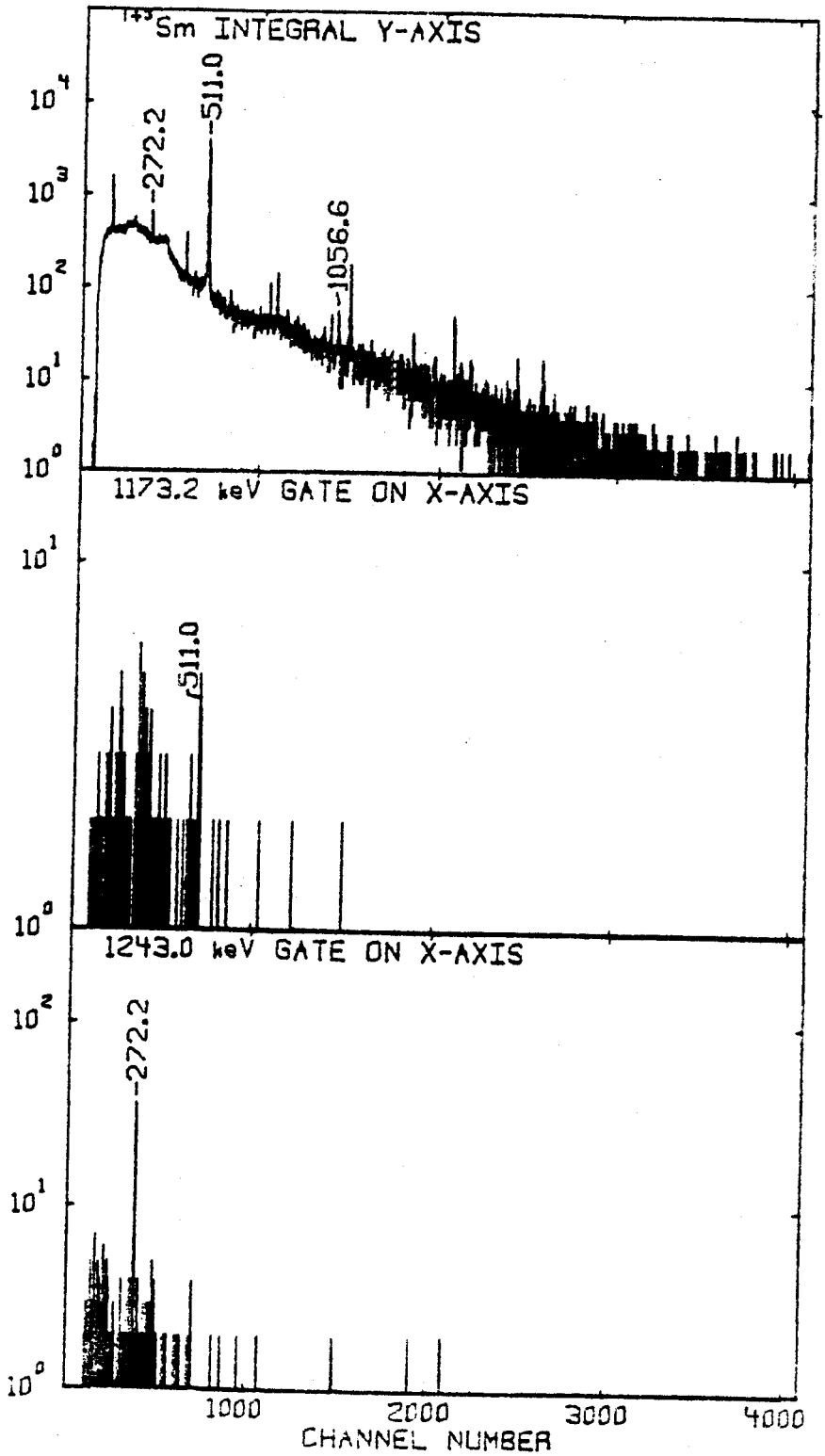

Figure 5-2. ^{143}Sm γ-γ coincidence spectra gating on the X axis and displaying the coincident Y axis.

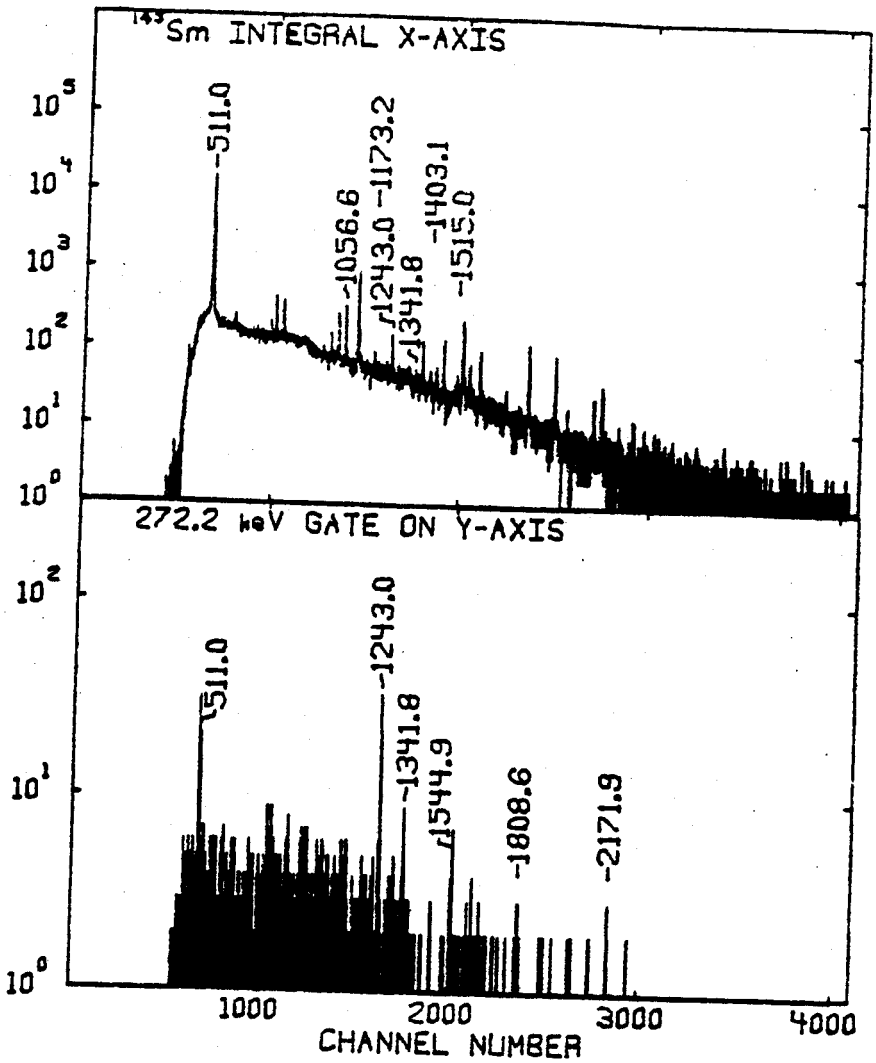

Figure 5-3. ^{143}Sm γ-γ coincidence spectra gating on the *X* axis and displaying the coincident *Y* axis.

Figure 5-3 (cont'd.)

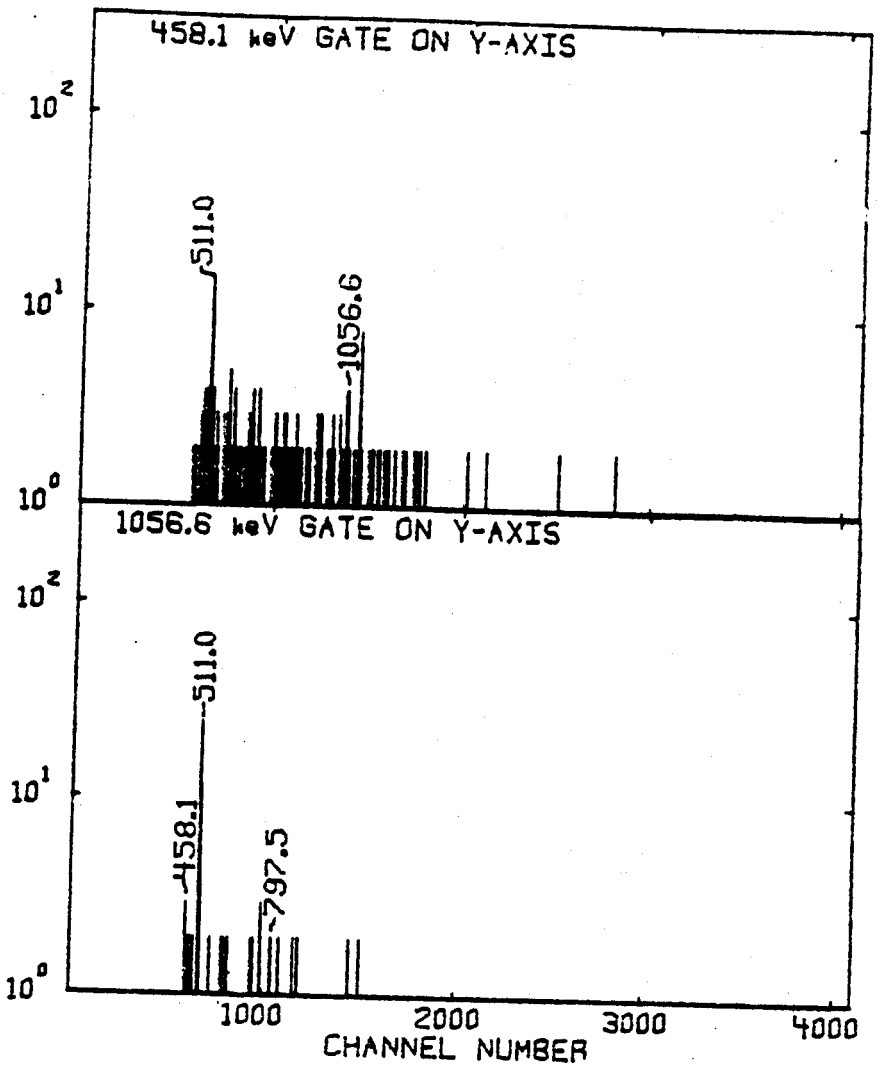

Table 5-2

^{143m}Sm Coincidence Summary

Gate (keV)	Coincident γ Rays
272.2(Y)	1243.0, 1341.8, 1544.9, 1808.6, 2171.9
458.1(Y)	1056.6
1056.6(Y)	458.1, 797.5?
1243.0(X)	272.2

Figure 5-4. ^{143}Sm decay scheme. All energies are given in keV, and transition intensities are given in terms of percent per disintegration of the parent. The 272.2-keV transition is corrected for internal conversion. The logft values are calculated from the tables by Gove (Go71).

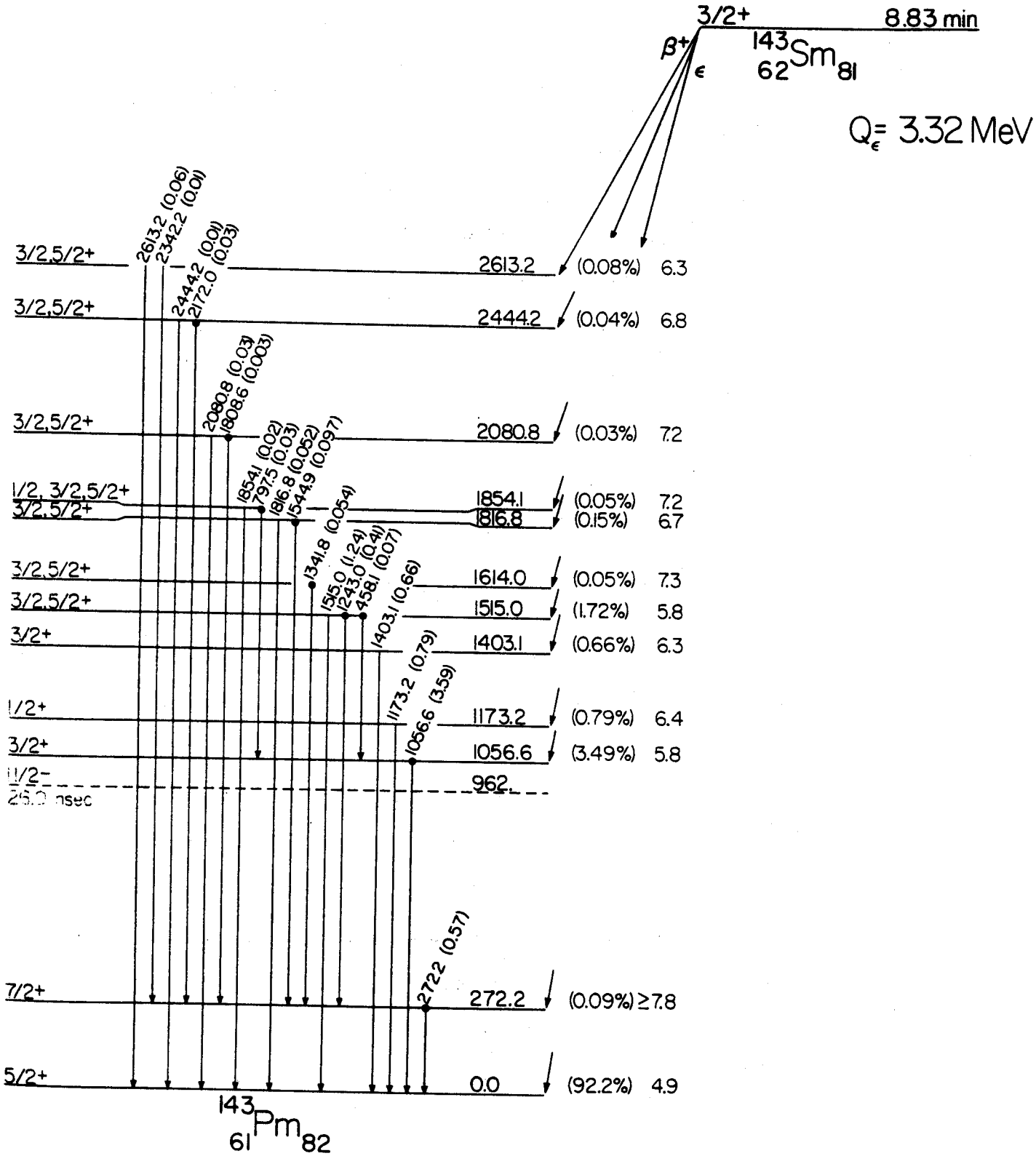
3/2+
8.83 min
β+
ε
143 62 Sm 81
Q_ε = 3.32 MeV
2613.2 (0.06)
2342.2 (0.01)
2444.2 (0.01)
272.0 (0.03)
2080.8 (0.03)
1808.6 (0.003)
1854.1 (0.02)
797.5 (0.03)
1816.8 (0.052)
544.9 (0.097)
1341.8 (0.054)
1515.0 (1.24)
1243.0 (0.41)
458.1 (0.07)
1403.1 (0.66)
1173.2 (0.79)
1056.6 (3.59)
272.2 (0.57)
3/2,5/2+
3/2,5/2+
3/2,5/2+
1/2, 3/2,5/2+
3/2,5/2+
3/2,5/2+
3/2,5/2+
3/2+
1/2+
3/2+
11/2−
2613.2 (0.08%) 6.3
2444.2 (0.04%) 6.8
2080.8 (0.03%) 7.2
1854.1 (0.05%) 7.2
1816.8 (0.15%) 6.7
1614.0 (0.05%) 7.3
1515.0 (1.72%) 5.8
1403.1 (0.66%) 6.3
1173.2 (0.79%) 6.4
1056.6 (3.49%) 5.8
962
7/2+
272.2 (0.09%) ≥7.8
5/2+
0.0 (92.2%) 4.9
143 61 Pm 82

decay via a single transition to the ground state. These γ rays were all very weak so that in the absence of further evidence for their placement, we have omitted them entirely.

The assigned spins and parities represent a combination of deductions from our own work and the conclusions of Wildenthal *et al.* (Wil71) for states observed via the ^{142}Nd(τ,*d*)^{143}Pm and ^{144}Sm(*d*,τ)^{144}Pm reactions as shown in Table 5-3. The results of the two studies are in good agreement for most states. We use the measured total ε decay energy of 3.32 MeV (Mat65) to calculate log*ft* values.

The relative γ-ray intensities listed in Table 5-1 were based on a value of 100 for the 1056.58-keV γ-ray transition. The relative x-ray intensity was not measured. Thus, the total ground state feeding was inferred from the total intensity of the annihilation peak.

Specific evidence for the placement of levels and transitions in the decay scheme is given as follows.

Ground, 272.18-, 962.0, 1056.58-, 1173.18- and 1403.06-keV states. These states we all populated strongly in the ^{142}Nd(τ,*d*) reaction where their spins were unambiguously determined as $5/2^+$, $7/2^+$, $11/2^-$, $3/2^+$, $1/2^+$, and $3/2^+$, respectively. The 962-keV state is not seen at all in β decay, which agrees with its assigned spin and the $3/2^+$ spin of the ^{143}Sm ground state.

The 272.18-keV state appears to be fed with a log*ft* of 7.8 indicative of a forbidden transition. This is in line with its $7/2^+$ spin assignment. This state is also established from coincidence data which confirm γ rays of 1242.95, 1341.81, 1544.87, 1808.64, and 2171.95 keV as being coincident with it.

The transition to the 1056.58-keV state proceeds with a log*ft* = 5.8

Table 5-3

Levels in ^{143}Pm From Beta Decay and Reaction Studies

This Work		^{142}Nd(τ,d) (Wil70)		^{144}Sm(t,α) (Han68)	
Energy	Assignment	Energy	Assignment	Energy	Assignment
0.0	$5/2^+$	0.0	$5/2^+$	0.0	5/2
272.2	$5/2^+$	270.	$7/2^+$	273.	$7/2^+$
		960.	$11/2^-$	964.	$11/2^-$
1056.6	$3/2^+$	1060.	$3/2^+$		
1173.2	$1/2^+$	1170.	$1/2^+$	1183.	$1/2^+$
1403.1	$3/2^+$	1400.	$3/2^+$	1409.	$3/2^+$
1515.0	$(3/2,5/2^+)$				
1614.0	$(3/2,5/2^+)$				
1816.8	$(1/2,3/2,5/2^+)$				
1854.1	$(1/2,3/2,5/2^+)$				
2080.8	$(3/2,5/2^+)$				
2444.2	$(3/2,5/2^+)$				
2613.2	$(3/2,5/2^+)$				

indicative of allowed transitions as predicted by its assigned spin. This level is further confirmed by weak coincidence data supporting feeding by 458.11-keV γ ray. The 1173.18- and 1403.06-keV states are fed with log*ft* values of 6.3 and 6.4, respectively. This strongly indicates allowed transitions, confirming the spin assignments. No coincidence information is available to confirm these levels further, but their placement appears to be quite certain, nevertheless.

1514.98-, 1613.99-, 1816.78-, 2080.83-, and 2444.17-keV states. These states are based solely on the available coincidence data and energy sums. They are presumably all well placed although in some cases the coincidence data are very weak. The log*ft* to the 1514.98-keV level is 5.8, indicative of an allowed transition. The log*ft*'s to the other levels are 7.3, 6.7, 7.2 and 6.8, respectively. While these values are high, they probably still indicate allowed transitions. The possible spins presented for these levels are based on both β-decay and γ-ray selection rules and generally indicate these levels to be either $3/2^+$ or $5/2^+$.

1854.08- and 2613.15-keV states. These levels are placed strictly on the basis of energy sums or differences. The log*ft*'s to these levels are 7.2 and 6.3, respectively, indicating allowed transitions, and they are clearly restrained to spin $3/2^+$ or $5/2^+$.

5.5 Discussion

Some 13 states have now been placed, with varying degrees of confidence, in ^{143}Pm.

5.5.1 Single-Particle States

The states at 0, 272.18, 962, 1173.18, and 1403.06 keV comprise the major components of all of the single-proton orbits between Z=50 and 82, viz., $d_{5/2}$, $g_{7/2}$, $h_{11/2}$, $s_{1/2}$, and $d_{3/2}$ respectively. This was clear from the ^{144}Sm(d,τ) and ^{142}Nd(τ,d) reactions by Wildenthal (Wil71) where the production of single particle states is predominant.

The $g_{7/2}$ state is very weakly fed and the logft of 7.8 clearly indicates that the transition is forbidden. Actually, this value was attained by assuming the theoretical prediction of 11% internal conversion. Otherwise, no net feeding is seen. The net intensity out of the $g_{7/2}$ level is not greater than the experimental uncertainties, so the logft value is by no means certain. It is, however, consistent with previous results for the $g_{7/2}$ feeding from ^{141}Nd and ^{145}Gd decay.

The $h_{11/2}$ state is not populated by β decay. It has been reported, however, that this state is populated in the decay of ^{143m}Sm (Fe70). The logft was found there to be 6.7. For such an allowed decay to take place there is the implication of at least some occupation of the $h_{11/2}$ orbit by proton pairs.

The predominant decay is to the $5/2^+$ ground state. The logft to this state is very low at 4.9. This β transition is extremely fast because it is a simple one step $(\pi d_{5/2}) \rightarrow (\nu d_{3/2})$ transition between simple single-particle states.

The ε/β^+ decays to the 1173.18- $s_{1/2}$ and 1403.06- $d_{3/2}$ keV states proceed somewhat slowly for allowed transitions, with logft values of 6.3 and 6.4, respectively. This can be seen to occur because the decays cannot go as directly as was the case to the ground state. In these

cases a rather complex particle rearrangement must occur in the proton shell which will necessarily hinder the transitions.

5.5.2 Three-Quasiparticle States

Somewhat peculiarly, the strongest β-fed excited states are not the single particle states, but the two states at 1056.58 and 1514.98 keV. These two states account for 57% of the excited state feeding, and the low logft's, both 5.8, indicate unhindered, allowed transitions. The 1056.58-keV state was seen weakly in the ^{142}Nd(τ,d) reaction studies by Wildenthal, but the extracted spectroscopic factor (C^2S) for this ℓ=2 transfer was only 0.05, indicating the structure of that state to be more complicated (or at least different) than what could be obtained by a simple dropping of a proton into a vacant or semi-vacant ^{142}Nd orbit. The 1514.98-keV state was not seen at all.

In Eppley's study of ^{145}Gd decay (Ep71) two states at 1757.8 and 1880.6 keV absorbed 72% of the β feeding to excited states. Both transitions proceeded with logft's of 5.6. The $11/2^-$ ^{145m}Gd also exhibited a significant β branch to the $11/2^-$ $h_{11/2}$ state in ^{145}Eu with a logft of 6.2 indicative of proton occupation of the $h_{11/2}$ state. The similarities between these states and those in ^{143}Pm are too great to be ignored. In ^{145}Eu it was shown that these states could be constructed as three quasiparticle states of the form $(\pi h_{11/2})^{2n-1}$ $(\nu h_{9/2})(\nu s_{1/2})^{-1}$ where the β transition could go formally as $(\pi h_{11/2}) \rightarrow (\nu h_{9/2})$.

Such a description leaves one major defect for ^{143}Pm, In our case the ground state of ^{143}Sm is $3/2^+$, but in ^{145}Gd the $1/2^+$ state drops below the $3/2^+$ in energy. Thus, if our situation is to be analogous,

the three-quasiparticle state must be constructed slightly differently as $(\pi h_{11/2})^{2n-1}(\nu h_{9/2})(\nu d_{3/2})^{-1}$. As the $s_{1/2}$ and $d_{3/2}$ states lie at nearly the same energy, the systematics of this system must be much like that in ^{145}Eu. A highly stylized description of the important transitions in the ^{143}Sm - ^{143}Pm system is offered in Figure 5-5.

Perhaps the most striking feature of these two states is how low in excitation they lie. Indeed the 1056.58-keV state lies below the $s_{1/2}$ and $d_{3/2}$ single particle states. This fact can in part be explained by the fact that a considerable part of the single particle strength is in these states. Additionally, these states are lowered by the energy gained in coupling the odd particles. To construct such states of low total angular momentum, the two odd particles, $(\nu h_{9/2})$ and $(\pi h_{11/2})$, must couple to minimum orbital angular momentum and therefore maximum total spin. This is suggestive of odd-odd (2-quasiparticle) coupling rules for the lowest configuration (Br60). Another feature of these two states is that their splitting is considerably larger than in ^{145}Eu. Perhaps this results from the fact that we are no longer coupling a third particle of zero orbital angular momentum where the two states might differ only in a spin flip of this third particle. In ^{143}Pm the $(\nu d_{3/2})$ particle carries two units of orbital angular momentum making it likely that the two states are very different in energy.

Clearly this description of the 1056.58- and 1514.98-keV states is speculative. In order to pin down this hypothesis more clearly it will be useful to look for other three-quasiparticle levels in ^{145}Eu and ^{143}Pm. Work is currently under way to find the higher spin states, particularly the $21/2^+$ in ^{145}Eu and the $23/2^+$ in ^{143}Pm, which should be present (Fi74e). It is our experience that such states may be

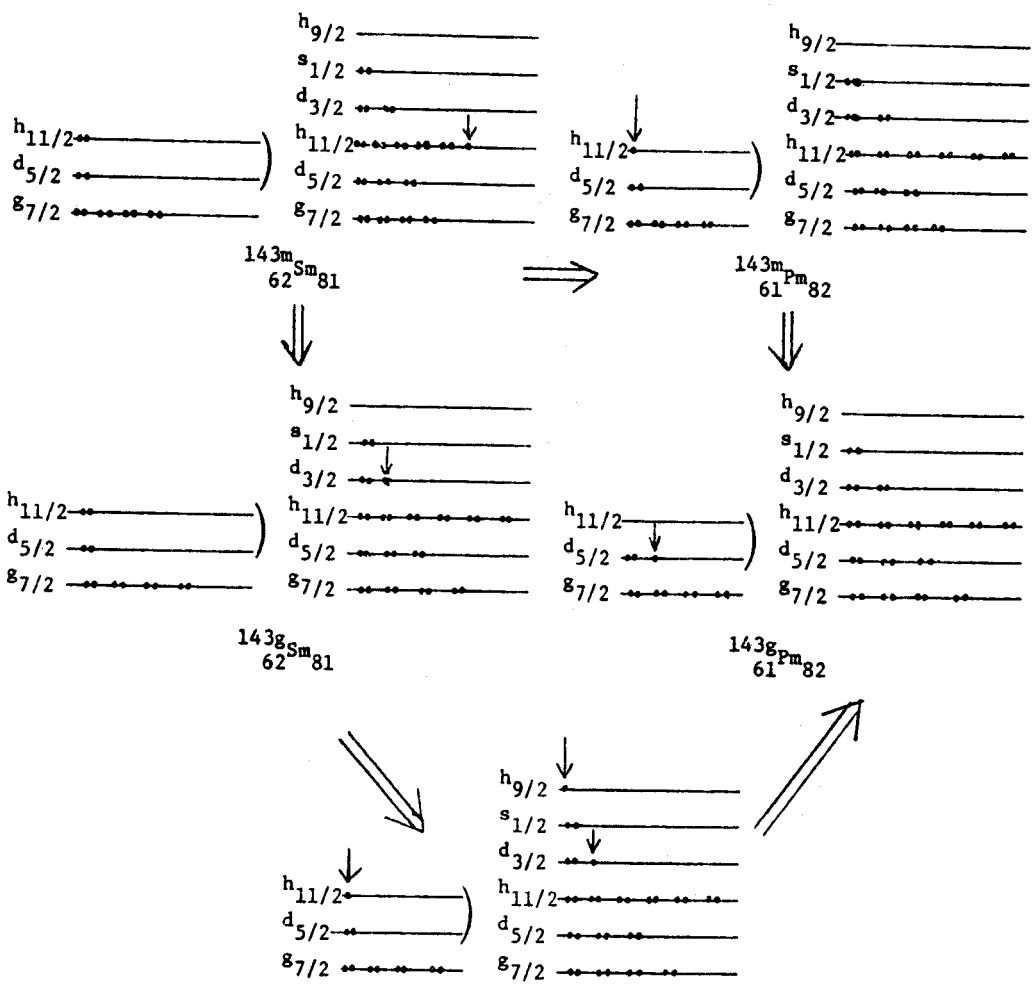

Figure 5-5. Stylized model of ^{143}Sm decay to single particle and 3-quasiparticle states in ^{143}Pm.

lying lower than most other 3-particle configurations and be recognizable by their relatively long half-lives.

5.5.3 Remaining States

Relatively little can be said about the remaining states at this time. Their decay properties indicate them all to be 3/2 or $5/2^+$ but their origins may be from multiparticle configurations or core excitations.

5.5.4 ε/β^+ Ratios

From our $\gamma^{\pm}$ gated spectrum (Figure 4-4) we obtained the relative β^+ feedings to five of the ^{143}Pm states. The deduced ε/β^+ ratios for the transitions to these states are listed in Table 5-4, where they are compared to the theoretical ratios calculated in Nuclear Data Table (Go71). We normalized the experimental values to theoretical values with the transition to the 1056.58-keV state, which we considered to be one of the most straightforward transitions in the entire decay scheme. It appears that at least one of the hindered transitions has strongly hindered β^+ branches leading to poor agreement with theory. This corroborates similar results for ^{145}Gd decay. It is clear that the theoretical considerations in ε/β^+ ratios need serious overhauling and work in that direction is currently in progress (Fi74b,Fi74c).

Table 5-4

Theoretical and Experimental $\varepsilon(tot)/\beta^+$ Branching Ratios for the Decay of ^{143}Sm

Energy (keV)	$\varepsilon(tot)/\beta^+$ Theoretical*	$\varepsilon(tot)/\beta^+$ Experimental
1056.58	9.7	≡9.7± 0.7
1173.18	13	63 ±10.
1403.06	29	35 ±5.
1514.98	49	30 ±7.

*Values from Nuclear Data Tables 10, p. 206 (1971).

Chapter VI

THE DECAY OF ^{140m}Pm

6.1 Introduction

Although no research was directed specifically at ^{140m}Pm, it was a common contaminant in several reactions so that data were inadvertently collected for it. Arlt *et al.* (Ar67) reported the decay of ^{140m}Pm with a 5.8-min half-life predominently feeding a 0.6-msec state. γ-ray transitions of 418.8, 771.2, 1025.9 and 1197.9-keV were also reported with the 418.8-keV transition being delayed. Bleyl *et al.* (Bl68) report the decay of ^{140g}Pm with a half-life of 9.2 sec, which is too short to be seen in these experiments.

6.2 Production of ^{140m}Pm

In this work ^{140m}Pm was produced in reactions such as ^{142}Nd(τ,$p4n$), ^{142}Nd(α,$p5n$), and ^{144}Sm(p,αn) at varying energies of the incident particles. Such reactions may be quite complex involving cluster stripping and indicate how weakly α and other charged particles are bound for these targets.

6.3 Decay of ^{140m}Pm

A rough measurement of the half-life of ^{140m}Pm gives a value of 5.9±0.6 min, which is in good agreement with the published value (5.8 min). These half-life data are shown in Table 6-1.

A singles Ge(Li) spectrum is shown in Figure 6-1. This spectrum was obtained in a ^{142}Nd(τ,$p4n$)^{140m}Pm reaction with 17-MeV incident τ.

Table 6-1

Half-life Data for the Decay of ^{140m}Pm

Energy (keV)	I_1(0-1 min)	I_2(1-4 min)	I_3(4-9 min)	I_4(9-19 min)
419.57	1.00[a]	2.25	2.46	2.10
773.74	1.00[a]	2.27	2.64	2.27
1028.19	1.00[a]	2.38	2.56	2.26

[a]Normalized to I=1 for the first interval.

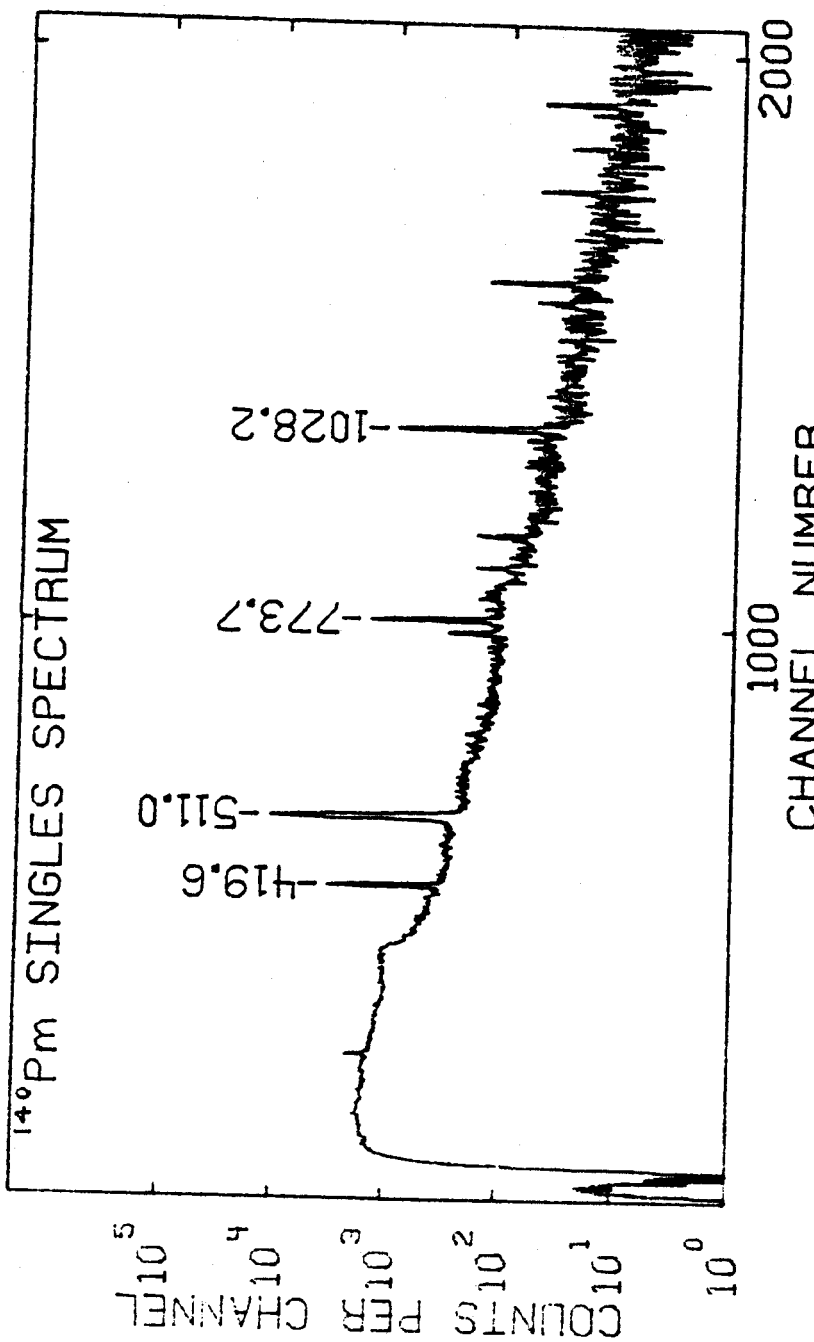

Figure 6-1. ^{140m}Pm singles spectrum taken with the 10.4% Ge(Li) detector.

The intended reaction was $^{142}Nd(\tau,2n)^{143}Sm$ but no ^{143}Sm production is seen indicating the cleanness of this reaction. A list of the γ rays and their relative intensities assigned to ^{140m}Pm is given in Table 6-2.

Coincidence data for ^{140m}Pm decay were also collected and the relevant spectra are shown in Figure 6-2. These data were produced in the $^{144}Sm(p,\alpha n)^{140m}Pm$ reaction where the primary products were ^{143}Eu and ^{143}Sm, discussed elsewhere in this thesis. Additionally, β^+ feeding data were also collected and the relative β^+ fed intensities are included in Table 6-2.

6.4 Conclusions and Results

The fact that gating on each of the transitions gives the other two transitions indicates that they do, indeed, form a cascade. Additionally, since we know that the 419.57-keV γ ray is delayed, we have confirmed that this transition lies uppermost in the cascade. It is too long-lived otherwise to be seen in coincidence experiments. These data say nothing about the order of the lower two levels in the cascade, but Arlt reports that the ground state ^{140g}Pm feeds a level at 771.2 keV so we can use this fact in sorting out a level scheme.

An interesting anomaly exists in these data. The β^+ feedings experiments have shown feeding through the 773.7- and 1028.2-keV rays but not the 419.6-keV γ ray. Since the 419.6-keV transition is long-lived (0.6 ms) there must be other feeding than just to the 2221.5-keV state. Otherwise, no significant feeding will be seen in the coincidence experiment to the lower lying levels. The ^{140m}Pm parent is reported to be an 8^- state so the lower states in ^{140}Nd should not be fed directly.

Table 6-2

Relative Singles and Coincidence Intensities for the β^+/ε Decay of ^{140m}Pm

Energy (keV)	$I_{singles}$	$I_{\beta^+ feeding}$
419.57±0.05	90±5	0.
773.74±0.06	99±5	83±17
1028.19±0.07	≡100	≡100±20
1197.9 ±0.2	6±1	-----

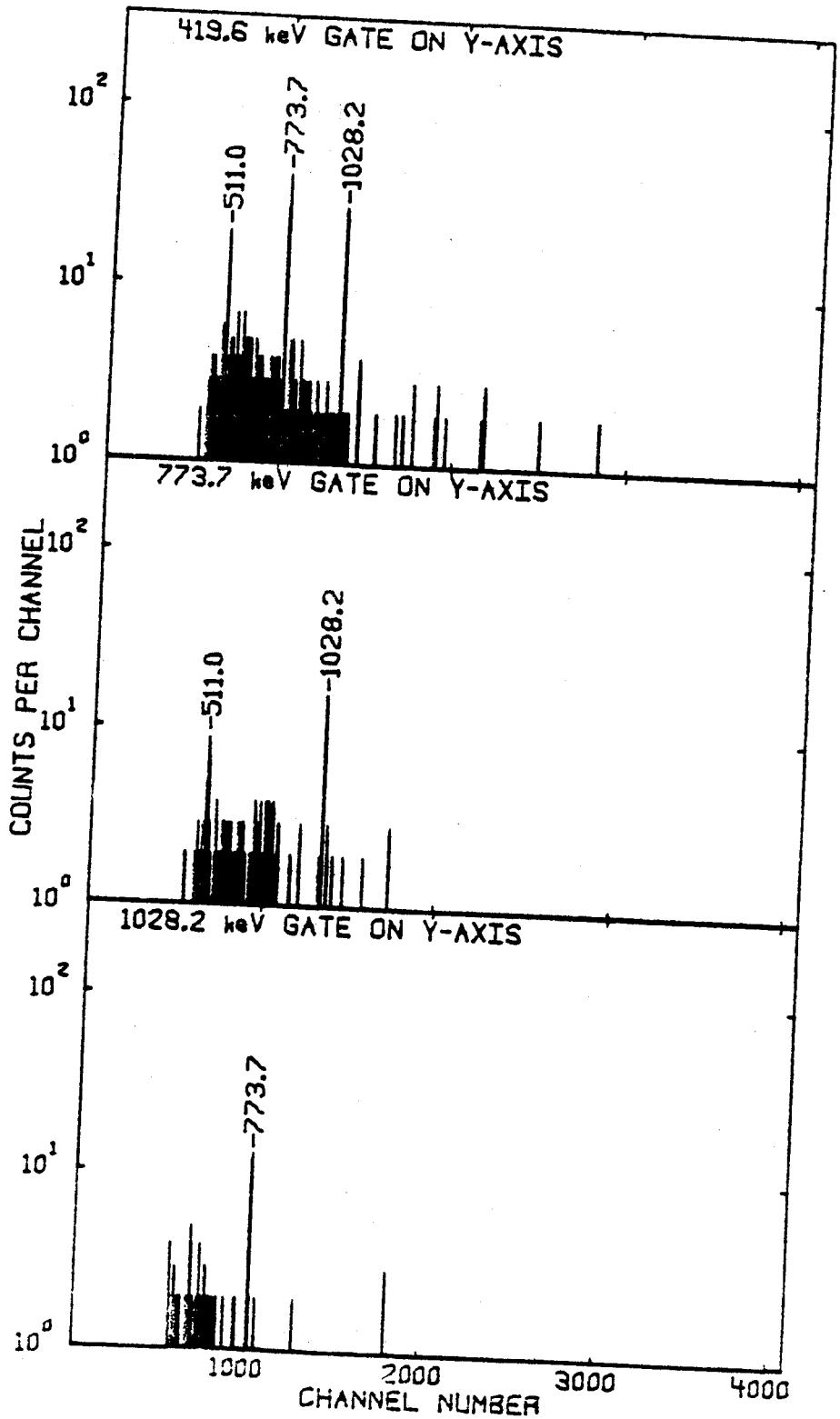

Figure 6-2. ^{140m}Pm γ-γ coincidence spectra.

Figure 6-2 (Cont'd.)

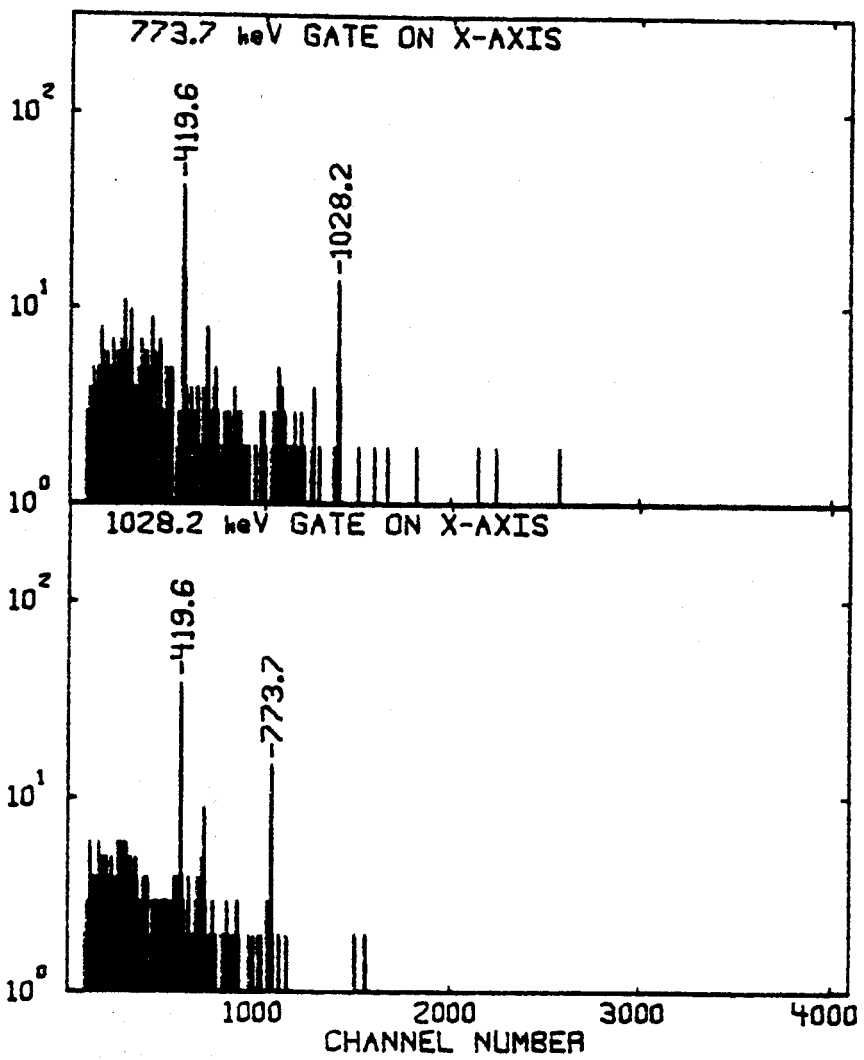

The highest spin state that could cascade to the 4^+ state at 1801.9 keV would be a 6^+ state but such a state could also not be fed directly. With Q_ε = 5.9±0.4 MeV (Ar67) it is possible for levels well up in the nucleus to be fed. Some of these might deexcite to the 4^+ state bypassing the 7^- state. Indeed the intensity of the 419.6-keV γ ray only accounts for 90% of the lower level feeding. Conversion can account for only about 4% more of this missing intensity. One other γ ray transition, which is not seen in coincidence experiments, of 1197.9 keV may account for the rest of the missing intensity and is placed tentatively in the decay scheme. It is likely that other, unseen, transitions must also exist. A tentative decay scheme for ^{140m}Pm decay is given in Figure 6-3.

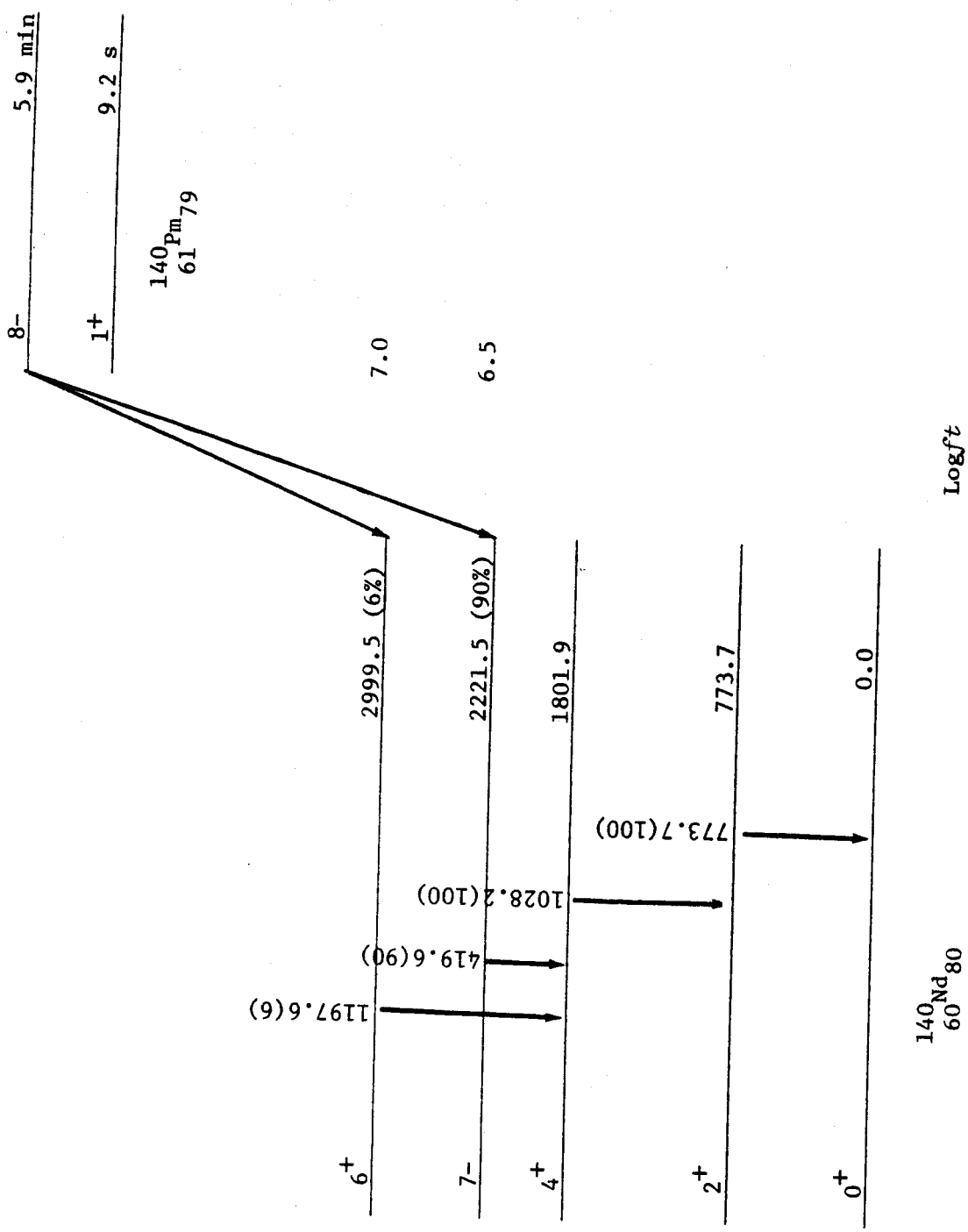

Figure 6-3. ^{140m}Pm decay scheme. All energies are given in keV and transition intensities are given in terms of percent per disintegration of the parent. Logft values are calculated from tables by Gove and Martin (Go71).

Chapter VII

MEASUREMENT OF β^+ ENDPOINT OF ^{63}Ga

The decay of 32.4-sec ^{63}Ga has been studied in great detail by Giesler *et al.* in this laboratory (Gi74). An important missing piece of data at this point is the β^+ endpoint energy for decay to the ground state of ^{63}Zn. From the systematics of this region, the β^+ endpoint has been predicted to be 4.6 MeV.

In order to measure this endpoint, a pilot-B plastic scintillator was constructed 4.5 cm in diameter and 9 cm deep. This scintillator was mounted on an EMI 9530B photomultiplier tube. The tube was operated at 1000 V and the resolution for 662-keV conversion electrons was 20% (FWHM). This was acceptable because the detector was designed primarily for high energy particles and even then only to measure endpoints. All sources were measured both with and without absorbers in front of the detector such that correction could be made for the contribution of γ-ray Compton electrons to the spectra.

Sources of ^{63}Ga were produced using 30-MeV protons from the Michigan State University Sector Focused Cyclotron on a natural Zn target. Because of the short half-life (32.4 sec) of ^{63}Ga, recoils from the target were collected by a He-thermalizer jet transport system and deposited in front of the detector on a moving tape transport so as not to allow a build up of longer lived activities. The energy calibration of the system was performed using ^{64}Ga and ^{144}Pr standards.

A modified Fermi-Kurie plot[2] for ^{63}Ga decay is shown in Figure 7-1. Cramer *et al.* (Cr62) indicate that a plot of the form

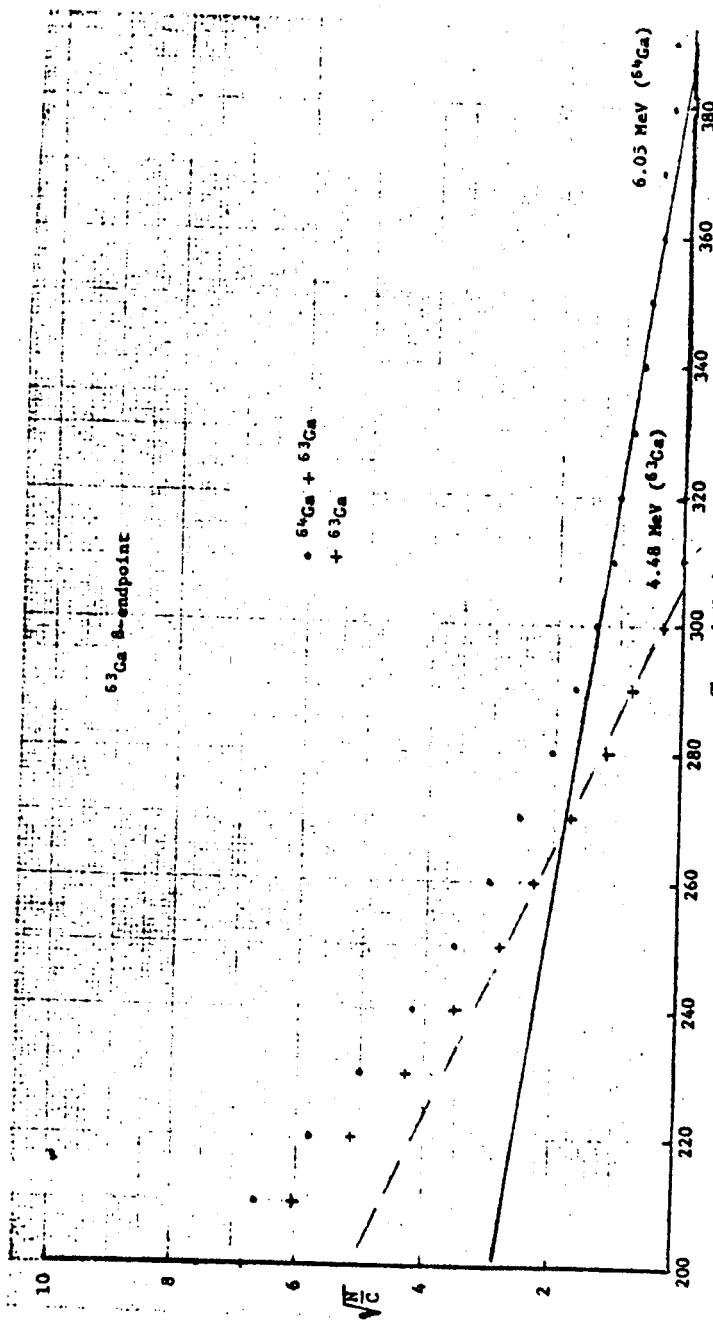

Figure 7-1. Adjusted Kurie plot of betas from ^{63}Ga and ^{64}Ga decay measured with a large Pilot-B plastic scintillator detector. Non-linearity at lower energies is due to the lower energy beta branches which were not resolvable in this plot.

$$\left(\frac{N(C)}{C^{const}}\right)^{1/2} \quad \text{vs } E$$

N(C) = number of counts in channel C

C = channel number

will give a fairly good endpoint. Since E≈C, we made the substitution, and the best value of the constant was 1. An endpoint of 4.5±0.1 MeV was measured after stripping out the higher energy ^{64}Ga endpoint. This is in good agreement with the predicted endpoint, however, transitions to other states in ^{63}Zn were not resolvable.

CHAPTER VIII

ε/β^+ BRANCHING RATIOS

8-1 Introduction to Beta Decay Theory

β-decay is a process by which energetically unstable nuclei may decay to more stable nuclei. Most generally, β decay appears as simply the transformation of a proton to a neutron or vice versa accompanied by creation or annihilation of an electron such as to conserve charge. Although the nucleons should be considered as bound particles, the three forms of β decay most commonly seen can be abbreviated as

$$\begin{aligned} &\beta^- \text{ decay} \quad n \rightarrow e^- + \bar{\nu} + p^+ && \text{a)} \\ &\beta^+ \text{ decay} \quad p^+ \rightarrow e^+ + \nu + n && \text{b)} \\ &e^- \text{ capture} \quad p^+ + e^- \rightarrow \nu + n && \text{c)} \end{aligned} \qquad (8\text{-}1)$$

where the neutrino ν and the antineutrino $\bar{\nu}$ are leptons originally postulated to conserve energy.

Studies of numerous examples of β decays have shown that the electrons are always emitted in a continuous spectrum of energy and momentum. Because the transition involves a known constant decay energy, W_o, it was apparent that the energy and momentum were not being conserved. Even considering the recoil energy, it was evident that momentum would not be conserved. In order to remedy this situation it was postulated by Pauli (Pa30) that a previously undetected particle called a neutrino was emitted, statistically sharing energy and momentum with the electron. This particle must be neutral and have half integral spin in order to fit in with what was known of β decay.

Strong indication that this approach was correct was found in its prediction of the β-energy spectrum. The basic assumption of statistical sharing of energy between the electron and neutrino is that the probability of a specific subgroup of states to emerge is proportional simply to the number of such states. Thus, if $d\lambda/\lambda$ is the fraction of decays involving momentum ranges $(d\vec{p}) = dp_x dp_y dp_z$ for the electron and $(d\vec{q})$ for the neutrino,

$$\frac{d\lambda}{\lambda} = \frac{(d\vec{p})(d\vec{q})}{\int\cdots\int (d\vec{p})(d\vec{q})} \tag{8-2}$$

where the denominator encompasses the total momentum space. This can easily be simplified by substitution to (Ko66)

$$\frac{d\lambda}{dW} = \left(\frac{\lambda}{f_o}\right) W(W_o - W)\,[W^2 - m^2c^4]^{1/2} \div [(W_o - W)^2 - \mu^2c^4]^{1/2}/(mc^2)^5 \tag{8-3}$$

where

$$f_o(p_o) = \int_o^{p_o} dpp^2 qK/(mc)^2 c \tag{8-4}$$

and

$W = c(p^2+m^2c^2)^{1/2}$ is the electron energy

$K = c(q^2+\mu^2c^2)^{1/2}$ is the neutrino energy

$W_o = W + K.$

The recoil energy has been neglected above.

An additional correction must be included for the Coulomb interaction between the electrons and the nucleus. This correction can be generalized as

$$F(Z,W) = \left|\frac{\psi_c}{\psi_o}\right|^2 \approx d\lambda \tag{8-5}$$

where $|\psi_o|^2$ is the free particle spacial density and $|\psi_c|^2$ is the spacial density of the electron at the nucleus.

By simple manipulation one can write

$$\frac{d\lambda}{\lambda dW} = cpW(W_o-W)^2F(Z,W)/f(Z,W_o)(mc^2)^5 \tag{8-6}$$

where

$$f(Z,W_o) = \int_{mc^2}^{W^o} dW \cdot cpW(W_o-W)^2F(Z,W)/(mc^2)^5 \tag{8-7}$$

This equation can be used to accurately predict the shape of many β spectra.

For convenience in discussion total decay rates (8-6) can be written

$$d\lambda = C\cdot F(Z,W)pWq^2dW/(mc)^5c^2 \tag{8-8}$$

where integration gives

$$\lambda \equiv \frac{\ell n2}{t} = Cf(Z,W_o) \tag{8-9}$$

or

$$ft = \ell n2/C \qquad (8\text{-}10)$$

Thus, reduced decay rates (ft) can be calculated for all β decays from analogy to well understood electromagnetic theory and this simple calculation indicates that the ft's should be identical. In reality, the reduced rates range widely from $10^3 \rightarrow \approx 10^{18}$ sec. These large deviations can be explained by such things as:

1) Angular momentum change - the half-spin leptons can carry off a total of only one unit of angular momentum unless they are ejected off-center from the nucleus. Such occurrences have a lower probability and, indeed, decays involving large angular momentum changes invariably proceed with larger ft values.

2) Parity mismatches - transitions between states of differing parity are seen to be greatly hindered.

3) Nuclear states - decays between very similar initial and final nuclear states are generally quite fast. Mirror and some $0^+ \rightarrow 0^+$ decays are particularly fast whereas other modes may be much slower.

For the continuation of this text I will discuss only "allowed" decays; that is, decays involving angular momentum transfer of 0 or 1 unit with no parity change. The discussion of "forbidden" decays is beyond the interest of this discussion although a thorough discussion is given by Konopinski (Ko66).

The emission of the leptons in allowed β decay may be such that their spins are antiparallel (singlet) or parallel (triplet). These general modes of decay are frequently called Fermi (F) and Gamow-Teller (GT)

decay, respectively. Their interaction strengths will be proportional to C_F^2 and C_{GT}^2. Clearly decays involving a change of one unit of nuclear angular momentum result from triplet decay, but decays involving no angular momentum change can be either singlet or triplet (an exception is $0^+ \rightarrow 0^+$ which can only be singlet emission). Thus, in neutron decay ($1/2^+ \rightarrow 1/2^+$) the reduced transition rate might be proportional to

$$(ft)_n^{-1} \approx C_F^2 + 3C_{GT}^2 \qquad (8\text{-}11)$$

where each of the three possible triplet spin projections to the nuclear axis are given equal weight to the singlet projection. Similarly, for ^{14}O ($0^+ \rightarrow 0^+$) where either of the two protons outside the core might β decay

$$(ft)_0^{-1} \approx 2C_F^2 \qquad (8\text{-}12)$$

The measured ft values for n and ^{14}O decay are 1180±35 sec (So59) and 3060±10 sec (He61) respectively. Thus,

$$\frac{C_{GT}^2}{C_F^2} = \frac{1}{3}\left[2\,\frac{(ft)_o}{(ft)_n} - 1\right] = 1.40 \pm 0.05 \qquad (8\text{-}13)$$

gives an estimate of these relative strengths. It should be noted that it was assumed that the core nucleons in ^{14}O did not contribute significantly to the decay rate. Here an assumption has been made that C_{GT}^2 and C_F^2 are basic constants irrespective of the decaying nucleus. If this approach sufficiently describes the β-decay force, a constant interaction strength is to be expected.

8.1.1 The Neutrino

Although this particle is almost impossible to detect, the neutrino's existence has been verified by Reines and Cowan (Re59) through anti-neutrino capture in protons. Coincident positrons and neutron reaction γ-rays were observed proving the neutrino's existence. It is also shown that more than one kind of neutrino exists as the above reaction is not observed from neutrinos created during positron decay (Da55). Further information is obtained about the neutrino from carefully measured statistical electron spectra. The higher energy data are very dependent on the neutrino rest mass μ. All experiments to date have indicated that the neutrino is probably massless, with an upper limit of 250 eV predicted by the ^{3}H spectrum (La52). Actually recent speculation on solar neutrino fluxes suggest that the neutrino might have a very small rest mass (Bah72), but this would not seriously affect any of the discussion here. Finally, in an ingenious experiment by Goldhaber et al. (Go58) it was indicated that the neutrinos emitted in ^{152}Eu electron capture had 100% negative helicity; that is they were all left-handed. This means that the neutrino's spin is lined up antiparallel to its direction of motion.

8.1.2 - The Electron

Because the neutrino appears to be fully left-handed, it is of interest to investigate the polarizations inherent to the electron. Most generally, the polarization of the emitted electron is defined as

$$P = \langle \vec{S}_e \cdot \vec{V} \rangle = \frac{d\lambda_{\uparrow\downarrow} - d\lambda_{\uparrow\uparrow}}{d\lambda_{\uparrow\downarrow} + d\lambda_{\uparrow\uparrow}} \qquad (8\text{-}14)$$

where the average projection of electron spin in the direction of motion

is proportional to the difference in decay rates producing parallel and antiparallel spins and motions. Clearly a positive polarization indicates dominance of right-handed particles while negative polarization leads to left-handed electrons. Measurements of electron polarizations for both positron and negatron decay have shown that (Wu57).

$$P = \pm v/c \text{ for } e^{\pm} \tag{8-15}$$

This indicates that the positron is the mirror image of the electron and indeed suggests that a good explanation of all antiparticles may be as mirror particles to the normal particles. Thus, it suggests that the antineutrino is fully a right handed particle. The electron does not appear to be fully polarized, however, so it is necessary at this point for a short diversion to explain this partial polarization.

The instantaneous measurement of the electron velocity can give only the two values $\pm c$. This is because the instantaneous velocity $u = \Delta X/\Delta t$, but in the limit $\Delta t \to 0$ the uncertainty principle tells us that the energy $\Delta E \geq \hbar/\Delta t \to \infty$. Infinite energy corresponds to $u = \pm c$. If the electron has a precise momentum $\vec{p} = (W/c^2)\,\vec{v}$, then $\vec{v}$ must be defined as the average of point motions alternating between states $u = \pm c$. If a is the probability amplitude for forward motion (+c)

$$|a|^2 (+c) + (1 - |a|^2)(-c) = v$$

$$|a|^2 = 1/2(1+v/c) \tag{8-16}$$

and

$$(1 - |a|^2 = 1/2(1 - v/c)$$

Therefore, if the negatron is fully left-handed, its spin must flip as it alternates between opposite velocity states. Thus,

$$P = (-1)\ 1/2\ (1+\frac{v}{c}) + (+1)\ 1/2(1-\frac{v}{c}) = -\frac{v}{c} \qquad (8\text{-}17)$$

indicating that beta-negatrons are indeed fully left-handed. Similarly, $P = +v/c$ is predicted for positrons.

8.1.3 - Angular Distribution of β Particles About Polarized Nuclei

The polarization of the negatron in the direction of nuclear orientation is written as

$$P = \frac{d\lambda\uparrow - d\lambda\downarrow}{d\lambda\uparrow + d\lambda\downarrow} = -\hat{I} \cdot \frac{\vec{v}}{c} = -(\frac{v}{c})\cos\theta \qquad (8\text{-}18)$$

for e^- where $d\lambda\uparrow,\downarrow$ represents decay rates for spin up and spin down respectively relative to the nuclear spin I. θ is simply the angle to initial nuclear spin of the emitted electron. Clearly the two decay rates $d\lambda\uparrow$ and $d\lambda\downarrow$ can be written

$$d\lambda\uparrow,\downarrow \approx 1\mp (\frac{v}{c})\cos\theta \qquad (8\text{-}19)$$

as seen by substitution into (8-18). For spin up, the projection of total lepton spin $S_Z = \vec{S}\cdot\hat{I}_i = M_S = +1$ and for spin down $M_S = -1$ so one can write

$$d\lambda(M_S) = 1 - M_S\ (\frac{v}{c})\ \cos\theta \qquad (8\text{-}20)$$

For transitions involving $M_S = 0$ there are equal numbers of spin up and

spin down decays washing out any anisotropy as predicted in (8-20). For singlet transitions $S = M_S = 0$ and only isotropic electron distributions are observed. In the case of triplet radiation $S = 1$ so $M_S = 0, \pm 1$, and in addition more than one orientation may arise in each form of angular momentum transfer as indicated in Figure 8-1. Generalizing (8-20) to $e^{\mp}$-decay for all transitions.

$$d\lambda(\theta) = 1 \mp \langle M_S \rangle \left(\frac{v}{c}\right) \cos\theta \tag{8-21}$$

For triplet transitions it can be shown that (Ko66)

	a)	b)	c)
	$I_f = I_i - 1$	I_i	$I_i + 1$
	$\langle M_S \rangle = 1$	$1/(I_i+1)$	$-I_i/(I_i+1)$

(8-22)

8.1.4 - Electron-Neutrino Angular Correlations

In this casethe projection of electron polarization in the neutrino direction $\vec{q}\cdot\vec{v}/c$ is the quantity of interest. Analogously to section 8.1.3 for positron decay

$$d\lambda\uparrow,\downarrow \approx 1 \pm \left(\frac{v}{c}\right) \cos\theta_{e\nu} \tag{8-23}$$

where $\theta_{e\nu}$ is the angle between the positron and neutrino emission directions. This will lead to

$$d\ (\theta_{e\nu}) \approx 1 + \langle 2S_{eZ} \rangle \left(\frac{v}{c}\right) \cos\theta_{e\nu} \tag{8-24}$$

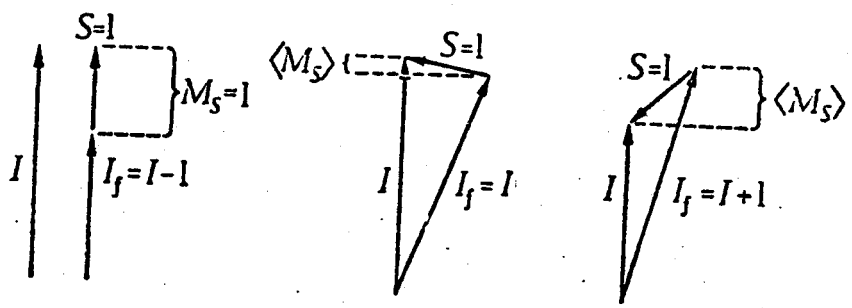

Figure 8-1. Possible orientations of lepton spin S to the nuclear spin I.

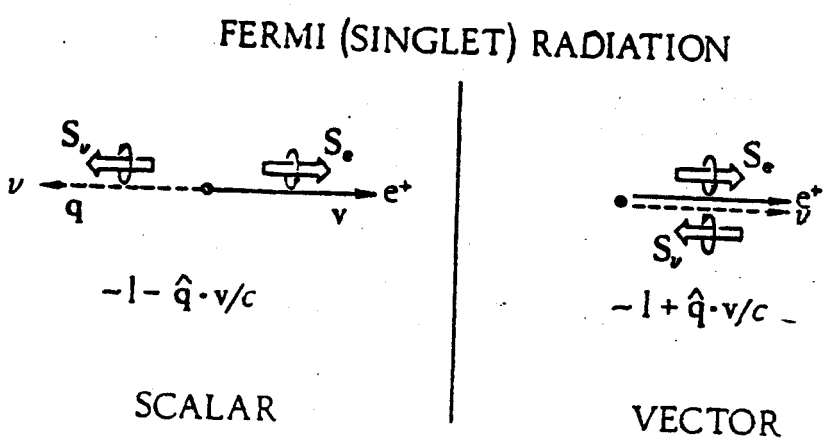

Figure 8-2. Electron-neutrino spin orientations.

where $\langle S_{eZ} \rangle$ is the average projection of electron spin on the neutrino momentum. Singlet radiation can be inferred to proceed in two general forms diagrammed in Figure 8-2. The "scalar" arrangement involves only right-handed particles while the "vector" involves left-handed particles. If C_S and C_V give the scalar and vector coupling strengths, then for Fermi transitions

$$d\lambda_F(\theta_{e\nu}) \approx 1 + a_F(\frac{v}{c})\cos\theta_{e\nu} \qquad (8\text{-}25)$$

where

$$a_F = \frac{C_V^2 - C_S^2}{C_V^2 + C_S^2}$$

allowing for the possible mixture of both terms. Measurements on ^{35}A mirror decay (He57, A159) which proceeds largely by Fermi emission gives $a_F = +0.97 \pm 0.14$ or $C_S^2/C_V^2 < 0.09$, indicating that the vector contribution is predominant.

For triplet radiation a similar picture of the emitted leptons is obtained by reversing the neutrino spin directions in Figure 8-2. Here the three orientations of the triplet radiation tend to wash out the correlation and one gets a "tensor" contribution

$$d\lambda_T(\theta_{e\nu}) \approx 1 + 1/3\ (\frac{v}{c})\cos\theta_{e\nu} \qquad (8\text{-}26)$$

yielding right-handed neutrinos and a "axial vector" contribution,

$$d\lambda_A(\theta_{e\nu}) \approx 1 - 1/3\ (\frac{v}{c})\cos\theta_{e\nu} \qquad (8\text{-}27)$$

yielding left-handed neutrinos. Analogous to the Fermi transitions, for Gamow-Teller transitions we write

$$d\lambda_{GT}(\theta_{e\nu}) \approx 1 + a_{GT}(\frac{v}{c})\cos\theta_{e\nu} \qquad (8\text{-}28)$$

where

$$a_{GT} = \frac{1}{3}(C_T^2 - C_A^2)/(C_T^2 + C_A^2)$$

Measurement of a_{GT} for ^{6}He (Jo63) and ^{23}Ne (Al59) yield

$$a(^6\text{He}) = -0.334\pm0.003$$
$$a(^{23}\text{Ne}) = -0.37\pm0.04 \qquad (8\text{-}29)$$

suggesting that $C_T^2/C_A^2 < 0.004$. This again strongly indicates participation of left-handed neutrinos with right-handed positrons. When a mixture of singlet and triplet radiation is seen, the correlation coefficient $a = xa_F + (1 - x)a_{GT}$. Plotting known values of x versus a in Figure 8-3, where lines corresponding to pure S or V and pure T or A are drawn, suggest dominance of A-V interactions or participation of left-handed particles and right-handed antiparticles. The mathematical reasoning for the names S, V, T, and A will be indicated in later sections. Thus, apparently,

$$a = \frac{1}{3}(4x - 1) \qquad (8\text{-}30)$$

where $a_F = 1$ and $a_{GT} = -1/3$.

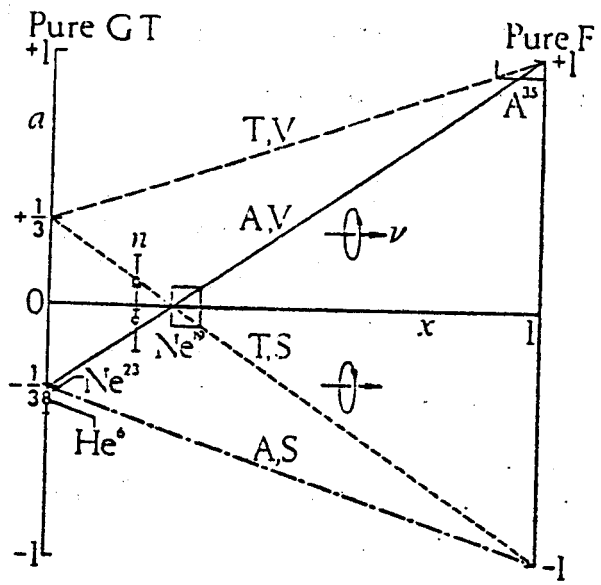

Figure 8-3. Mixing of correlation coefficient.

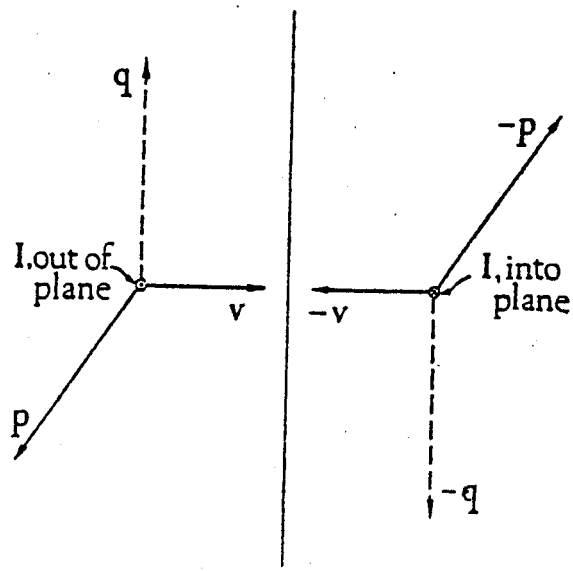

Figure 8-4. Time Reversal.

8.1.5 - Neutron Decay

The simplest form of β decay should be the neutron decay ($1/2^+ \rightarrow 1/2^+$) in which only the single nucleon participates. If all possible correlations are to be considered between the nucleon and the two leptons,

$$d\lambda \approx 1 + a_n \hat{q}\cdot\frac{\vec{v}}{c} + \hat{I}\cdot\left[A_n \frac{\vec{v}}{c} + B_n\hat{q} + D_n\hat{q}\times\frac{\vec{v}}{c}\right] \qquad (8\text{-}31)$$

The last term concerns time invariance, and reversing all motions ($t \rightarrow -t$) as in Figure 8-4 should give equally valid results where a component $D_n(-\hat{I})\cdot[(-\hat{q})\times(-\frac{\vec{v}}{c})]$ would exist. If both cases are equally probable, the two parts will cancel. Measurements of the decay of polarized neutrons in a given arrangement as well as oppositely polarized neutrons in the same experimental arrangement will clearly offer a test of time invariance. Such an experiment (Bu58a) has shown that $D_n = 0.04\pm0.07$, suggesting that β decay is indeed time invariant. From here on it is assumed that $D_n = 0$.

Looking at unpolarized neutrino beams yields average coefficients $\bar{A}_n = \bar{B}_n = \bar{D}_n = 0$, since the associated anisotropies average to zero. This leaves only a_n for the neutron and the fraction of decay resulting from the vector interaction is clearly

$$x_n = \frac{C_V^2}{C_V^2 + 3C_A^2} \qquad (8\text{-}32)$$

so

$$a_n = \frac{1}{3}(4x_n - 1) = \frac{C_V^2 - C_A^2}{C_V^2 + 3C_A^2} \qquad (8\text{-}33)$$

As shown previously from ^{14}O data $C_A^2/C_V^2 = 1.40\pm0.05$, yielding

$$x_n = 0.192\pm0.007 \tag{8-34}$$

For pure axial vector decay it was previously shown (8-22) that for $I_i = I_f = 1/2$,

$$A'_A = -\langle M_S \rangle = \frac{-1}{I_i+1} = -\frac{2}{3} \tag{8-35}$$

so for neutron decay the triplet contribution to A is

$$A_A = -\frac{2}{3}(1-x_n) = \frac{-2C_A}{C_V^2 + 3C_A^2} = -0.539\pm0.005 \tag{8-36}$$

Since the antineutrino is right-handed, clearly $B_n = -A_n = \langle M_S \rangle = 2/3$, so

$$B_A = -A_A = 0.539 \tag{8-37}$$

From recoil proton-electron angular distributions it was found (Bu58b) that

$$A_n = -0.11\pm0.02, \quad B_n = +0.88\pm0.15 \tag{8-38}$$

Because vector radiation is isotropic, the only other contribution to A_n and B_n could be the interference term

$$A_{AV} = B_{AV} = 2|C_A C_V|/(C_V^2 + 3C_A^2) = 2[\tfrac{1}{3}(1-x_n)x_n]^{1/2} \tag{8-39}$$

such that

$$A_n = A_A \pm A_{AV} \text{ and } B_n = B_A \pm B_{AV} \tag{8-40}$$

where we can calculate from 8-39

$$A_{AV} = B_{AC} = \pm 0.46 \pm 0.02 \tag{8-41}$$

If one chooses the positive sign,

$$A_n = -0.54 + 0.46 = -0.08 \pm 0.02$$

$$B_n = +0.54 + 0.46 = 1.00 \pm 0.02 \tag{8-42}$$

agreement with experiment is well within the experimental errors.

The experimental implications of the preceding section are indicated in Figure 8-5.

There are four possible orientations, corresponding to $M_S = 0, \pm 1$. In polarized neutron decay the $M_S = -1$ orientation cannot be constructed. The $M_S = 1$ orientation does not specify the recoil proton direction because the electron and neutrino alone can conserve momentum. This orientation does, however, indicate the sign of $B_A \approx \hat{I} \cdot \vec{q}$ and $A_A \approx \hat{I} \cdot \vec{v}$. The two cases involving $M_S = 0$ differ only in the net polarization predicted for the recoil proton. Clearly, the first case in Figure 8-5 predicts the signs of $A_{AV} \approx \hat{I} \cdot \vec{v}$ and $B_{AV} \approx \hat{I} \cdot \vec{q}$ as being negative, while the last case indicates both signs are positive. The experimental results indicate that the last case is correct so we can thus predict that the recoil proton will have a net left-handed polarization. Of course, this polarization is too

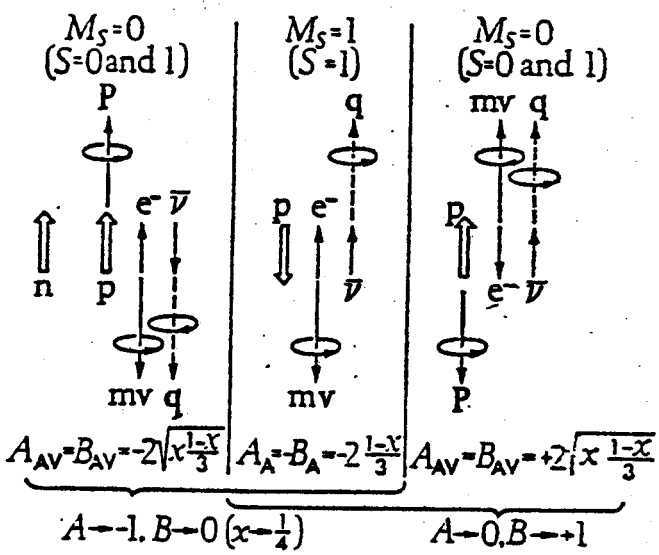

Figure 8-5. Screw sense of the proton recoil.

difficult to detect, since $P = v_p/c$ is quite small, but a general statement of the form of β decay may be made.

8.1.6 - General Theory of Beta-Decay

All of the data so far have indicated that in the β decay process all particles participate fully through their left-handed states and all antiparticles appear in their right-handed states. These decays proceed through two forms, a singlet or Fermi decay of strength proportional to C_V^2 and a triplet or Gamow-Teller decay proportional to C_A^2. Two other forms involving tensor forces proportional to C_T^2 and scalar forces proportional to C_S^2 are not measurably observed in any studies to date.

8.2 Mathematical Derivation of Allowed β-Decay Theory

8.2.1 Transition Probabilities

For the general decay type, $n + \nu = p + e^-$, the β-interaction energy density can be given by (Ko66)

$$h_\beta = 8^{1/2} g J(pn) J(e\nu) + c.c. \qquad (8\text{-}43)$$

where g, the "Fermi coupling constant" gives the strength of the interaction, and

$$J(pn) = \psi_p^\dagger \Gamma^X \tau_+ \psi_n \qquad (8\text{-}44a)$$

$$J(e\nu) = \psi_e^\dagger \Gamma^X \psi_\nu \qquad (8\text{-}44b)$$

represent the transition currents for the transformations $n \rightarrow p$ and

$\nu \rightarrow e^-$. ψ_p, ψ_n, ψ_e and ψ_ν represent the wave functions for the corresponding particles and Γ^X represents the form of the β interaction. τ_+ is the isospin operator converting a neutron into a proton. It is apparent that the β interaction operator, H_β, in the Hamiltonian of the nucleon can be inferred from $\langle\psi_f^+|H_\beta|\psi_i\rangle = h_\beta$ to be

$$H_\beta = 8^{1/2} g \Gamma^X \tau_+ J(e\nu) + h.c. \tag{8-45}$$

This may be expanded to an entire nucleus of A nucleons to get

$$H_\beta(A) = 8^{1/2} g \sum_{a=1}^{A} \Gamma^{X^a} \tau_+^a [J(e\nu)]_{\vec{r}}^a + h.c. \tag{8-46}$$

where the electron-neutrino current is now evaluated at the position of the transforming nucleon $\vec{r}^a$.

Expressing the variables of the nuclear system in the complete set of eigenstates $|k\rangle\exp(-iE_k t/\hbar)$ where $\langle\ell|k\rangle = \delta_{\ell k}$; if H_A is the energy Hamiltonian for a nucleus, $H_A|k\rangle = E_k|k\rangle$, then H_β can be treated as a perturbation to the isolated nuclear system. Then any state in the perturbed system may be represented by

$$|(t)\rangle = \sum_k |k\rangle a_k(t) e^{-iE_k t/\hbar} \tag{8-47}$$

where $|(t)\rangle$ is not of the set $|k\rangle$ but a time dependent state. $|a_k(t)|^2$ is the probability of finding the nucleus in state $|k\rangle$ at time t. The time dependent equation of motion

$$(i\hbar \frac{\partial}{\partial t})|(t)\rangle = (H_A + H_\beta)|(t)\rangle \tag{8-48}$$

must apply, so upon substitution of (8-47) into the above and projection on some state, $\langle f|\exp(iE_f t/\hbar)$ we get

$$i\hbar\dot{a}_f(t) = \sum_k \langle f|H_\beta|k\rangle a_k(t) e^{i(E_f-E_k)t/\hbar} \tag{8-49}$$

These transition equations can be used to find the growth in time of various nuclear states from a specific initial state. Obviously, $a_k(t = -\infty) = \delta_{ki}$, and before any new states grow in appreciably,

$$i\hbar\dot{a}_f(t) = \langle f|H_\beta|i\rangle e^{-iW_o t/\hbar} \tag{8-50}$$

where $W_o = E_i - E_f$. This takes into account only first order processes, i.e. *direct* i → f transitions. Second order transitions like i → k → f, represented by $\langle f|H_\beta|k\rangle\langle k|H_\beta|i\rangle$, would not be expected to be significant as they are proportional to first-order effects by the factor g (β coupling strength) which is small.

To analyze transition rates further, knowledge of the time dependence of β coupling is required. Through straightforward Fourier analysis,

$$\langle f|H_\beta|i\rangle = \int_{-\infty}^{\infty} dw \langle f|H_\beta|i\rangle_\omega e^{i\omega t} \tag{8-51}$$

where

$$\langle f|H_\beta|i\rangle_\omega = \int_{\infty}^{\infty} \left(\frac{dt}{2\pi}\right) \langle f|H_\beta|i\rangle e^{-i\omega t} \tag{8-52}$$

Time integration of (8-50) gives

$$i\hbar a_f(\infty) = \int_{-\infty}^{\infty} dt \int_{-\infty}^{\infty} d\omega \langle f|H_\beta|i\rangle_\omega e^{-i(\omega - W_o/\hbar)t} \tag{8-53a}$$

$$= 2\pi \int_{-\infty}^{\infty} d\omega \langle f|H_\beta|i\rangle_\omega \delta(\omega - W_o/\hbar) \tag{8-53b}$$

$$= 2\pi \langle f|H_\beta|i\rangle_{W_o/\hbar} \tag{8-53c}$$

This is consistent with (8-52) and

$$|a_f(\infty)|^2 = \hbar^{-2} \left| \int_{-\infty}^{\infty} dt \langle f|H_\beta|i\rangle e^{iW_o t/\hbar} \right|^2 \tag{8-54}$$

which is the final probability fraction.

The oscillations in the β-coupling theory come from the neutrino-electron current in $J(e\nu)$. In general, the neutrino wave function can be expressed in free spherical and plane waves while the electron is adequately described by Coulomb-distorted spherical and plane waves. The wave field should be composed of a superposition of all energy eigenstates, including "negative energy" states. Thus, it is convenient to represent ψ_e or ψ_ν as

$$\psi = \int_{W>0} dW \sum_k \left[u_k e^{-iWt/\hbar} + u_k^C e^{+iWt/\hbar} \right] \tag{8-55}$$

where u_k and u_k^C (charge conjugate) are time dependent Dirac spinors of arbitrary normalizations and phases. Thus, Fourier analysis of the $J(e\nu)$ trivally gives frequency relations $\omega = (\pm W \pm cq)/\hbar$ for electron energies W and neutrino energies cq. Time dependence in $J(E\nu)$ comes out in form

$$J(\bar{e}\bar{\nu}) = (\psi_e^\dagger \Gamma^X \psi_\nu^C)_{t=0} e^{i(W+cq)t/\hbar} \tag{8-56a}$$

$$J(e^{+}\nu) = (\psi_c^{C\dagger}\Gamma^{X}\psi_\nu)_o\, e^{-i(W+cq)t/\hbar} \tag{8-56b}$$

$$J(e^{-}\nu) = (\psi_c^{\dagger}\Gamma^{X}\psi_\nu)_o\, i^{(W-cq)t/\hbar} \tag{8-56c}$$

$$J(e^{+}\bar{\nu}) = \psi_e^{C\dagger}\Gamma^{X}\psi_\nu^{C})_o\, e^{-i(W-cq)t/\hbar} \tag{8-56d}$$

where proton-to-neutron transformations are proportional to τ_- and can be written by exchanging $\psi_\nu = \psi_e$. The probability of reaching a given final state $|f\rangle$ can now be written for $p \to n + e^{+} + \nu$ as

$$|a_f(\infty)|^2 = \hbar^{-2}|\langle f|H_\beta|i\rangle|^2 \left|\int_{-\infty}^{\infty} dt\; e^{-i(W+cq+W_o)t/\hbar}\right|^2 \tag{8-57}$$

The first of the two conjugate time integrals is simply $2\pi\hbar\delta(W + cq + W_o)$, corresponding to conservation of energy. The second integral exists for $W + cq = -W_o$; hence the second time integral becomes $I = \int_{-\infty}^{\infty} dt \to \infty$. Thus, if the decay rate per nucleus is $d\lambda = |a_f(\infty)|^2/T$

$$d\lambda = (2\pi/\hbar)|\langle f|H_\beta|i\rangle|^2\delta(W + cq + W_o) \tag{8-58}$$

Assuming both lepton waves are normalized to unity in V, the desired rate is obtained by multiplying (8-58) by

$$(d\vec{p})(d\vec{q})V^2/(2\pi\hbar)^6 \tag{8-59}$$

where we can substitute $d\vec{p} = p^2 dp d\hat{p}$ and $d\vec{q} = q^2 dq d\hat{q}$ to get

$$\frac{d\lambda}{dp} = \frac{p^2q^2(d\hat{p})(d\hat{q})V^2}{(2\pi)^5\hbar^7 c}\,|\langle f|H_\beta|i\rangle|^2 \tag{8-60}$$

for decays in which the electron and the neutrino momenta end in the specific ranges $(d\vec{p})$ and $(d\vec{q})$. The δ-function is eliminated by integrating over the infinitesimal range of neutrino energy, remembering that $\int cdq\ \delta(W + cq + W_o) = 1$. $(\hat{p})$ and $(\hat{q})$ give the proton and neutrino solid angles. Integration over all solid angles simplifies (8-60) to

$$\frac{d\lambda}{dp} = \frac{p^2 q^2 V^2}{2\pi^3 \hbar^7 c} |\langle f|H_\beta|i\rangle|^2 \qquad (8\text{-}61)$$

The above equation cannot be trivially integrated to obtain the rate constant explicitly without knowledge of momentum (energy) dependence of $|\langle f|H_\beta|i\rangle|^2$. Clearly, Coulomb interactions of the electron with the nucleus may be significant, so the matrix element is generally factored, giving

$$|\langle f|H_\beta|i\rangle|^2 = F(Z,W_o)\xi^2 \qquad (8\text{-}62)$$

where $F(Z,W_o)$ contains the Coulombic interaction between the electron and the nucleus. Integrating (8-61)

$$= \frac{\xi^2}{2\pi^3 \hbar^7 c} \int_o^{p_o} dp\ p^2 q^2 F(Z,W)$$

$$\lambda = (2\pi^3 \hbar^7 c)^{-1} f(Z,W_o)\xi^2 \qquad (8\text{-}63)$$

where $f(Z,W_o)$ is generally evaluated numerically. This result should be correct for all forms of β decay, both induced and spontaneous. Although this form is essentially exact, $f(Z,W_o)$ and ξ^2 need to be further

elaborated before actual calculations may be performed. Nevertheless, a preliminary investigation of the case of competing positron decay and electron capture decay indicates some interesting possibilities. The rates of these forms of decay in a given nucleus are

$$\lambda_\varepsilon = (2\pi^3\hbar^7 c)^{-1} f_\varepsilon(Z,W_o)\xi_\varepsilon \tag{8-64a}$$

and

$$\lambda_{\beta+} = (2\pi^3\hbar^7 c)^{-1} f_{\beta+}(Z,W_o)\xi_{\beta+} \tag{8-64b}$$

Assuming that the β-interaction force is identical in all forms of β-decay (i.e. there is only one β force), then to first order $\xi_\varepsilon = \xi_{\beta+}$ and

$$\frac{\lambda_\varepsilon}{\lambda_{\beta+}} = \frac{f_\varepsilon}{f_{\beta+}} \tag{8-65}$$

This quantity is experimentally measurable and, because $f(Z,W_o)$ is composed strictly of electromagnetic effects, such values are straightforwardly calculated. Thus, such calculations should be easily compared to experiment to test their accuracy. In addition, the assumption $\xi_\varepsilon = \xi_{\beta+}$ can be tested to confirm the β theory presented here.

8.2.2 Lepton Wave Functions

Since the neutrino is presumably an essentially non-interacting particle, its description as a free spherical wave will be sufficient. Any wave function chosen must satisfy the Dirac equations

$$W\Phi = c\vec{\sigma}\cdot\vec{p}\,\vec{\Theta} + mc^2\,\Phi \tag{8-66}$$

$$W\,\Theta = c\vec{\sigma}\cdot\vec{p}\vec{\Phi} - mc^2\Theta \tag{8-67}$$

where $W = (c^2p^2 + m^2c^4)^{1/2}$ is the energy of the particle in question. Φ and Θ are Pauli spinors representing forward and retrograde motion and composing the four-component spinor,

$$\psi = \begin{pmatrix}\Phi(r)\\ \Phi(r)\end{pmatrix} e^{-iWt} \tag{8-68}$$

In order to obtain eigenstates of total angular momentum $\vec{j} = \vec{\ell} + \vec{s}$ one must consider superpositions of spin eigenfunctions $\vec{\chi}_{\pm 1/2}$ and angular momentum eigenfunctions $\vec{\chi}_{\ell m}$ defined such that

$$\vec{\chi}^{\dagger}_{j\mu}\vec{\chi}^{\dagger}_{j'\mu'} = \delta_{jj'}\delta_{\mu'\mu} \tag{8-69}$$

In the case of orbital angular momentum, $\vec{\chi}_{\ell m} \rightarrow Y_{\ell m}(\theta,\phi)$, the familiar spherical harmonic function. Thus, an eigenstate of $\vec{j}$ can be expressed as

$$\vec{\chi}_{\ell\mu}(\theta,\phi) = \sum_{\rho=\pm 1/2}\vec{\chi}_{\rho}Y_{\ell\mu-\rho}<\ell(\mu-\rho)\tfrac{1}{2}(\rho)\,|\,j(\mu)> \tag{8-70}$$

where

$\kappa = \pm 1, \pm 2, \pm 3, \ldots$

$\mu = \pm 1/2, \pm 3/2, \ldots, \pm j$

$j = |\kappa| - 1/2$

$\ell = j + 1/2 = \kappa$ for $\kappa > 0$

$\ell = j - 1/2 = -(\kappa+1)$ for $\kappa < 0$.

The orthonormality condition

$$\int d\Omega \vec{\chi}^{\dagger}_{\kappa\mu} \vec{\chi}_{\kappa'\mu'} = \delta_{\kappa\kappa'}\delta_{\mu\mu'} \tag{8-71}$$

applies, and the coupling term in 8-70 is simply the vector addition coefficient connecting the two eigenstates. If we then introduce a radial dependence, $g_\kappa(r)$, the spinor $\Phi(\vec{r}) = g_\kappa(r)\vec{\chi}_{\kappa\mu}(\hat{r})$, and the Dirac equation, becomes

$$\vec{\Theta}(\vec{r}) = (W+1)^{-1}\left(\frac{d}{dr} + \frac{1+\kappa}{r}\right) g_\kappa \vec{\chi}_{-\kappa\mu} \tag{8-72}$$

so the Dirac four-component spinor takes the form,

$$\psi_{\kappa\mu}(\vec{r}) = \begin{pmatrix} g_\kappa(r)\vec{\chi}_{\kappa\mu}(\hat{r}) \\ i f_{-\kappa}(r)\vec{\chi}_{-\kappa\mu}(\hat{r}) \end{pmatrix} e^{-iWt/\hbar} \tag{8-73}$$

where

$$f_{-\kappa}(r) = (W+1)^{-1}\left(\frac{d}{dr} + \frac{1+\kappa}{r}\right) g_\kappa(r)$$

$$g_\kappa(r) = -(W-1)^{-1}\left(\frac{d}{dr} + \frac{1+\kappa}{r}\right) f_{-\kappa}(r)$$

$g_\kappa(r)$ and $f_{-\kappa}(r)$ can be chosen proportional to spherical Hankel functions $h_\ell(pr)$, giving

$$g_\kappa = N_W h_{\ell(\kappa)} \rightarrow f_{-\kappa} = \hat{\kappa} N_W [(W-1)/(W+1)]^{1/2} h_{\ell(-\kappa)} \tag{8-74}$$

where N_W is a normalization constant and $\hat{\kappa} = \kappa/|\kappa|$. Since the neutrino

is emitted in a continuous spectrum of energies, the wave function should represent a superposition of eigenstates,

$$\psi(\vec{r},t) = \int dW \sum_{K\mu} a_{WK\mu}\psi_{K\mu}(\vec{r},t) \qquad (8\text{-}75)$$

where $a_{WK\mu}$ is defined such that $\sum_{K\mu}|a_{WK\mu}|^2 dW$ is the probability of finding a particle in the range dW and

$$\S(d\vec{r})|\psi|^2 = \int dW \sum_{K\mu}|a_{WK\mu}|^2 = 1 \qquad (8\text{-}76)$$

The eigenfunction for the emitted electron is necessarily more complicated by the Coulomb potential V(r), so Coulomb distortion can be created by substituting W - V(r) in the above equations.

8.2.3 The β Interaction

Presumably, the internal variables of any particle can be described by four-component Dirac spinors resulting from intrinsic spins ±1/2 and intrinsic velocity ±c. Thus, the radial part of the particle wavefunction is assumed separable from the intrinsic parts. The total particle wavefunction can be written as

$$\psi = \psi_1(\vec{r})u_{+1/2}(+c) + \psi_c u_{-1/2}(+c) + \psi_3 u_{+1/2}(-c) +$$

$$+ \psi_4 u_{-1/2}(-c) \qquad (8\text{-}77)$$

which can be written in matrix form as

$$\psi(\vec{r}) = \begin{pmatrix} \psi_1(\vec{r}) \\ \psi_2(\vec{r}) \\ \psi_3(\vec{r}) \\ \psi_4(\vec{r}) \end{pmatrix} \equiv \begin{pmatrix} \Phi = \psi_1 \vec{\chi}_{1/2} + \psi_2 \vec{\chi}_{-1/2} \\ \Theta = \psi_3 \vec{\chi}_{1/2} + \psi_4 \vec{\chi}_{-1/2} \end{pmatrix} \tag{8-78}$$

where $\chi_{\pm 1/2}$ are eigenspinors represented by

$$\vec{\chi}_{+1/2} = \begin{pmatrix} 1 \\ 0 \end{pmatrix} \vec{\chi}_{-1/2} = \begin{pmatrix} 0 \\ 1 \end{pmatrix} \tag{8-79}$$

Similarly, the four-component eigenspinors can be constructed as

$$u_{1/2}(+c) = \begin{matrix} 1 \\ 0 \end{matrix} \vec{\chi}_{1/2} = \begin{pmatrix} 1 \\ 0 \\ 0 \\ 0 \end{pmatrix} \quad u_{-1/2}(+c) = \begin{pmatrix} 1 \\ 0 \end{pmatrix} \vec{\chi}_{-1/2} = \begin{pmatrix} 0 \\ 1 \\ 0 \\ 0 \end{pmatrix}$$

$$u_{1/2}(-c) = \begin{pmatrix} 0 \\ 1 \end{pmatrix} \vec{\chi}_{1/2} = \begin{pmatrix} 0 \\ 0 \\ 1 \\ 0 \end{pmatrix} \quad u_{-1/2}(-c) = \begin{pmatrix} 0 \\ 1 \end{pmatrix} \vec{\chi}_{-1/2} = \begin{pmatrix} 0 \\ 0 \\ 0 \\ 1 \end{pmatrix} \tag{8-80}$$

Eigenvectors can be constructed to project the eigenvalues for the various spin projections, giving the equations,

$$\sigma_z u_{+1/2}(\pm c) = +u_{+1/2}(\pm c); \quad \sigma_z u_{-1/2}(\pm c) = -u_{-1/2}(\pm c) \tag{8-81}$$

resulting in

$$\sigma_z = \begin{pmatrix} 1 & 0 & 0 & 0 \\ 0 & -1 & 0 & 0 \\ 0 & 0 & 1 & 0 \\ 0 & 0 & 0 & -1 \end{pmatrix} = \begin{pmatrix} \sigma_z' & 0 \\ 0 & \sigma_z' \end{pmatrix} \tag{8-82}$$

where σ_z' are the Pauli spinors. Similarly, an eigenvector can be created to project intrinsic velocity giving

$$\alpha_z = \begin{pmatrix} 1 & 0 & 0 & 0 \\ 0 & 1 & 0 & 0 \\ 0 & 0 & -1 & 0 \\ 0 & 0 & 0 & -1 \end{pmatrix} = \begin{pmatrix} 1 & 0 \\ 0 & -1 \end{pmatrix} \tag{8-83}$$

Also, an eigenvector can be constructed to project out chirality such that the eigenvalue +1 refers to left-handed states and -1 for right-handed states. Thus

$$\gamma_5 u_{\mp 1/2}(\pm c) = +u_{\mp 1/2}(\pm c); \quad \gamma_5 u_{\pm 1/2}(\pm c) = -u_{\pm 1/2}(\pm c) \tag{8-84}$$

where

$$\gamma_5 = \begin{pmatrix} -1 & 0 & 0 & 0 \\ 0 & 1 & 0 & 0 \\ 0 & 0 & 1 & 0 \\ 0 & 0 & 0 & -1 \end{pmatrix} \equiv \begin{pmatrix} -\sigma_z' & 0 \\ 0 & \sigma_z' \end{pmatrix} = -\sigma_z \alpha_z \tag{8-85}$$

Actually a total of 16 independent 4-dimensional matrices may be constructed, including

$$\rho_1 = \begin{pmatrix} 0 & 1 \\ 1 & 0 \end{pmatrix}, \quad \rho_2 = \begin{pmatrix} 0 & -i \cdot 1 \\ i \cdot 1 & 0 \end{pmatrix}, \text{ and } \rho_3 = \begin{pmatrix} 1 & 0 \\ 0 & -1 \end{pmatrix}$$

Also,

$$\sum = \begin{pmatrix} \sigma & 0 \\ 0 & \sigma \end{pmatrix}; \quad \rho_1 \sum, \ \rho_2 \sum, \ \rho_3 \sum; \quad \rho_0 = \begin{pmatrix} 1 & 0 \\ 0 & 1 \end{pmatrix} \tag{8-86}$$

where $\sigma_z = \sum_3$, $\alpha_z = \rho_3$, and $\gamma_5 = -\rho_3 \sum_3$. Also, historically, $\rho_3 = \alpha_z = \beta$ and $\vec{\alpha} = \rho_1 \vec{\sum}$.

It is clearly desirable that solutions to the Dirac equation

$$W\psi = (c\vec{\alpha}\cdot\vec{p} + \beta mc^2)\psi \tag{8-87}$$

lead to real physical quantities and that $\psi^\dagger\psi$ be an invariant scalar. If this is to include relativistic invariance, it is necessary to treat the time coordinate as the fourth component of a four-vector $\omega_\mu(\vec{w}, ic\psi^\dagger\psi)$ on equal footing with the three special vectors. For this to be true,

$$\vec{\nabla}\cdot\vec{w} + d(\psi^\dagger\psi)/dt \equiv \sum_\mu d\omega/_\mu dX_\mu = 0 \tag{8-88}$$

where it turns out that

$$\vec{w} = c\psi^\dagger\vec{\alpha}\psi \tag{8-89}$$

Since $\omega_\mu(c\psi^\dagger\vec{\alpha}\psi, ic\psi^\dagger\psi)$ is a 4-vector, $\psi^\dagger\psi$ is not a scalar and $c\psi^\dagger\alpha\psi$ represents the special components. The scalar expression,

$$\psi^\dagger H\psi = c(\psi^\dagger\alpha\psi) + (\psi^\dagger\beta\psi)mc^2 = W\psi^\dagger\psi \tag{8-90}$$

shows that the multiplication of $\bar{\psi} = \psi^\dagger\beta$ into ψ, not $\psi^\dagger$, produces an invariant scalar product. Since $\beta^2 = 1$, denote the current density 4-vector as $\omega_\mu(c\,\bar{\psi}\beta\alpha\psi, ic\bar{\psi}\beta\psi)$, where the internal dynamical variable components are

$$\gamma_\mu = (-i\beta\alpha, \beta) \tag{8-91}$$

with properties of a 4-vector. The current 4-vector is simply

$$\omega_\mu = ic\bar{\psi}\gamma_\mu\psi \tag{8-92}$$

and the Dirac equation becomes

$$(\gamma_\mu d/dX_\mu + mc/\hbar)\psi = 0 \tag{8-93}$$

Thus, the entire dependence on inner variables is expressed as a function of γ_μ. Indeed, all possible internal motions can be expressed in terms of γ_μ, which can be used to generate the sixteen independent 4-dimensional matrices. If all possible internal motions can be represented by four 4-component spinors, then it follows that any internal variable must be representable by a 4×4 matrix. Thus, an arbitrary function can be written generating all sixteen possible spinors using the anticommutation property,

$$1/2(\gamma_\mu\gamma_\nu + \gamma_\nu\gamma_\mu) = \delta_{\mu\nu} \tag{8-94}$$

and constructing all possible products,

$$f = f_o + \sum_\mu f_\mu\gamma_\mu + \sum_{\mu\neq\nu} f_{\mu\nu}\gamma_\mu\gamma_\nu +$$

$$+ \sum_{\substack{\mu\neq\nu\neq\rho \\ \mu\neq\rho}} f_{\mu\nu\rho}\gamma_\mu\gamma_\nu\gamma_\rho + f_5\gamma_x\gamma_y\gamma_z\gamma_4 \tag{8-95}$$

where f can coincide with an arbitrary matrix having sixteen parameters. Note that only five distinct types of products can be created. The first

two include a scalar and a 4-component vector whose properties are already quite clear.

The six products $\gamma_\mu\gamma_\nu = -\gamma_\nu\gamma_\mu$ form components of a second-rank tensor. This tensor may be represented as

$$\sigma_{\mu\nu} = (\gamma_\mu\gamma_\nu - \gamma_\nu\gamma_\mu)/2i = -i\gamma_\mu\gamma_\nu \quad (\mu \neq \nu) \tag{8-96}$$

where the factor i makes the component hermitian. The spacial components form the circular relationship

$$\sigma_x\sigma_y = (\gamma_x\gamma_y - \gamma_y\gamma_x)/2i = (\vec{\gamma}\times\vec{\gamma})_z/2i \equiv (\vec{\alpha}\times\vec{\alpha})_z/2i \tag{8-97}$$

and symbolically

$$\sigma = (\vec{\alpha}\times\vec{\alpha})/2i \tag{8-98}$$

The space-time component has the form

$$\sigma_{x4} = -i\gamma_x\gamma_4 = \alpha_x \tag{8-99}$$

so the total array of tensor components is

$$(\alpha_{\mu\nu}) = \begin{pmatrix} 0 & \sigma_z & -\sigma_y & \alpha_x \\ -\sigma_z & 0 & \sigma_x & \alpha_y \\ \sigma_y & \sigma_x & 0 & \alpha_z \\ -\alpha_x & -\alpha_y & -\alpha_z & 0 \end{pmatrix} = \sigma_{\mu\nu}(\vec{\sigma},\vec{\alpha}) \tag{8-100}$$

The last term becomes simply

$$\gamma_5 = \gamma_x\gamma_y\gamma_z\gamma_4 \tag{8-101}$$

As was shown previously, this undergoes changes under right-to left-handed frame inversions ($\vec{r} \to -\vec{r}$). In all other changes of reference frame this behaves like an invariant scalar hence this quantity is termed a pseudoscalar.

Finally, the four components $\gamma_\rho\gamma_\mu\gamma_\nu$ can be written as

$$\omega_\mu = i\gamma_5\gamma_\mu \tag{8-102}$$

which behaves like a 4-vector under all operations except space inversion where $\vec{\omega} = i\gamma_5\vec{\gamma}$ does not change signs. For this reason ω_μ is termed an axial vector. Thus, the possible inner variables can be written,

$$f = f_o + \sum f_\mu\gamma_\mu + i\sum f_{\mu\nu}\sigma_{\mu\nu} + \sum f'_\mu\omega_\mu + f_5\gamma_5 \tag{8-103}$$

in terms of the five covariants

scalar,	1
vector,	$\gamma_\mu(-i\beta\alpha,\beta)$
tensor,	$\sigma_{\mu\nu}(\vec{\sigma},\vec{\alpha})$
axial vector,	$\omega_\mu(\beta\sigma,-i\beta\gamma_5)$
pseudoscalar,	γ_5

Each has the covariance shown only under the operation

$$\bar{\psi}\Gamma^X\psi \equiv \psi^\dagger\beta\Gamma^X\psi \tag{8-104}$$

where Γ^X is the covariant in question.

8.2.4 H_β

The β interaction current between nuclear states can be written as $\langle f|H_\beta|i\rangle$ where it has been shown that most generally (8-46)

$$H_\beta = 8^{1/2}g \sum_X \sum_{a=1}^{A} \beta^a\Gamma^{X^a}\tau_\pm^a\psi_e^\dagger\beta^a\Gamma^{X^a}\psi_\nu + \text{h.c.} \tag{8-105}$$

The interaction is summed over all nucleons as well as all interactions.

Two interactions that are quite similar are the vector (V) and axial vector (A) interactions. These are written in the form

$$V : \gamma_\alpha \qquad A : \gamma_\alpha\gamma_5 \tag{8-106}$$

Each consists of four components, which can be taken as

$$\Gamma_\alpha^{V+A} \approx (\gamma_\alpha + \gamma_\alpha\gamma_5) \approx \gamma_\alpha(1 + \gamma_5) \tag{8-107}$$

Assuming each form contributes proportionally to $1/2C_V$, $-1/2C_A$, respectively,

$$\Gamma_\alpha^{V+A} = 1/2\gamma_\alpha(C_V - C_A\gamma_5) \tag{8-108}$$

so that

$$H_\beta^{VA} = 2^{1/2}g \sum_{a=1}^{A} \beta^a\gamma_\alpha^a(C_V - C_A\gamma_5^a)\tau_\pm^a[J_\alpha(e\nu)]_{\vec{r}}^a + \text{h.c.} \tag{8-109}$$

Also, since $\gamma_4^a \equiv \beta^a$ and $\vec{\gamma}^a = -i\beta\vec{\alpha}^a$ and the lepton current $J_\alpha(e\nu)$ is composed of components $J_4^a, \vec{J}^a$, it is easy to rearrange the above to

$$H_\beta^{VA} = 2^{1/2} g \sum_a \tau_\pm^a \{J_4^a(C_V - C_A\gamma_5^a) - i\vec{J}^a(C_V\vec{\alpha}^a + C_A\vec{\sigma}^a)\} + \text{h.c.} \qquad (8\text{-}110)$$

where $-\gamma_5\vec{\alpha} = \vec{\sigma}$. Since nuclei are considerably smaller than lepton wavelengths, the lepton current J_α need only be evaluated to first order at the nuclear center, $r = 0$. Thus, as an approximation, $J_\alpha^a(r_a = 0) \equiv J_\alpha^o$ leading to

$$\langle f|H_\beta^{VA}|i\rangle = 2^{1/2} g\{J_4^o[C_V \textstyle\int 1 - C_A \int \gamma_5] - iJ^o[C_A \int \vec{\sigma} + C_V \int \alpha]\} + \text{h.c.} \qquad (8\text{-}111)$$

where

$$\textstyle\int 1 = \langle f|\sum_a \tau_\pm^a|i\rangle, \quad \int \gamma_5 = \langle f|\sum_a \tau_\pm^a\gamma_5^a|i\rangle$$

$$\textstyle\int \vec{\sigma} = \langle f|\sum_a \tau_\pm^a\vec{\sigma}^a|i\rangle, \quad \vec{\alpha} = \langle f|\sum_a \tau_\pm^a\vec{\alpha}^a|i\rangle \qquad (8\text{-}112)$$

A further simplification may be made because nuclei are not relativistic particles. In this case $\vec{\alpha}$ and $\gamma_5 = -\sigma_i^a\alpha_i^a$ become "negligible" because the velocity operator $\vec{\alpha}^a$ takes on a magnitude proportional to v^a/c. Thus, to first order,

$$\langle f|H_\beta^{VA}|i\rangle \approx 2^{1/2} g\{C_V J_4^o \textstyle\int 1 - iC_A \vec{J}^o \cdot \int \vec{\sigma}\} \qquad (8\text{-}113)$$

Several interesting results can be inferred from the above β-transition amplitude. Most interestingly, the Vector and axial vector interactions

separate into different terms. Transition selection rules may be obtained for each interaction form. For the vector interaction,

$$\langle f|\sum_a \tau_\pm^a|i\rangle \equiv \langle I'|\sum_a \tau_\pm^a|I\rangle \approx \vec{\chi}^{\dagger}_{I'M'}\vec{\chi}_{IM} = \delta_{I'I}\delta_{M'M} \quad (8\text{-}114)$$

where $\vec{\chi}_{IM}$, $\vec{\chi}_{I'M'}$ represent the angular momentum eigenstates $\approx Y_{LM}$. Similarly, for the axial vector interaction

$$\langle f|\sum_a \tau_\pm^a \vec{\sigma}^a|i\rangle \equiv \langle I'|\sum_a \tau_\pm^a \vec{\sigma}^a|I\rangle \approx \vec{\chi}_{I'M'}\vec{\sigma}\vec{\chi}_{IM} \quad (8\text{-}115)$$

where $\vec{\sigma}$ projects out states $I' = I$, $I \pm 1$. In addition, terms $I' = I = 0$ vanish. Also, the parity operation,

$$P\psi_i(r_1,\ldots,r_A) \equiv \psi_i(-r_1,\ldots,-r_A) \quad (8\text{-}116)$$

leads to another selection rule. Since $P^2 = 1$,

$$P^2\langle f|H_\beta|i\rangle = \langle f|H_\beta|i\rangle \quad (8\text{-}117)$$

This can only be true if the initial and final states have identical parities. Thus, selection rules for the Vector and axial vector interactions are

Vector (V): $\int 1 = 0$ unless $\Delta I = 0$, $\Pi_i\Pi_f = +1$ (Fermi rules)

Axial Vector (A): $\int \sigma = 0$ unless $\Delta I = 0$ or 1, $\Pi_i\Pi_f = +1$ (Gamow-Teller rules)

$= 0$ when $I = I' = 0$

These rules, better known As Fermi and Gamow-Teller rules, indicate that Vector and axial vector interactions can both contribute to β transitions in which the nucleons do not change in angular momentum, except for $0^+ \rightarrow 0^+$ transitions when only vector interactions can occur. Transitions involving a change of one unit of angular momentum can only contain axial vector contributions. In addition, these rules indicate that no transitions can take place between states of opposite parity.

Actually, the non-existence of higher-order transitions involving parity change is a result of two approximations made previously, i.e., $r_a = 0$ and nonrelativistic nucleon motion. This is termed the "allowed approximation" and the above rules are actually for "allowed" transitions. Indeed, "forbidden" transitions do exist, but their transition rates are assumed to be considerably slower than allowed transitions as they involve higher order terms in r and v/c and will be ignored for the present.

Similarly, the Scalar (S), Tensor (T), and Pseudoscalar (P) contributions to the interaction are

$$\Gamma^{STP} \approx (1 + \sigma_{\mu\nu} + \gamma_5) = (1 - i(\vec{\sigma} + \vec{\alpha}) + \gamma_5) \qquad (8\text{-}118)$$

Discarding the relativistic terms as before,

$$\Gamma^{STP} \approx (1 - i\vec{\sigma}) \qquad (8\text{-}119)$$

and proportionality constants C_S, C_V lead to

$$\Gamma^{STP} = (C_S - iC_T\vec{\sigma}) \qquad (8\text{-}120)$$

Thus, as before

$$H_\beta^{STP} = 2^{1/2} g \sum_{a=1}^{A} \beta^a (C_S - i\vec{\sigma}^a C_T) \tau_\pm^a [J_\alpha(e\nu)]_{\vec{r}^a}$$

$$= 2^{1/2} g \sum_a \tau_\pm^a \beta^a \{J_4^a(C_S) - i\vec{J}^a(C_T \vec{\sigma}^a) \qquad (8\text{-}121)$$

This form is quite similar to that for V-A terms except that the terms are proportional to $\beta^a = \gamma_\alpha^a$. Thus the β-interaction current contains the terms $\langle f | \sum_a \tau_\pm^a \beta^a | i \rangle$ and $\langle f | \sum_a \tau_\pm^a \beta^a \vec{\sigma}^a | i \rangle$. In the case of non relativistic particles, $\beta\psi \approx \psi$, so for the nucleons the above terms can be simplified. It must be remembered, however, that this simplification is unwarranted for leptons. The β interaction becomes

$$\langle f | H_\beta | i \rangle \approx 2^{1/2} g \{(C_V + C_S) J_4^o \int 1 - i(C_A + C_T) \vec{J}^o \cdot \int \vec{\sigma}\} \qquad (8\text{-}122)$$

The terms $\int 1$ and $\int \vec{\sigma}$ can be simplified using the Wigner-Eckart relation

$$\langle \delta' I' M' | S_{Jm}^\dagger | \delta I M \rangle = \langle I'(M') J(m) | I(M) \rangle \langle S_J \rangle \qquad (8\text{-}123)$$

where $\langle S_J \rangle$ is the reduced matrix element which is independent of angular momentum orientations. Thus,

$$\int 1 = \langle I'(M') 0(0) | I(M) \rangle \langle 1 \rangle = \delta_{I'I} \delta_{M'M} \langle 1 \rangle \qquad (8\text{-}124a)$$

$$\int \sigma_m^\dagger = \langle I'(M') 1(m) | I(M) \rangle \langle \sigma \rangle \qquad (8\text{-}124b)$$

where $\langle 1 \rangle$ is the singlet (Fermi) β moment and $\langle \sigma \rangle$ is the triplet (Gamow-

Teller) moment. Note that

$$\langle\sigma\rangle^2 = \sum_m |\int\sigma_m|^2 = |\int\sigma_x|^2 + |\int\sigma_y|^2 + |\int\sigma_z|^2 \qquad (8\text{-}125)$$

The three spacial components of the transition current can be written

$$\vec{J}\cdot\int\vec{\sigma} \equiv \sum_m J_m\int\sigma_m^\dagger = \langle\sigma\rangle\sum_m J_m\langle I'(M')1(m)|I(M)\rangle \qquad (8\text{-}126)$$

The selection rules suggest that the allowed transition current terms can be divided into those leading to no angular momentum change and those involving a change of one unit of angular momentum between the initial and final nuclear states. This leads to

$$|\langle f|H_\beta|i\rangle|^2 = 2g^2\{|(C_S+C_V)J_4\int 1 - i(C_T+C_A)J_o\int\sigma_z|^2 +$$

$$(C_T+C_A)^2[|J_{+1}|^2|\int\sigma_{-1}|^2 + |J_{-1}|^2|\int\sigma_{+1}|^2]\} \qquad (8\text{-}127)$$

where the leptons carry away angular momentum equal but opposite in sign to the nucleons. This can be separated into a purely Scalar-Vector part, a Tensor-Axial vector part, and a factor containing all four interactions as follows

$$|\langle f|H_\beta|i\rangle|^2_{SV} = \delta_{II'}2g^2(C_S+C_V)^2\langle 1\rangle^2|J_4|^2 \qquad (8\text{-}128a)$$

$$|\langle f|H_\beta|i\rangle|^2_{TA} = 2g^2(C_T+C_A)^2\langle\sigma\rangle^2\sum_m |J_m|^2\langle I'(M-m)1(m)|I(M)\rangle^2 \qquad (8\text{-}128b)$$

$$|\langle f|H_\beta|i\rangle|^2_{STVA} = \delta_{II'}2g^2(C_S+C_V)(C_T+C_A)\langle 1\rangle\langle\sigma\rangle[I/(I+1)]^{1/2}$$

$$(M/I)(iJ_o^*J_4 + c.c.) \qquad (8\text{-}128c)$$

For randomly oriented nuclei it is necessary to average overall orientations $-I \leq M \leq I$ by the operator $(2I+1)^{-1}\sum_M$. The S-V term is not a function of orientation, so

$$(2I+1)^{-1}\sum_M |\langle f|H_\beta|i\rangle|^2_{SV} = \delta_{I'I}2g^2(C_S+C_V)^2\langle 1\rangle^2|J_4|^2 \qquad (8\text{-}129)$$

The cross term in STVA is linear in M, so

$$(2I+1)^{-1}\sum_M |\langle f|H_\beta|i\rangle|^2_{STVA} = 0 \qquad (8\text{-}130)$$

Finally, the TA term requires the average vector addition coefficient

$$(2I+1)^{-1}\sum_M [(2I+1)/3]\langle I'(m-M)I(M)|1(m)\rangle^2 \equiv 1/3 \qquad (8\text{-}131)$$

where the initial coefficient has been reordered by use of symmetry relations. This leads to

$$(2I+1)^{-1}\sum_M |\langle f|H_\beta|i\rangle|^2_{TA} = 2g^2(C_A+C_T)^2\langle\sigma\rangle^2 \cdot \frac{1}{3}\sum_m |J_m|^2 \qquad (8\text{-}132)$$

The β-interaction forms were proportional to

$$\Gamma^{VA} \approx 1/2\gamma_\alpha(1+\gamma_5) \quad \Gamma^{ST} \approx 1/2\gamma_\alpha(1-\gamma_5) \qquad (8\text{-}133)$$

The terms $1/2(1\pm\gamma_5)$ are informative when one writes

$$\psi \equiv 1/2(1+\gamma_5)\psi + 1/2(1-\gamma_5) \qquad (8\text{-}134)$$

where the two parts are orthogonal eigenstates of γ_5 with eigenvalues +1 and -1, respectively. Remembering that γ_5 is the chirality operator, lepton states

$$\phi = 1/2(1\pm\gamma_5)\psi \tag{8-135}$$

can be created in which the property $\gamma_5\phi = \pm\phi$ holds for $1/2(1\pm\gamma_5)$. Thus, $1/2(1\pm\gamma_5)$ selects out intrinsically left- and right-handed components from ψ, where

$$1/2(1\pm\gamma_5)\phi = \phi \tag{8-136}$$

befitting a projection. Therefore, the essential difference in the two pairs of interactions is that the V-A form will lead to intrinsically left-handed particles while the ST form involves only right-handed particles. Thus, the lepton wave functions involved in the β-interaction need only the forms

$$\Phi_e(\pm z) = 1/2(1\pm\gamma_5)\psi_e(\pm z); \quad \phi_\nu = 1/2(1\pm\gamma_5)\psi_{\bar{\nu}} \tag{8-137}$$

The lepton current may now be written in a form inclusive of all first order interactions

$$J_\alpha = \phi_e^\dagger \beta\gamma_x \phi_{\bar{\nu}} \tag{8-138}$$

It is desirable to evaluate the following terms in the β interaction.

$$|J_\alpha|^2 = \Phi_e^\dagger \beta\gamma_\alpha \phi_{\bar{\nu}} \phi_{\bar{\nu}}^\dagger \beta\gamma_\alpha \Phi_e \tag{8-139}$$

The neutrino wave function product $\phi_{\bar{\nu}}\phi_{\bar{\nu}}^\dagger$ can be evaluated using the free particle wave function

$$\psi_\nu = \left(\frac{1}{2V}\right)^{1/2} \left(\frac{1}{\vec{\sigma}\hat{q}}\right) \vec{\chi}_\nu e^{i(\hat{q}\cdot\vec{r}-cqt)/\hbar} \tag{8-140}$$

where

$$\sum_\nu \phi_{\bar{\nu}}\phi_{\bar{\nu}} = \frac{1}{8V}(1\pm\gamma_5)^2(1 \mp \vec{\sigma}\cdot\hat{q}) = \frac{1}{4V}(1\pm\gamma_5)(1 \mp \vec{\sigma}\cdot\hat{q}) \tag{8-141}$$

Then

$$\sum_\nu |J_4|^2 = \Phi_e^\dagger \beta^2 \phi_{\bar{\nu}} \phi_{\bar{\nu}}^\dagger \beta^2 \Phi_e$$

$$= \frac{1}{4V} \Phi_e^\dagger (1\pm\gamma_5)(1 \mp \vec{\sigma}\cdot\hat{q})\Phi_e$$

$$= \frac{1}{2V} \Phi_e^\dagger (1 \mp \vec{\sigma}\cdot\hat{q})\Phi_e \tag{8-142}$$

Similarly,

$$\frac{1}{3}\sum_m |J_m|^2 = \frac{1}{2V} \Phi_e \frac{1}{3} \sum_m [\sigma_m^\dagger (1 \mp \vec{\sigma}\cdot\hat{q})\sigma_m]\Phi_e$$

$$= \frac{1}{2V} \Phi_e^\dagger \frac{1}{3} \sum_m [1 \pm (\vec{\sigma}\cdot\hat{q})_m]\Phi_e$$

$$= \frac{1}{2V} \Phi_e^\dagger (1 \pm \vec{\sigma}\cdot\hat{q})\Phi_e \tag{8-143}$$

8.2.5 The Neutrino Wave Function

As was shown previously, a free particle can be described as the four-component spinor

$$\psi = \begin{pmatrix} \vec{\phi} \\ \theta \end{pmatrix} e^{i(\vec{p}\cdot\vec{r} - Wt)/\hbar} \tag{8-144a}$$

which must obey the relativistic equation of motion

$$i\hbar \frac{d\psi}{dt} = H\psi = (-i\hbar c\vec{\alpha}\cdot\vec{\nabla} + \beta mc^2)\psi = (c\vec{\alpha}\cdot\vec{p} + \beta mc^2)\psi \tag{8-144b}$$

Substitution gives the pair of equations

$$W\vec{\phi} = c\vec{\sigma}\cdot\vec{p}\theta + mc^2\phi \tag{8-145a}$$

$$W\vec{\theta} = c\vec{\sigma}\cdot\vec{p}\phi - mc^2\vec{\theta} \tag{8-145b}$$

which can be solved to give

$$\theta = (W + mc^2)^{-1} c\vec{\sigma}\cdot\vec{p}\,\vec{\phi} \tag{8-146a}$$

$$\phi = (W - mc^2)^{-1} c\vec{\sigma}\cdot\vec{p}\,\vec{\theta} \tag{8-146b}$$

If $W>0$, then $\theta<\phi$ and in the nonrelativistic limit where $p<<mc$, $W = (c^2p^2 + m^2c^4)^{1/2} \to mc^2$, then $\theta \to 0$. Thus, particles with $W > 0$ are considered "normal particles". Alternately, "antiparticles" with $W < 0$ give θ as the large component in the nonrelativistic limit. In either case, one

can choose one of the Pauli spinors as a linear combination of the Pauli spin eigenstates, $\vec{\chi}_{\pm 1/2}$ mentioned previously. Thus, for +W choose $\phi \approx \chi_{\pm 1/2}$ and normalization such that

$$(d\vec{r})\psi_{\mu}^{\dagger}\psi_{\mu'} = \delta_{\mu\mu'} \tag{8-147}$$

giving

$$\psi_{\pm 1/2} = \left(\frac{W+mc^2}{2WV}\right)^{1/2} \begin{pmatrix} c\vec{\sigma}\cdot\vec{p}/(W+mc^2) \\ 1 \end{pmatrix} \vec{\chi}_{\pm 1/2} e^{i(\vec{p}\cdot\vec{r}-Wt)/\hbar} \tag{8-148}$$

Similarly for $W < 0$ choose $\theta \approx \vec{\chi}_{\pm 1/2}$. The antiparticle ($W < 0$) wavefunction ψ^C can then be written

$$\psi^C_{\pm 1/2} = \mp \left(\frac{W+mc^2}{2WV}\right)^{1/2} \begin{pmatrix} c\vec{\sigma}\cdot\vec{p}/(W+mc^2) \\ 1 \end{pmatrix} \vec{\chi}_{\mp 1/2} e^{i(\vec{p}\cdot\vec{r}-Wt)/\hbar} \tag{8-149}$$

where ψ^C describes a normal particle of $-W$, $-\vec{p}$ and $-\mu\hbar$ spin projection equivalent to an antiparticle of $+W$, $+p$, and $+\hbar$. A charge conjugation operator relating particles and antiparticles by $\psi^C_{\mu} = C\psi^*_{\mu}$ can be formulated, giving $C \equiv \gamma_2$. The leading signs are added merely to allow an arbitrary phase.

The term $\vec{\sigma}\cdot\hat{p} = \pm 1$ ($\hat{p} = \vec{p}/p$) is of particular interest in that it gives particle polarizations for spin parallel (+1) or antiparallel (-1) to $\vec{p}$. The polarization of particles participating in β decay is a measurable quantity, and $\vec{\sigma}\cdot\hat{p}$ is termed the helicity operator. $\psi_{\pm 1/2}$ will be eigenstates of the helicity operator if the $\vec{\chi}_{\pm 1/2}$ are defined relative to $\vec{p}$ as a quantization axis.

Unfortunately, it is not the helicity, but chirality, which will

determine the β strengths. Chirality eigenstates will, nevertheless, lead to predictions of polarizations. As an example, the left-handed helicity state $\psi_{-1/2}$ is an eigenstate of both $\vec{p}$ and $\vec{\sigma}\cdot\hat{p} = -1$. The "intrinsically" left-handed chirality states $u_{\mp 1/2}(\pm c)$ are eigenstates of intrinsic velocity $c(\vec{\alpha}\cdot\hat{p}) = \pm c$ and chirality

$$\gamma_5 = -(\vec{\sigma}\cdot\hat{p})(\vec{\alpha}\cdot\hat{p}) = +1 \tag{8-150}$$

as referred to the axis $\hat{p}$. A general way to project out the components of each chirality is through the identity

$$\psi \equiv 1/2(1 + \gamma_5)\psi + 1/2(1 - \gamma_5)\psi \tag{8-151}$$

where, since $\gamma_5^2 = +1$, the two parts are orthogonal eigenstates of γ_5 with eigenvalues +1 and -1, respectively. The left-handed projection is denoted

$$\phi = 1/2(1 + \gamma_5)\psi = +\gamma_5\phi \tag{8-152}$$

and $1/2(1 + \gamma_5)\phi = \phi$ as befits a projection. The left-handed projection of $\psi_{\pm 1/2}$ can be most conveniently found by using the unitary transformation

$$U = 2^{-1/2}\begin{pmatrix} 1 & -1 \\ 1 & 1 \end{pmatrix} \tag{8-153}$$

giving the representation, $\gamma_5 \to \rho_3$, $\beta \to \rho$. Thus,

$$\phi^{L}_{\pm 1/2} = 1/2(1 + \gamma_5)U^{\dagger}\psi_{\pm 1/2}U$$

$$= \frac{1}{4}\left(\frac{W+mc^2}{2WV}\right)^{1/2}\left[\begin{pmatrix}1 & 0\\ 0 & 1\end{pmatrix} + \begin{pmatrix}1 & 0\\ 0 & -1\end{pmatrix}\right]\begin{pmatrix}1 & -1\\ 1 & 1\end{pmatrix}\left(c\vec{\sigma}\cdot\vec{p}/\frac{1}{(W+mc^2)}\right)\vec{\chi}_{\pm 1/2}\cdot e^{i(\vec{p}\cdot\vec{r}-Wt)/\hbar}$$

$$= \frac{1}{2}\left(\frac{W+mc^2}{2WV}\right)^{1/2}\begin{pmatrix}1 & -1\\ 0 & 0\end{pmatrix}\left(c\vec{\sigma}\cdot\vec{p}/\frac{1}{(W+mc^2)}\right)\begin{pmatrix}1 & 1\\ -1 & 1\end{pmatrix}\vec{\chi}_{\pm 1/2}e^{i(p\cdot r-Wt)/\hbar}$$

$$= \frac{1}{2}\left(\frac{W+mc^2}{W}\right)^{1/2}\begin{pmatrix}1\\ -1\end{pmatrix}(1-c\vec{\sigma}\cdot\vec{p}/(W+mc^2))\vec{\chi}_{\pm 1/2}e^{i(\vec{p}\cdot\vec{r}-Wt)/\hbar}$$

$$= \begin{pmatrix}1\\ -1\end{pmatrix}U_{\pm 1/2}(2V)^{-1/2}e^{i(\vec{p}\cdot\vec{r}-Wt)/\hbar} \qquad (8\text{-}154)$$

where

$$U^{L}_{\pm 1/2} = 1/2\left(\frac{W+mc^2}{W}\right)^{1/2}\left(1 - \frac{c\vec{\sigma}\cdot\vec{p}}{(W+mc^2)}\right)\vec{\chi}_{\pm 1/2} \qquad (8\text{-}155)$$

Normalization at unit density (V=1) gives

$$\phi^{\dagger}_{\pm 1/2}\phi_{\pm 1/2} = \vec{U}^{\dagger}_{\pm 1/2}\vec{U}_{\pm 1/2} = 1/2(1 \mp cp_z/W) \qquad (8\text{-}156)$$

since $(\vec{\sigma}\cdot\vec{p})^2 = p^2$. For right-handed projections, $1/2(1 - \gamma_5)$,

$$\phi^{R}_{\pm 1/2} = \begin{pmatrix}1\\ 1\end{pmatrix}\vec{u}_{\pm 1/2}\cdot(2V)^{-1/2}e^{i(\vec{p}\cdot\vec{r}-Wt)/\hbar} \qquad (8\text{-}157)$$

and

$$\vec{U}^{R}_{\pm 1/2} = 1/2\left(\frac{W+mc^2}{W}\right)^{1/2}[1 \mp c\vec{\sigma}\cdot\vec{p}/(W+mc^2)]\vec{\chi}_{\pm 1/2} \qquad (8\text{-}158)$$

where normalization gives

$$\phi^{R}_{\pm 1/2}\phi^{R}_{\pm 1/2} = \vec{u}^{R}_{\pm 1/2}u^{R}_{1/2} = 1/2(1\pm cp_z/W) \tag{8-159}$$

If $\hat{p}$ is the quantization axis, $cp_z/W = v/c$, and the relative intensities of the two helicities is

$$d\lambda\rightarrow/d\lambda\leftarrow = |\phi_{1/2}|^2/|\phi_{-1/2}|^2 = (1-v/c)/(1+v/c) \tag{8-160}$$

yielding a polarization, -v/c. The projection $1/2(1 + \gamma_5)$ on the antiparticle state yields

$$\phi^{C^L}_{\mu} = 1/2(1 + \gamma_5)c\psi^{*}_{\mu} = c[1/2(1 - \gamma_5)\psi_{\mu}]^{*} \tag{8-161}$$

since $c = \gamma_2$, γ_5 anticommute. Thus, antiparticle states are generated in their net right-handed polarizations by $1/2(1 + \gamma_5)$, so

$$\phi^{C^L}_{\pm 1/2} = 1/2(1+\gamma_5)\psi^{C}_{\pm 1/2} = \pm\begin{pmatrix}1\\-1\end{pmatrix}u_{\mp 1/2}(2V)^{-1/2}e^{-i(\vec{p}\cdot\vec{r}-Wt)/\hbar} \tag{8-162}$$

and

$$\phi^{C\dagger}_{\pm 1/2}\phi^{C^L}_{\pm 1/2} = u^{\dagger}_{\mp 1/2}u_{\mp 1/2} = 1/2(1\pm cp_z/W) \tag{8-163}$$

yielding a net polarization v/c.

Similarly, $1/2(1-\gamma_5)$ will generate net left-handed polarizations of antiparticle states where

$$\phi^{R}_{\pm 1/2} = \pm\binom{1}{1}\vec{u}_{\mp 1/2}(2V)^{-1/2}e^{-i(\vec{p}\cdot\vec{r}-Wt)/\hbar} \tag{8-164}$$

and

$$\phi^{R^{\dagger}}_{\pm 1/2}\phi^{R}_{\pm 1/2} = 1/2(1 \mp cp_z/W) \tag{8-165}$$

Thus, states generated by $1/2(1\pm\gamma_5)$ can be identified by the net polarization of the emitted particle.

This formalism is given for a free particle such as the neutrino. Indeed, if the neutrino is a massless particle and $W \to c\vec{q}$, $\vec{p} \to \vec{q}$

$$\phi^{L}_{\nu} = \binom{1}{-1}\vec{u}_{\nu}(2V)^{1/2}e^{i(\hat{q}\cdot\vec{r}-ct)q/\hbar} \tag{8-166a}$$

$$\phi^{R}_{\nu} = \pm\binom{1}{1}\vec{u}_{\nu}(2V)^{-1/2}e^{i(\hat{q}\cdot\vec{r}-ct)q/\hbar} \tag{8-166b}$$

$$\phi^{L^{C}}_{\nu} = \pm\binom{1}{-1}\vec{u}_{-\nu}(2V)^{-1/2}e^{-i(\hat{q}\cdot\vec{r}-ct)q/\hbar} \tag{8-166c}$$

$$\phi^{R^{C}}_{\nu} = \pm\binom{1}{1}\vec{u}_{-\nu}(2V)^{-1/2}e^{-i(\hat{q}\cdot\vec{r}-ct)q/\hbar} \tag{8-166d}$$

where

$$\vec{u}_{\nu} = 1/2(1-\vec{\sigma}\cdot\vec{q})\vec{\chi}_{\nu} \tag{8-167}$$

distorted spherical waves. These solutions lead to more complicated equations, yet yield no further implications of physical significance and won't be discussed here.

8.2.6 ε/β^+ Branching Ratios

The β interaction H_{fi} can be written as

$$H_{fi} = 2^{1/2} g[\ 1\psi_e^\dagger (C_V+\beta C_S)\phi_\nu - i\ \vec{\sigma}\psi_e^\dagger (C_A+\beta C_T)\phi_\nu] \qquad (8\text{-}168)$$

In $|H_{fi}|^2$ terms of the types

$$c_i^2\psi_e^\dagger\phi_\nu\phi_\nu^\dagger\psi_e;\quad c_j^2\psi_e^\dagger\beta\phi_\nu\phi_\nu^\dagger\beta\psi_e;\quad c_ic_j\psi_e^\dagger\beta\phi_\nu\phi_\nu^\dagger\ \psi_e$$

appear. Normalization properties of the wave functions reduce the first two terms to c_i^2 and c_j^2, respectively. The third term can be evaluated using the trace method (Wo66) where

$$c_ic_j\psi_e^\dagger\beta\phi_\nu\phi^\dagger\psi_e = c_ic_jTr(\psi_e^\dagger\beta\phi_\nu\phi^\dagger\psi_e)$$

$$= c_ic_jTr(\beta\phi_\nu\phi_\nu{}^\dagger\psi_e\psi_e{}^\dagger) \qquad (8\text{-}169)$$

Considering negatron decay where it appears that the electron is a particle (+W) and the neutrino an antiparticle (-cq), it is desirable to be able to project out the correct energy state from the wave function. For the electron, the Dirac equation can be written

$$(c\vec{\alpha}\cdot\vec{p} + \beta mc^2)\psi_e^\dagger = +|W|\psi_e^\dagger \qquad (8\text{-}170)$$

We want an operator with the property,

$$\Lambda_e^+\psi_e = \psi_e \text{ if } W > 0;$$
$$= 0 \text{ if } W < 0 \qquad (8\text{-}171)$$

Such an operator can be constructed as

$$\Lambda_e^+ = \frac{c\vec{\alpha}\cdot\vec{p} + \beta mc^2 + |W|}{2|W|} \quad \frac{1}{2}\left(1 + \frac{\beta mc^2}{|W|} + \frac{\vec{\alpha}\cdot\vec{V}}{c}\right) \tag{8-172}$$

Similarly, for the antineutrino (massless)

$$\Lambda_\nu^- = \frac{c\vec{\alpha}\cdot\vec{q} - |cq|}{-2|cq|} = \frac{1}{2}(1 - \vec{\alpha}\cdot\hat{q}) \tag{8-173}$$

where

$$\begin{aligned} \Lambda_\nu^- \phi_\nu &= \phi_\nu \quad \text{if } cq < 0 \\ &= 0 \quad \text{if } cq > 0 \end{aligned} \tag{8-174}$$

Since only positive energy electron states and negative energy neutrino states are produced,

$$\psi_e \psi_e^\dagger = \Lambda_e^+ \psi_e \psi_e^\dagger = \Lambda_e^+ \tag{8-175a}$$

$$\phi_\nu \phi_\nu^\dagger = \Lambda_\nu^- \phi_\nu \phi_\nu^\dagger = \Lambda_\nu^- \tag{8-175b}$$

applying the closure properties of wave functions. The matrix element simplifies to

$$\mathrm{Tr}(\beta\Lambda_\nu^-\Lambda_e^+) = \mathrm{Tr}\left[\frac{1}{4}\beta\left(1 + \frac{\beta mc^2}{|W|} + \frac{\vec{\alpha}\cdot\vec{V}}{c}\right)(1 - \vec{\alpha}\cdot\hat{q})\right]$$

$$= \mathrm{Tr}\left[\frac{1}{4}\left(\beta + \frac{mc^2}{|W|} + \frac{\beta\vec{\alpha}\cdot\vec{V}}{v/c}\right)(1 - \vec{\alpha}\cdot\hat{q})\right] \tag{8-176}$$

To interpret these terms it is necessary to realize that the terms linear in β and $\vec{\alpha}$ vanish since

$$\mathrm{Tr}\beta = 0; \quad \mathrm{Tr}\alpha = 0 \tag{8-177}$$

and terms proportional to the 4×4 unit matrix are easily evaluated, since $\mathrm{Tr}1 = 4$. Thus, for e^- decay,

$$c_i c_j \psi_e^\dagger \beta \phi_\nu \phi_\nu^\dagger \psi_e = \mathrm{Tr}(\beta \Lambda_\nu^- \Lambda_e^+) = c^i c^j \frac{mc^2}{|W|} \tag{8-178}$$

Positron decay yields negative energy electrons and positive energy neutrinos, so the analogous result is

$$\mathrm{Tr}(\beta \Lambda_\nu^+ \Lambda_e^-) = -c_i c_j \frac{mc^2}{|W|} \tag{8-179}$$

Similarly for terms proportional to $\int\sigma$ we get terms like

$$\psi_e^\dagger \beta \vec{\alpha} \phi_\nu \phi_\nu^\dagger \beta \vec{\sigma} \psi_e = \mathrm{Tr}(\beta \vec{\sigma} \Lambda_\nu^+ \beta \vec{\sigma} \Lambda_e^-) \tag{8-180}$$

$$= \mathrm{Tr}(\sigma \Lambda_\nu^+ \sigma \Lambda_e^-)$$

$$= \mathrm{Tr}[\tfrac{1}{4}\vec{\sigma}(1 + \frac{\beta mc^2}{|W|} + \frac{\vec{\alpha}\cdot\vec{v}}{c})\sigma(1-\vec{\alpha}\cdot\hat{q})]$$

$$= \mathrm{Tr}[\tfrac{1}{4}\vec{\sigma}(1-(\frac{\vec{\alpha}\cdot\vec{v}}{c})(\vec{\alpha}\cdot\hat{q})\sigma]$$

$$= \mathrm{Tr}[\tfrac{1}{4}\vec{\sigma}\cdot\vec{\sigma}]$$

$$= 1$$

where

$$(\vec{\alpha}\cdot\vec{v})(\vec{\alpha}\cdot\hat{q}) = (\vec{\sigma}\cdot\vec{v})(\vec{\sigma}\cdot\hat{q}) = \vec{v}\cdot\hat{q} + i(\vec{\sigma}\cdot\vec{v}X\hat{q}) \tag{8-181}$$

$\mathrm{Tr}(\sigma) = 0$ and $\frac{\vec{v}\cdot\hat{q}}{c^2} = \frac{v}{c}\cos\theta_{e\nu} = 0$ averaging over all electron and neutrino orientations.

Also, for terms such as

$$\psi_e^{\dagger}\beta\vec{\sigma}\phi_\nu\phi_\nu^{\dagger}\sigma\psi_e = \mathrm{Tr}(\beta\sigma\Lambda_\nu^{+}\sigma\Lambda_e^{-})$$

$$= \mathrm{Tr}[\tfrac{1}{4}\beta\sigma(1-\vec{\alpha}\cdot\hat{q})\sigma(1 + \frac{\beta mc^2}{|W|} + \frac{\vec{\alpha}\cdot\vec{v}}{c})]$$

$$= \mathrm{Tr}[\tfrac{1}{4}\sigma\frac{mc^2}{|W|}\sigma]$$

$$= \frac{mc^2}{|W|} \tag{8-182}$$

for negatron decay. The matrix element in full form thereby reduces to

$$|H_{fi}|^2 = 2g^2\{|\textstyle\int 1|^2(C_V^2 + C_S^2 \pm 2C_VC_S\frac{\gamma_o mc^2}{W}) + |\int\vec{\sigma}|^2(C_A^2 + C_T^2$$

$$\pm 2C_AC_T\frac{\gamma_o mc^2}{W})\} \tag{8-183}$$

for $e^{\mp}$ decay

where $\gamma_o = (1 - \alpha^2z^2)^{1/2}$ is included from the Coulomb analysis of the problem. Of particular interest are the cross terms containing c_ic_j which have an energy dependence. The nature of these terms will be shown

to be important as their existance can be tested experimentally. The above matrix element will be written more economically as

$$|H_{fi}|^2 = \xi[1 \pm \gamma_o b(\frac{mc^2}{W})] \text{ for } e^{\mp} \tag{8-184}$$

where

$$\xi = 1/2[(C_V^2 + C_S^2)\langle 1\rangle^2 \ (C_A^2 + C_T^2)\langle \sigma\rangle^2] \tag{8-185}$$

and

$$b\xi = [C_V C_S \langle 1\rangle^2 + C_A C_T \langle \sigma\rangle^2] \tag{8-186}$$

The transition rate shown in (8-64) can be written as

$$\lambda = (2\pi^3 \hbar^7 c)^{-1} |H_{fi}|^2$$

$$= g^2 F(\mp Z, W)(2\pi^3 \hbar^7 c)^{-1} \xi[1 \pm \gamma_o b(\frac{mc^2}{\langle W\rangle})] \text{ for } e^{\mp} \text{ decay} \tag{8-187}$$

where $\langle W\rangle$ is the main electron energy necessitated by integration to get λ. For electron capture the same general equation occurs where

$$\lambda_\varepsilon = g^2(2\pi^3 \hbar^7 c)^{-1} F_\varepsilon(Z,W)\xi[1 + \gamma_o b(\frac{mc^2}{\langle W\rangle})] \tag{8-188}$$

and $F_\varepsilon(Z,W)$ contains the Coulomb contributions to electron capture. Both $F_{\beta+}$ and F_ε are calculated functions, so the relative branching ratios when both forms compete is given by

$$R = \frac{\lambda_\varepsilon}{\lambda_{\beta^+}} = \frac{F_\varepsilon}{F_{\beta^+}} \left[\frac{1 + \gamma_o b\langle W^{-1}\rangle}{1 - \gamma_o b\langle W^{-1}\rangle}\right]$$

$$= R_o \left[\frac{1 + \gamma_o b\langle W^{-1}\rangle}{1 - \gamma_o b\langle W^{-1}\rangle}\right] \qquad (8\text{-}189)$$

for $m = c = 1$.

Also, since $\lambda = \ell n 2/t_{1/2}$

$$f_{\beta^+}t = \ell n 2[\xi(1 - \gamma_o b\langle W^{-1}\rangle)]^{-1} \qquad (8\text{-}190)$$

$$f_\varepsilon t = \ell n 2[\xi(1 + \gamma_o b\langle W^{-1}\rangle)]^{-1} \qquad (8\text{-}191)$$

The ft values differ in that the energy dependence cannot be completely separated from the matrix element. If $b = 0$, both terms are equivalent and only $C_A + C_V$ terms of $C_S + C_T$ terms may contribute. If $b \neq 0$, then all four forms may contribute, at least as far as cross terms.

8.3 Implications of the Allowed Assumptions

Although the allowed assumptions are generally valid for numerous allowed decays, there are also examples of allowed spectral shapes that are not adequately explained by the theory (Dan68). Indeed the overlap between the allowed and forbidden log*ft* values is great enough to imply that by analogy higher order corrections to allowed decay may not be as small as initially assumed. Any breakdown in the allowed assumption will be most sensitively measured in ε/β^+ decay branching ratios. No thorough

investigation of the consequences of higher order corrections will be presented here, but the more salient aspects will be discussed.

When we include off-center ($r \neq 0$) decay terms, we can obtain an infinite number of correction terms. Those matrix elements most likely to contribute are of order $\approx(qR)^2$ or $(qR)\cdot(v/c)$ and are presented in Table 8-1. There are up to ten such elements which can contribute to simple allowed decay. These terms can cause large affects on ε/β^+ ratios through VA interference which appears quite analogously to Fierz-type interference. The similar case of second-forbidden unique transitions has been shown to offer ε/β^+ ratios six times as large as those calculated for allowed decay. Unfortunately, no such calculations are available for the allowed corrections so we must only assume they are of a similar magnitude.

When we consider higher order matrix elements, it is important that we also include Pseudoscalar terms. Although Scalar and Tensor forces may be eliminated, the lower limit of $C_P < 90C_A$ (Ko66) leaves plenty of room for such an affect. Keeping all the terms in the transition amplitude,

$$\langle f|H_\beta|i\rangle = 2^{1/2} g\, J_4^0[(C_S+C_V)\int 1 - (C_A+C_P)\int\gamma_5] - i\bar{J}^0[(C_A+C_T)\int\bar{\sigma} + (C_V+C_T)\int\bar{\alpha}] \qquad (8\text{-}192)$$

where the complete allowed matrix element now contains the Fierz terms

$$b\xi = 2[C_S C_V\langle 1\rangle^2 + C_A C_T\langle\vec{\sigma}\rangle^2 + C_A C_P\langle\gamma_5\rangle^2 + C_S C_T\langle\vec{\alpha}\rangle^2] \qquad (8\text{-}193)$$

Of particular interest would be the $C_A C_P$ interference which could lead to

Table 8-1

Matrix Elements Contributing to Allowed Transitions (Sc66)

Matrix Element	Selection Rules I	$\Pi_i\Pi_f$	Forbidden	Power of qR	Power of v_N/c	Type of Transition
$\int 1$	0	(+)	---	0	0	Allowed
$\int\vec{\sigma}$	0,1	(+)	0-0	0	0	
$\int 1(\vec{r}/R)^2$	0	(+)	---	2	0	Corrections to Allowed Transitions
$\int i(\vec{\alpha}\cdot\vec{r})/R$	0	(+)	---	1	1	
$\sqrt{3}\int i\gamma_5\vec{r}/R$	0,1	(+)	0-0	1	1	
$\sqrt{3/2}\int(\vec{\alpha}\times\vec{r})/R$	0,1	(+)	0-0	1	1	
$\int\vec{\sigma}(r/R)^2$	0,1	(+)	0-0	2	0	
$3/\sqrt{2}\int\frac{(\vec{\sigma}\cdot\vec{r})\vec{r}-\frac{1}{3}\vec{r}^2}{R^2}$	0,1	(+)	0-0	2	0	
$\sqrt{15/2}\int R_{ij}/R^2$	0,1,2	(+)	0-0	2	0	2nd Forbidden (ΔI=2,3) and corrections to allowed transitions (ΔI=0,1)
$\sqrt{3/2}\int iA_{ij}/R$	0,1,2	(+)	1/2-1/2	1	1	
$\sqrt{5/2}\int iT_{ij}/R^2$	0,1,2	(+)	0-1	2	0	
$6\sqrt{15/2}\int B_{ijk}/R^2$	0,1,2,3	(+)	0-0,1/2-1/2, 0-1,0-2,101, 1/2-3/2	2	0	

With $R_{ij} = (r_i r_j - 1/3\delta_{ij} r^2)$ $\quad A_{ij} = \gamma_5 B_{ij} = \{\alpha_i r_j + \alpha_j r_i - \frac{2}{3}\delta_{ij}(\vec{\alpha}\cdot\vec{r})\}$ etc.

$B_{ij} = \{\sigma_i r_j + \sigma_j r_i - \frac{2}{3}\delta_{ij}(\vec{\sigma}\cdot\vec{r})\}$ $\quad T_{ij} = (\vec{\sigma}\times\vec{r})_i r_j + (\vec{\sigma}\times\vec{r})_j r_i$

significant anomalies in ε/β^+ ratios. Of course these terms would appear to be of the same order as the other allowed correction terms in Table 8-1, but their implications would lead to the advent of beta decay through right-handed helicity states. Pseudoscalar forces have been eliminated in pion decay studies so if one accepts a unified weak interaction theory, they should not appear in beta decay. Nevertheless, this factor should be investigated because any such correction would be intriguing.

8.4 Experimental Measurement of ε/β^+ Ratios

8.4.1 ^{145g}Gd

8.4.1A Decay of ^{145}Gd - Relative positron feedings to states in ^{145}Eu were measured in γ-γ triple coincidence experiments described in Chapter 2. A spectrum of γ-ray transitions in ^{145}Eu in coincidence with annihilation radiation is presented in Figure 8-6. The relative positron fed intensities inferred from this spectrum are shown in Table 8-2. In Table 8-3 the net positron feeding to known levels in ^{145}Eu, calculated from the gross intensities, is presented. It is important to remember that the high efficiency of the 8×8 in. NaI(Tl) annulus causes coincident summing which lessens the coincidence intensity of cascade transitions. This is evident in the 1072.0-keV deexcitation of the 1880.6-keV level where the intensity is only 40% of that seen in singles spectra. The intensities in Table 8-3 take into account the above phenomena although, fortunately, the vast majority of decay is through direct ground state transitions.

The electron capture decay of ^{145}Gd was studied through x-γray coincidence experiments as described in Chapter 2. The integral

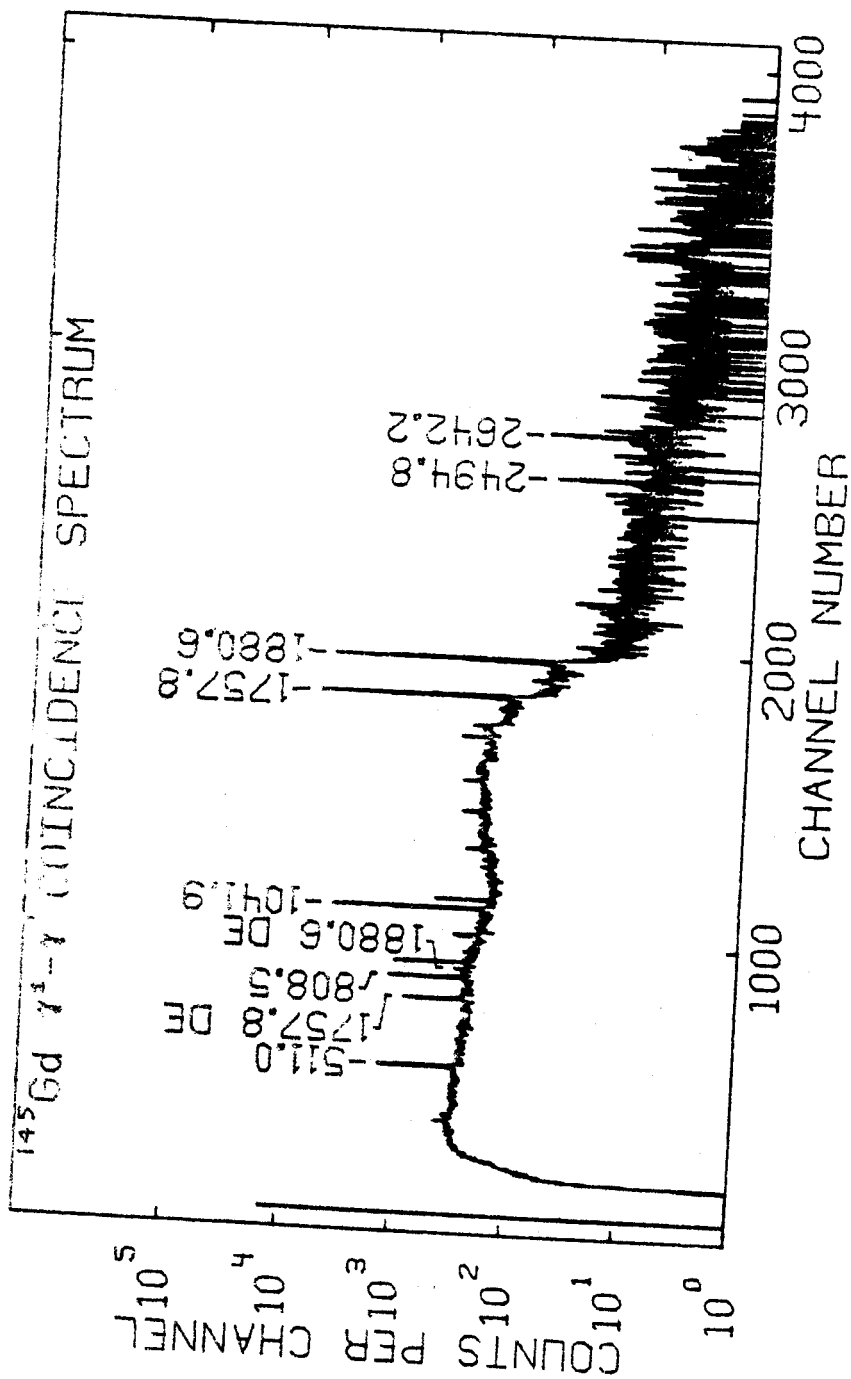

Figure 8-6. ^{145g}Gd β^+-γ coincidence spectrum.

Table 8-2

Experimental Positron and Electron Capture Relative

γ-ray Intensities for ^{145}Gd Decay

Energy (keV)*	$I_{\beta+}$	$I_{\varepsilon(K)}$
329.5	0.24	7.46
808.5	6.26	24.9
949.6	0.88	1.62
953.4	1.08	4.21
1041.9	32.2	19.8
1072.0	2.99	7.10
1719.4	0.63	3.41
1757.8	≡100†	≡100†
1784.4	0.17	2.86
1845.4	0.12	2.82
1880.6	86.5	95.8
2203.3	0.15	2.96
2494.8	1.75	4.58
2642.2	2.10	8.43

*Value taken from Eppley et al. Phys. Rev. C, 3, p. 282 (1971).

†All values normalized to 1757.8-keV ≡100.

Table 8-3

Experimental Positron and Electron Capture Relative

β-Feeding Intensities for ^{145}Gd Decay

Energy (keV)	$I_{\beta+}$(NET)*	I_{ε}(NET)*
329.5	0	1.39
808.5	1.31	14.0
1041.9	32.2	23.2
1757.8	101.†	119.†
1845.4	0.12	3.30
1880.6	89.5	120.
2494.8	1.75	5.37
2642.2	2.10	9.88

*Corrected for net feedings into or out of each level.

†Normalized such that ε/β^{+}=1.17 for transitions to the 1757.8-keV level.

coincidence spectra for the x-ray leg, the γ-ray leg are shown at the top of Figure 8-7. At the bottom of the same figure is a γ-ray spectrum showing coincidences with prompt x-rays. In this spectrum the gate was set across the total K x-ray peaks. The relative electron capture fed intensities are shown in Table 8-2. Table 8-3 shows the inferred electron capture feeding to the known levels in ^{145}Eu. Again corrections are made for coincidence summing in the x-ray detector although here we see only a <15% effect. In order to use coincidence information quantitatively it is necessary to know whether the γ-rays are prompt. In Figure 8-8 the TAC spectra corresponding to each gamma ray is shown. Broad peaks with long tails would be evidence of delayed transitions and clearly none of the transitions studied here are delayed in the time scale of the experiment.

8.4.1B ε/β^+ Branching Ratios in the Decay of ^{145g}Gd - ε/β^+ branching ratios have been calculated incorporating screening and finite nuclear size corrections. These values are tabulated in Nuclear Data Tables (Go71) and are presented in Table 8-4. In addition, experimental values can be calculated from the relative positron and electron capture feedings given in Table 8-3. Several assumptions must still be made in order to get the experimental values. First, the relative K-capture intensities must be converted to total capture intensities using tables supplied in Lederer's Tables of the Isotopes (Led68). These corrections are straightforward and do not affect the relative intensities to any large degree. Another correction which might seem important is the x-ray fluorescence yield, but as this does not change the relative intensities, it is ignored here. Finally, the only major correction left is to normalize the two sets of intensity ratios. In this case

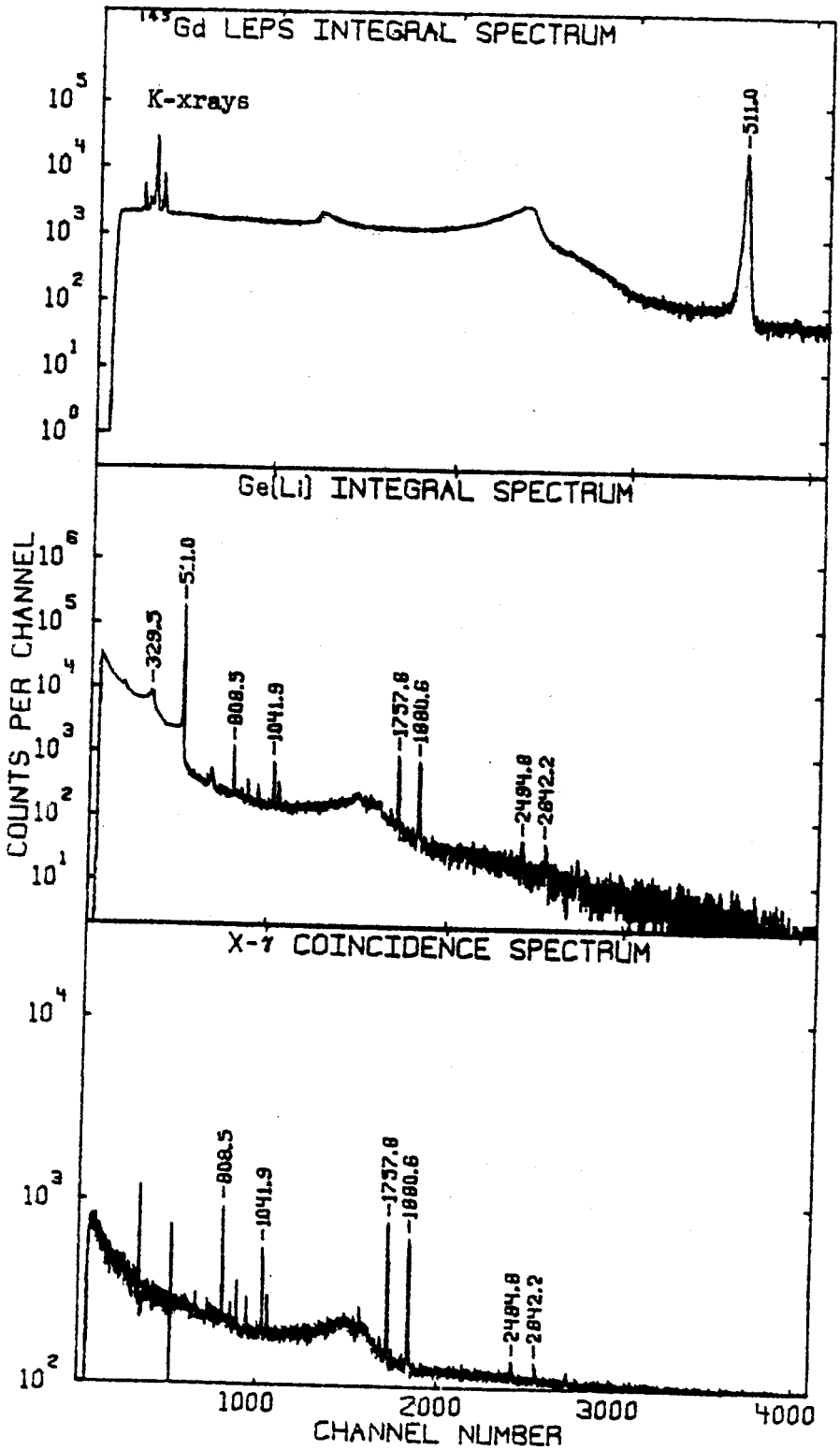

Figure 8-7. ^{145g}Gd x-γ integral coincidence and coincidence spectra.

Figure 8-8. ^{145g}Gd x-γ coincidence TAC spectra. The integral TAC peak is 20 nsec FWHM.

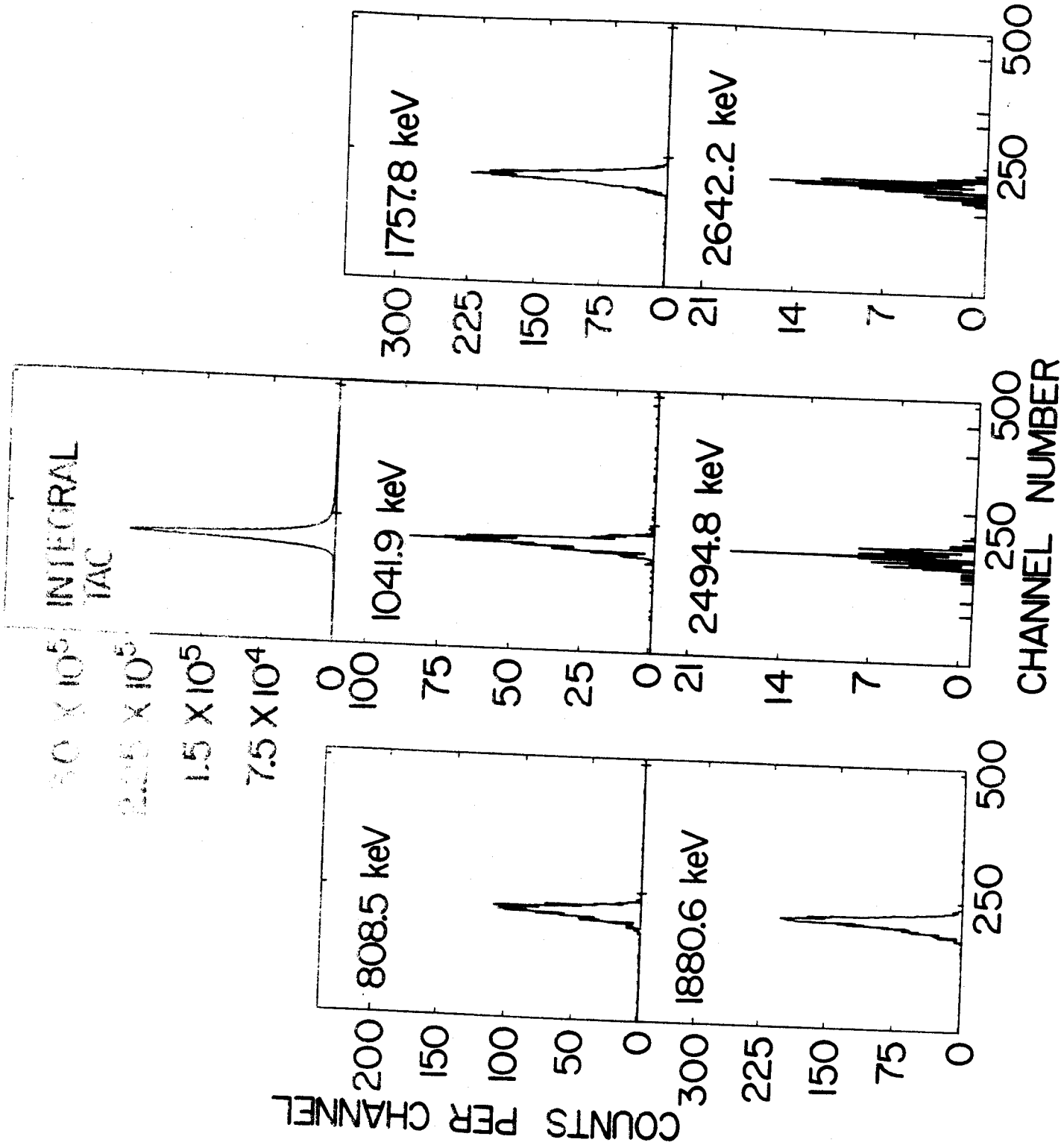
INTEGRAL
TAC
1.5 X 10^5
7.5 X 10^4
0
808.5 keV
1880.6 keV
1041.9 keV
2494.8 keV
17578 keV
2642.2 keV
COUNTS PER CHANNEL
CHANNEL NUMBER

Table 8-4

Theoretical and Experimental ε/β^+ Branching Ratios for ^{145}Gd Decay

Energy (keV)	$(\varepsilon(\text{tot})/\beta^+)^*$ theoretical	$(\varepsilon(\text{tot})/\beta^+)^\dagger$ experimental
808.5	0.45	10.7 ± 2.0
1041.9	0.60	0.72±0.05
1757.8	1.17	≡1.17±0.05
1880.6	1.37	1.34±0.05
2494.8	3.39	3.07±0.3
2642.6	4.41	4.70±0.5

*Values from Nuclear Data Tables 10, 205-317 (1971)

†Values from data in Table 8-3.

normalizations are made to the theoretical ratio for the 1757.8-keV level. This is a level where good statistics exist and the γ-transition seems straightforward and fast. If the theoretical ratios are indeed correct, the only difference in normalization would be statistical. Even if the theory is sometimes incorrect, previous data suggest that "normal allowed" transitions are correctly predicted. In any case the final intensities should correctly predict the total singles intensity.

Comparison of the theoretical and experimental ε/β^+ values show generally good agreement for all of the strong transitions except the transition to the 808.5-keV level. This level is well placed experimentally (Wa71) and its feeding is quite well understood (Ep71). The anomaly in this value is well beyond statistical significance.

Table 8-5 presents a comparison of the inferred singles intensities from coincidence to levels in ^{145}Eu with measured singles intensities. For the higher levels agreement is quite good but some discrepancies are seen for the lower levels particularly the 808.5- and 1041.9-keV levels. Those differences are still small enough to not change any arguments given previously, but they are, nonetheless, interesting. Explanations of the missing intensity cannot be made from experimental arguments because most of the transitions fit the experimental singles intensities quite reasonably. Some error may involve the choice of normalization to the 1757.8-keV level ε/β^+ feeding ratio, but this is clearly not a great source of error. Also, errors in the decay scheme should not be significant. Feedings from above to the lower levels are expected, and we have already seen evidence of misplaced transitions. This source of error would tend to lower singles intensities below their present values without as great an affect on coincidence feeding intensities.

Table 8-5

% β-Feeding to Levels in ^{145}Eu from ^{145}Gd Decay Singles and ε/β^+-Feeding Coincidence Experiments

Energy (keV)	% β(Singles)*	% β(coincidence)†
808.5	5.13	3.30
1041.9	9.93	8.74
1757.8	35.7	35.7
1880.6	36.3	≡35.2
2494.8	1.33	1.14
2642.2	1.98	1.93

*From Eppley et al., Phys. Rev. C, 3, p. 282 (1971)

†Inferred from relative β-feedings normalized to Eppley's singles intensity at 1757.8-keV.

Finally, a potentially exciting cause of these discrepancies is anomalies in K/L capture ratios. If some ε/β^+ ratios are anomalous, it corresponds that K/L capture ratios might also be errant. If L-capture is enhanced, the intensities can all fall into line.

The significance of these results and other results discussed later will be explored in Section 8.5.

8.4.2 ^{143g}Sm and ^{143}Eu

8.4.2A Decay of ^{143g}Sm and ^{143}Eu - The decays of ^{143}Eu and ^{143}Sm were discussed in considerable detail earlier in this thesis. Positron feeding ratios were measured through a $\gamma^{\pm}$-γ experiment similar to that described in the previous section. The activities for ^{143}Eu and ^{143}Sm were produced simultaneously and coincidences all measured in one spectrum. The differences in energies between transitions in the two spectra were sufficiently large to give clean results. A spectrum of positron fed transitions for ^{143}Eu and ^{143}Sm was shown in Figure 4-4. The total positron fed γ-ray intensities are shown in Table 8-5 which are the corrected intensities for total feeding into and out of each level.

Because no corresponding x-γ coincidence information is available, it is necessary to infer relative electron capture feedings from the singles intensities and the relative positron feedings. In order to do this, the ε/β^+ ratio for a "fast", well understood transition must be taken as the theoretical value. This was done for feeding to the 1056.65-keV level in ^{143}Sm and the 1107.15-keV level in ^{143}Eu. The results are shown in Table 8-6.

Table 8-6

β-Feedings from Decays of ^{143}Sm and ^{143}Eu to Levels in ^{143}Pm and ^{143}Sm Respectively

	E(keV)	I_{β^+}(total)[a]	I_{ε}(total)[b]
^{143}Sm	1056.69	99.6	966.
	1173.11	3.8	237.
	1403.11	5.6	196.
	1514.92	16.8	509.
^{143}Eu	1107.15	92.8	47.7
	1536.69	51.1	31.9
	1565.85	24.2	16.8
	1715.14	18.3	13.7
	1912.60	52.3	56.0

[a] From $\gamma^{\pm}$-γ triple-coincidence experiments.

[b] Inferred from singles intensities and theoretical value of $\varepsilon(tot)/\beta^+$ of 9.7 to the 1056.69-keV level of ^{143}Pm and the value 0.51 to the 1107.15-keV level of ^{143}Sm.

8.4.2B ε/β^+ Branching Ratios in the Decays of ^{143}Eu and ^{143}Sm - Theoretical $\varepsilon(tot)/\beta^+$ branching ratios for ^{143}Eu and ^{143}Sm are presented in Table 8-7. These values are calculated as discussed in Section 8.4.1B. Next to these values in Table 8-7 are the calculated experimental values for $\varepsilon(tot)/\beta^+$. In this case the statistical certainty is not nearly as good as the ^{145}Gd data and larger errors are expected.

The $\varepsilon(tot)/\beta^+$ branching ratios measured for ^{143}Sm agree quite well with theory for the transitions to the 1056.69-, 1403.11-, and 1514.93-keV levels. The value to the 1173.11-keV level shows yet another anomaly where the theory does not predict the correct $\varepsilon(tot)/\beta^+$ branching ratios. The ^{143}Eu ratios all agree quite well with theory.

These results and their implications will be discussed later in Section 8.5.

8.5 Discussion of Anomalous ε/β^+ Ratios

The results of the previous section indicate two concrete examples of anomalous ε/β^+ ratios. Since most of the data agrees with theory, these anomalies stand out quite sharply. It is imperative, nevertheless, that all experimental doubt be removed.

One concern is that a long-lived γ-ray transition might lead to erroneous results. There is no reason to expect such a transition as the anomalous levels have been observed in charged particle spectroscopy and are well understood (Jo71,Ch71,Wo71, and Wil71). These levels de-excite via high energy, low multipole transitions which would not likely lead to significantly delayed states. The 808.5-keV state of ^{145}Eu has been measured to deexcite promptly and the other cases should likewise

Table 8-7

Theoretical and Experimental $\varepsilon(tot)/\beta^+$ Branching Ratios for the Decays of ^{143}Eu and ^{143}Sm

	Energy (keV)[a]	$[\varepsilon(tot)/\beta^+]^b$ theoretical	$[\varepsilon(tot)/\beta^+]$ experimental
^{143}Eu	1107.15	0.46[c]	0.51±0.06[d]
	1536.69	0.69	0.62±0.06
	1565.85	0.72	0.69±0.15
	1715.14	0.83	0.75±0.17
	1912.60	1.02	1.07±0.11
^{143}Sm	1056.58	9.7	9.7 ±0.7
	1173.18	13.	63. ±10.
	1403.06	29.	35. ±5.
	1514.98	49.	30. ±7.[e]

[a] Values from Chapters 4 and 5.

[b] Values from Nuclear Data Tables 10, p. 206 (1971).

[c] Q_ε value chosen as 5.5 MeV to get best comparison with experiment.

[d] Data normalized to this value for best fit with theory.

[e] This point will fall in line if an error of 100 keV is assumed in the Q_ε value.

be fast.

Another possible flaw could be an error in the decay scheme. This is not likely as each decay is quite simple with most of the γ-ray strength accounted for. Any unplaced transitions are too weak to significantly affect the results. Nevertheless, the measured ratios could vary several percent and care should be taken in using these numbers.

Finally, choice of normalization to theory and errors in the decay energies can cause considerable deviations in the results but not individual anomalies. Correction for L-capture does not significantly alter relative electron capture feedings, and adjustments for deexcitations through cascades are generally small and always straightforward. Corrections were made for feedings from above, where necessary, using experimental coincidence efficiencies, however these changes were quite small.

This leaves little alternative but to believe that the ε/β^+ ratio anomalies are real. Other interesting features have already been published about these decays (Mc69,Ep71), so an attempt will be made to tie this information together. Clearly these anomalies can offer new insights into beta decay theory.

A pictorial description of ^{145}gGd decay is given in Figure 8-9. The 1757.8- and 1880.6-keV levels in ^{145}Eu are 3-quasiparticle states of the general form $(\pi h_{11/2})(\nu h_{9/2})(\nu s_{1/2})^{-1}$ as described by Eppley et al. (Ep71). Such states are seen elsewhere and described by McHarris et al. (Mc69) and in Chapter 5 of this thesis. The 808.5- and 1041.9-keV states are essentially the $(\pi s_{1/2})$ and $(\pi d_{3/2})$ single particle states respectively. Transitions to the 3-quasiparticle states are fast (logft = 5.8) because they involve primarily the breaking of a $(\pi h_{11/2})^2$ pair and the formation

Figure 8-9. Stylized model of ^{145}gGd decay to single-particle and 3-quasiparticle states in ^{145}Eu.

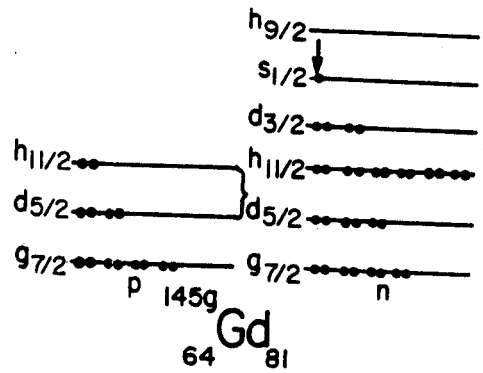
h9/2
s1/2
d3/2
h11/2
d5/2
g7/2
p
n
145g
64Gd81

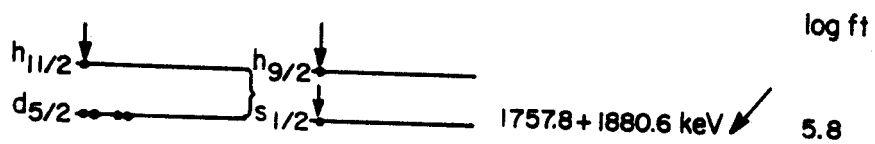
log ft
h11/2
h9/2
d5/2
s1/2
1757.8 + 1880.6 keV
5.8


d3/2
1041.9 keV
6.7


s1/2
808.5 keV
7.1

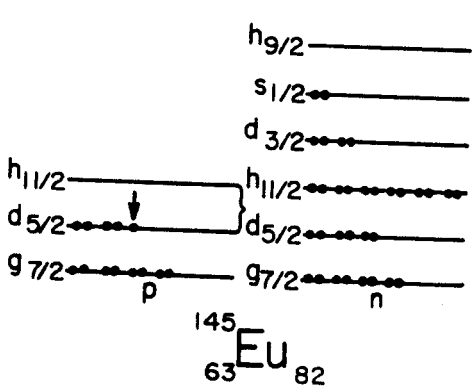
h9/2
s1/2
d3/2
h11/2
h11/2
d5/2
d5/2
g7/2
g7/2
p
n
145
63Eu82

of a $(\pi h_{9/2})$ particle. Decay to the single particle states is not so straightforward. Here a $(\pi d_{5/2})^2$ pair is broken, a $(\nu s_{1/2})^2$ is formed, and a $(\pi d_{5/2})$ particle is promoted to a $(\pi d_{3/2})$ or $(\pi s_{1/2})$ state. Although this is considered to be a single-step process, it will certainly proceed slowly. That is borne out by the large logft values of 7.1 and 6.7 to the 808.5- and 1041.9-keV states respectively.

A similar case exists for ^{143}Sm decay. The ground state of ^{143}Sm is essentially the $(\nu d_{3/2})$ single particle. The fastest transition (logft = 4.9) is to the ground state of ^{143}Pm. This involves the breaking of a $(\pi d_{5/2})^2$ pair and formation of a $(\nu d_{3/2})^2$ pair which is quite straightforward. Almost as fast (logft = 5.8) are transitions to the $(\pi h_{11/2})$-$(\nu h_{9/2})(\nu d_{3/2})$ 3-quasiparticle states at 1056.6- and 1515.0-keV described in Chapter 5. Transitions to the $(\pi d_{3/2})$ and $(\pi s_{1/2})$ single particle states at 1173.2- and 1403.1-keV in ^{143}Pm are slower (logft = 6.4). Again the transition rates parallel those in ^{145}Gd for similar reasons.

The ^{143}Sm transitions to single particle states are faster than those corresponding transitions from ^{145}Gd. This may be because the ^{143}Sm case involves essentially $(\pi d_{5/2}) \rightarrow (\nu d_{3/2})$, $\Delta I = 1$ while the ^{145}Gd case involves $(\pi d_{5/2}) \rightarrow (\nu s_{1/2})$, $\Delta I = 2$. Such a transition is necessarily more complex. Anomalies occur for the hindered transitions from ^{145}Gd and ^{143}Sm to the single particle states in the daughters. A small anomaly of $\simeq$15% may exist in transitions to the $(\pi d_{3/2})$ states. These transitions are somewhat simpler, involving the promotion $(\pi d_{5/2}) \rightarrow (\pi d_{3/2})$, $\Delta l = 0$ rather than the more complex $(\pi d_{5/2}) \rightarrow (\pi s_{1/2})$, $\Delta \ell = 2$ transition.

Although the allowed decay of near N=82 nuclei to single particle states can be strongly hindered, forbidden transitions to the single

particle states are seen to be enhanced ($\log ft$ = 7.2-7.8). Despite the fact that there may be some uncertainty in these numbers, the trend is unmistakable. These transitions should be straightforward, and it is also evident here that forbidden transitions may proceed more rapidly with larger A. There is no obvious reason why the forbidden transitions might be enhanced, but this appears to be the case.

These decay peculiarities must be involved in the anomalous ratios. The most complex transitions from ^{145}Gd and ^{143}Sm decay give the greatest anomalies. The decay to the 808.5-keV, ($\pi s_{1/2}$) state of ^{145}Eu deviates by a factor of 24 from the theoretical ε/β^+ value, and decay to the 1173.1-keV state of ^{143}Pm varies by a factor of 5. The implications of this chapter will be explored more directly in the following section.

8.6 Possible Implications of Anomalous ε/β^+ Ratios

Anomalous ε/β^+ ratios will occur when interference terms appear in the matrix element. They may contain an energy dependence and occur with opposite signs for ε or β^+ decay. More radical explanations of the anomalies such as fundamental differences in electron capture and positron emission seem to contradict too much of the established evidence to be considered at this time.

Interference can take several forms. The allowed assumption permits terms of the form $C_S C_V$ and $C_A C_T$. Measurements of ε/β^+ ratios for allowed decays such as ^{22}Na (Sh54) indicate these terms are small or are zero. Thus, it appears that scalar and tensor terms may be ruled out. Dispensing with the allowed assumption, the terms $C_S C_T$ and $C_A C_P$ arise. The $C_S C_T$ term should be quite small from previous experiments, but the $C_A C_P$ term needs

further investigation. This term occurs with the nuclear matrix element $\int \gamma_5$ which changes parity for a given first order transition. Thus, to contribute to allowed decay it appears in second order proportional to $\int \gamma_5 \frac{\vec{r}}{R}$. Clearly, the $C_A C_P$ term should be small if it exists at all. Nevertheless, finding such a contribution would be quite exciting. The pseudoscalar force allows the participation of right-handed particles in beta decay, a fact never yet observed. This might jeopardize two component neutrino theory. Pion decay studies indicate that π-e/π-μ decay ratios (An59) indicate the lack of pseudoscalar contribution. A unified weak interaction theory suggests that $C_P = 0$. Experimentally this is difficult to determine as measurements of $0 \rightarrow 0$, $\Delta\pi$ = yes beta spectra (Bh60) indicate only $C_P < 90 C_A$. Thus, pseudoscalar forces are not entirely ruled out of beta decay. A small pseudoscalar contribution should exist with $C_P \simeq (1/20)\ C_A$ (Bh60), but this would not be expected to lead to a significant effect.

The question arises as to why the pseudoscalar term could possibly be significant in the anomalous ε/β^+ ratios. Although the transitions are allowed, their large logft's indicate that the allowed matrix elements must be small. Thus, higher order terms like the pseudoscalar may not be small relative to the allowed terms. This is suggested by the fast forbidden transitions observed in these nuclei.

If the pseudoscalar term is indeed possible, certainly numerous other higher order terms may be present. Indeed, at least ten matrix elements may contribute to allowed decay in second order and these are listed in Table 8-1. These terms can introduce an interference of the form $C_A C_V$ which does not exist if the r = 0 assumption is made. Studies of forbidden decays indicate that large deviations from allowed theory

for ε/β^+ ratios are to be expected (Ber63,Ber68,Dan68, and Pe58) for higher order matrix elements. Calculated predictions are not possible for cases where several matrix elements may contribute, because each term affects the ε/β^+ ratio differently and no assumptions can be made without the relative contributions. For unique forbidden cases only one matrix element is important so the ratio is predicted by the equation (Be63)

$$\left(\frac{\lambda_\varepsilon}{\lambda_+}_{\text{unique forbidden}}\right) = \frac{2(W_o+1)}{(W_o-1)}\left(\frac{\lambda_\varepsilon}{\lambda_+}\right)_{\text{Allowed}} \qquad (8\text{-}194)$$

For the ^{145}Gd anomaly this would predict a ratio 2.6 times the allowed ratio and, for the ^{143}Sm anomaly, a ratio 3.8 times as large. Other matrix elements may give much higher values. Of particular interest may be the J = 2 matrix elements which may promote $(\pi d_{5/2}) \rightarrow (\nu s_{1/2})$ transitions strongly. Clearly $(\nu d_{3/2} \rightarrow \pi f_{7/2})$ transitions are fast so a strong similarity may be observed.

In conclusion, one must lean towards the contribution of normal higher order terms to explain the anomalies. This does not basically alter the current theory and pulls together several observed facts. Pseudoscalar forces do not seem so likely, but it is important that this prospect be further investigated.

8.7 Further Work on Anomalous ε/β^+ Ratios

In order to better understand the anomalous ε/β^+ ratios a series of difficult experiments should be performed. ^{145}Gd with its longer half-life and documented anomaly is a prime target. ^{143}Sm and ^{143}Eu are more

difficult due to short half-lives and the preponderance of decay to the ground state of the daughter.

Of primary importance are the measurements of the beta spectra. The endpoints for these nuclei are not well measured, and the spectral shapes should be sensitive to the various forbidden matrix elements. Unfortunately, these experiments must be β-γ coincidence measurements to simplify the problems because of the complexity of the decay scheme. The anomalous β^+ branches are weak so one is forced to demand a very small chance to true coincidence ratio. The use of magnetic spectrometers is probably difficult or impossible, and the inherent problems with Si(Li) leave only plastic detectors as likely β^+-spectrometers for this experiment. This may be marginally sufficient to get gross beta shapes, but will severely limit minute analysis of the contribution of different matrix elements.

In addition, β-γ (directional) and β-γ (circular polarized) coincidence experiments will also give valuable data concerning the matrix elements. Unfortunately, the directional experiment gives an isotropic distribution of betas for intermediate states of spin 0 or 1/2. The ^{145}Gd and ^{143}Sm cases involve spin 1/2 states so they cannot yield useful information. Their circular polarization correlation would be useful, but this experiment may be impossible to perform. Direct measurements of positron or neutrino helicity would be of great value in searching for pseudoscalar forces, but these experiments are also difficult.

It is certainly also valuable to search for new anomalous cases. Good prospects would be ^{143}Gd and ^{147}Dy which should also decay similarly to ^{145}Gd. Also certain allowed transitions with large logft values should be good candidates. It might be very valuable to pursue

cases where beta spectrum shape information is available. One such case is ^{56}Co. The β^+-spectrum gives a shape factor of the form $-1\ 1 + b \langle W^{-1} \rangle$ with b = 0.2 - 0.3. An interference term of this size would give an ε/β^+ ratio 50% larger than the allowed value.

Work should also proceed on the theoretical aspects of this problem. Calculations are needed to estimate the size of the higher order matrix elements as well as the allowed matrix elements. It would be worthwhile to estimate the relative participation of each matrix element in order to arrive at a better theoretical ratio.

Finally, the missing singles intensities strongly suggest that we measure the K/L capture ratios. If the anomalous decays proceed because of the higher order matrix elements, we expect to see considerable L_{III}, M, N... capture which has been shown (Br58) to be very important in forbidden decays. This information would give yet another handle on the important matrix elements.

BIBLIOGRAPHY

BIBLIOGRAPHY

A

[Al59] J. Allen, R. Burman, W. Hermansfeldt, P. Stahelin, and T. Braid, Phys. Rev. 116 (1959) 134.

[An59] H. L. Anderson, T. Fugii, R. H. Miller, and L. Tau, Phys. Rev. Lett. 2 (1959) 53.

[Ar53] W. Arber and P. Stähelin, Helv. Phys. Acta. 26 (1953) 433.

[Ar67] R. Arlt, G. Baier, G. Musiol, L. K. Peker, G. Pfrepper, and H. Strusny, JINR-P6-3540 (1967).

[At66] A. H. W. Aten and J. C. Kapteijn, Physica 32 (1966) 1159.

[Au69] HYDRA, a program written for the MSU Cyclotron Laboratory Sigma-7 computer by R. Au (1969).

[Au70] POLYPHEMUS, a program written for the MSU Cyclotron Laboratory Sigma-7 computer by R. Au (1970).

[Au73] IIEVENT, a program written for the MSU Cyclotron Laboratory Sigma-7 computer by R. Au (1973).

B

[Ba68] EVENT, a program written for the MSU Cyclotron Laboratory Sigma-7 computer by D. Bayer (1968).

[Ba70] MOD7, a program written for the MSU Cyclotron Laboratory Sigma-7 computer by D. Bayer and R. Au (1970).

[Ba71] TOOTSIE, a program written for the MSU Cyclotron Laboratory Sigma-7 computer by D. Bayer (1971).

[Bah72] J. N. Bahcall, N. Cabibbo, and A. Yahil, Phys. Rev. Lett. 28 (1972) 316.

[Be69] M. J. Berger, S. M. Seltzer, S. E. Chappell, J. C. Humphreys and J. W. Motz, Nucl. Instr. Meth. 69 (1969) 181.

[Bee68] D. B. Beery, W. H. Kelly, and Wm. C. McHarris, Phys. Rev. 171 (1968) 1283.

[Bee69] D. B. Beery, W. H. Kelly, and Wm. C. McHarris, Phys. Rev. 188 (1969) 1875.

[Beh71] H. Behrens and W. Buhring, Nucl. Phys. A162 (1971) 111.

[Bel66] Ya. I. Belyanin, E. J. Biryukov, and N. S. Shimanskaya, Izv. Akad. Nauk. SSSR, Ser. Fiz. 30 (1966) 1130.

[Ber63] D. Berenyi, Nucl. Phys. 48 (1963) 121.

[Ber68] D. Berenyi, Rev. Mod. Phys. 40 (1968) 390.

[Bern69] F. M. Bernthal, Ph.D. Thesis, University of California, Berkeley, UCLR-18651 (1969).

[Bh60] C. P. Bhalla and M. E. Rose, Phys. Rev. 120 (1960) 1415.

[Bi70] E. I. Biryukov and N. S. Shimanskaya, Soviet Journal of Nucl. Phys. 11 (1970) 138.

[Bl68] H. Bleyl, H. Munzel, and G. Pfennig, Radiochim Acta 9 (1968) 173.

[Bla72] FERMPLOT, a program written for the MSU Cyclotron Laboratory Sigma-7 computer by J. Black (1972).

[Bo57] F. Boehm and A. H. Wapstra, Phys. Rev. 106 (1957) 1364.

[Bohr69] A. Bohr and B. R. Mottelson, Nuclear Structure, W. A. Benjamin, Inc., New York (1969).

[Br58] H. Brysk and M. E. Rose, Rev. Mod. Phys. 30 (1958) 1169.

[Br60] M. H. Brennan and A. M. Bernstein, Phys. Rev. 120 (1960) 927.

[Bu58a] M. Burgy, V. Krohn, T. Novey, G. Ringo, and V. Telegdi, Phys. Rev. Lett. 1 (1958) 324.

[Bu58b] M. Burgy, V. Krohn, T. Novey, G. Ringo, and V. Telegdi, Phys. Rev. 110 (1958) 1214.

C

[Ca71] D. C. Camp and G. L. Meredith, Nucl. Phys. A166 (1971) 349.

[Ch71] A. Chaumeaux, G. Bruge, H. Faraggi and J. Picard, Nucl. Phys. A164 (1971) 176.

[Cr62] J. G. Cramer, Jr., B. J. Farmer, and C. M. Cass, Nucl. Instr. Meth. 16 (1962) 289.

D

[Da55] R. Davis, Phys. Rev. 97 (1955) 766.

[Dan68] H. Daniel, Rev. Mod. Phys. 40 (1968) 659.

[DeF68] D. DeFrenne, K. Hyde, L. Dorikens-Vanpraet, M. Dorikens, and J. Demuynck, Nucl. Phys. A110 (1968) 273.

[DeF70] D. DeFrenne, E. Jacobs, and J. Demuynck, Z. Physik 237 (1970) 327.

[Dew72] M. K. Dewanjic and I. L. Preiss, J. Inorg. Nucl. Chem. 34 (1972) 1105.

[Do69] R. E. Doebler, G. C. Giesler, K. L. Kosanke, R. B. Firestone, R. A. Warner, A. Croft, B. Jeltema, C. Morgan, et al., unpublished.

E

[Eb57] M. E. Ebel and G. Feldman, Nucl. Phys. 4 (1957) 213.

[En66] H. A. Enge, Nuclear Physics, Addison-Wesley Publishing Co., Inc., Redding, Mass. (1966).

[Ep71] R. E. Eppley, Wm. C. McHarris, and W. H. Kelly, Phys. Rev. C3, (1971) 282.

[Ev55] R. D. Evans, The Atomic Nucleus, McGraw-Hill Publishing Co., Inc., New York (1955).

F

[Fe70] J. Felsteiner and B. Rosner, Phys. Lett. 31B (1970) 12.

[Fi74a] R. B. Firestone, R. A. Warner, Wm. C. McHarris and W. H. Kelly, ε/β^+ Decay of ^{143}Sm to be published.

[Fi74b] R. B. Firestone, R. A. Warner, Wm. C. McHarris and W. H. Kelly, Anomalous ε/β^+ Ratios from ^{145}Gd, ^{143}Sm and ^{143}Eu Decays, to be published.

[Fi74c] R. B. Firestone, R. A. Warner, Wm. C. McHarris and W. H. Kelly, Possible explanations of anomalous ε/β^+ ratios, to be published.

[Fi74d] R. B. Firestone, R. A. Warner, Wm. C. McHarris and W. H. Kelly, ε/β^+ of ^{143}Eu to be published.

[Fi74e] R. B. Firestone, R. A. Warner, Wm. C. McHarris and W. H. Kelly to be published.

[Fit72] M. L. Fitzpatrick, K. W. D. Ledingham, J. Y. Gourlay, and J. G. Lynch, "K-Electron Capture to Positron Emission Ratios in Allowed Transitions - A Critical Analysis", Proceedings of the International Conference on Inner Shell Ionization Phenomena and Future Applications, 17-22 April, 1972, p. 2013.

[Fr66] G. Friedlander, J. W. Kennedy, and J. M. Miller, Nuclear and Radiochemistry, John Wiley and Sons, Inc., New York (1966).

G

[Geh73] R. J. Gehrke, Nucl. Phys. A204 (1973) 26.

[Ger58] J. B. Gerhart, Phys. Rev. 109 (1958) 897.

[Gi71] G. C. Giesler and R. B. Firestone, unpublished.

[Gi73] G. C. Giesler, Wm. C. McHarris, R. A. Warner and W. H. Kelly, to be published.

[Gi74] G. C. Giesler, Wm. C. McHarris, R. A. Warner and W. H. Kelly, to be published.

[Go71] N. B. Gove and M. J. Martin, Nucl. Data Tables 10 (1971) 205.

[Gold58] M. Goldhaber, L. Gnodzins, and A. Sunyar, Phys. Rev. 109 (1958) 1015.

[Gr66] J. T. Grissom, D. R. Koehler, and B. G. Gibbs, Nucl. Anstr. Meth. 45 (1966) 190.

H

[Ha61] J. H. Hamilton, L. M. Langer, D. R. Smith, Phys. Rev. 123 (1961) 189.

[Han68] O. Hansen, O. Nathan, and Vistisen, Nucl. Phys. A113 (1968) 75.

[He57] Hermannsfeldt, Maxson, Stahelin, and Allen, Phys. Rev. 107 (1957) 641.

[He61] D. Hendrie and J. Gerhart, Phys. Rev. 121 (1961) 846.

J

[Ja57a] J. D. Jackson, S. B. Fteiman, and H. W. Wyld, Phys. Rev. 106 (1957) 517.

[Ja57b] J. D. Jackson, S. B. Trieman, and H. W. Wyld, Nucl. Phys. 4 (1957) 206.

[Jo63] C. Johnson, F. Pleasanton, and T. Carlson, Phys. Rev. 132 (1963) 1149.

[Jo71] R. K. Jolly and E. Kashy, Phys. Rev. C4 (1971) 887.

K

[Ko60] K. Kotajima and H. Morinago, Nucl. Phys. 16 (1960) 231.

[Ko65] K. Kotajima, K. W. Brockman, and G. Wolzak, Nucl. Phys. 65 (1965) 109.

[Kon66] E. J. Konopinski, The Theory of Beta Radioactivity, Clarendon Press, Oxford (1966).

[Kos70] K. L. Kosanke, H. P. Hilbert, and C. B. Morgan, Annual Report MSU Cyclotron Laboratory (1970-71) 45.

[Kos73] K. L. Kosanke, Ph.D. Thesis, Michigan State University, East Lansing, Michigan, 1973.

L

[La52] L. M. Langer and R. D. Moffot, Phys. Rev. 88 (1952) 689.

[Lav73] N. Lavi, Nucl. Intr. Meth. 107 (1973) 197.

[Led68] C. M. Lederer, J. M. Hollander, and I. Perlman, Table of Isotopes, Sicth Edition, John Wiley and Sons, Inc., New York (1968).

[Lee56] T. D. Lee and C. N. Yang, Phys. Rev. 104 (1956) 254.

[Lee65] T. D. Lee and C. S. Wu, "Weak Interactions", Annual Rev. of Nucl. Science, 15 (1965) 381.

[Lin71] E. W. A. Lingeman and J. Konijn, Nucl. Instr. Meth. 94 (1971) 389.

M

[Ma66] H. P. Malon, H. Munzel, and G. Pfennig, Radiochim Acta 5-1 (1966) 24.

[Mar702 P. Marmier and E. Sheldon, Physics of Nuclei and Particles, Academic Press, Inc., New York (1969).

[Mat65] J. H. E. Mattauch, W. Thiele, and A. H. Wapstra, Nucl. Phys. 67 (1965)1.

[Mc69] Wm. C. McHarris, D. B. Beery, and W. H. Kelly, Phys. Rev. Lett, 22 (1969) 1191.

[Me70] R. A. Meyer, Private Communication, May, 1970.

[Mo71] Calculated by C. Morgan from tables, Rev. Mod. Phys. 41 (1969), and Introduction to Nuclear Physics and Chemistry, Harvey (1969) p. 428.

[Mo73] EVENT RECOVERY, a program written for the MSU Cyclotron Laboratory Sigma-7 computer by C. B. Morgan, R. Au, G. C. Giesler, and D. B. Beery (1973).

[Mow70] R. S. Mowatt, Canadian J. Phys. 48 (1970) 2606.

P

[Pa30] A letter from W. Pauli to friends reprinted in Beta Decay by Wu and Moszkowski (Wu66) p. 385.

[PDP73] PHA programs from DEC, Inc., modified by G. C. Giesler, S. Bradford, and R. Howard.

[Pe58] M. L. Perlman, J. P. Welker, and M. Wolfsberg, Phys. Rev. 110 (1958) 381.

[Ph70] M. E. Phelps, D. G. Sarantites, and W. G. Winn, Nucl. Phys. A149 (1970) 647.

[Pi73] W. F. Piel, Nucl. Phys. A203 (1973) 369.

R

[Re59] F. Reines and C. Cowan, Phys. Rev. 113 (1959) 273.

[Ro69] J. T. Routti and S. G. Prussin, Nucl. Instr. Meth. 72 (1969 125. We used a variant of SAMPO adopted for the MSU Cyclotron Laboratory Sigma-7 computer by T. Arnett, C. Merritt, C. B. Morgan, and W. H. Kelly.

[Rob60] B. L. Robinson and R. W. Fink, Rev. Mod. Phys. 32 (1960) 117.

[Ros58] M. E. Rose, Internal Conversion Coefficients, Interscience Publishers, Inc., New York (1958).

S

[Sa69] J. J. Sapyta, E. G. Funk, J. W. Mihelich, Nucl. Phys. A139 (1969) 161.

[Sc66] H. F. Schopper, Weak Interactions and Nuclear Beta Decay, North-Holland Publishing Co., Inc., Amsterdam (1966).

[Se57] J. Serpe, Nucl. Phys. 4 (1957) 183.

[Seg65] E. Segre, Nuclei and Particles, W. A. Benjamin, Inc., New York (1965).

[Sh53] R. Sherr and J. B. Gerhart, Phys. Rev. 91 (1953) 909.

[Sh54] R. Sherr and R. H. Miller, Phys. Rev. 93 (1954) 1076.

[Sie65] K. Siegbahn, editor, Alpha, Beta and Gamma-Ray Spectroscopy, North-Holland Publishing Co., Inc., Amsterdam (1965).

[So59] A. Sosnovskii, P. Spivak, Yu. Prokoviev, and Yu Dobrynin, Soviet Phys. (JETP), 35 (1959) 739.

[St66] P. C. Stevenson, Processing of Counting Data, NAS-NS3109 (1966).

W

[Wa59] A. H. Wapstra, G. J. Nijgh, and R. Van Lieshout, Nuclear Spectroscopy Tables, North-Holland Publishing Co., Inc., Amsterdam (1959).

[Wi67] J. B. Willet and E. H. Spejewski, Nucl. Intr. Meth. 52 (1967) 77.

[Wil71] B. H. Wildenthal, E. Newman, and R. L. Auble, Phys. Rev. 3C (1971) 1199.

[Wilk70] D. H. Wilkinson, Nucl. Instr. Meth. 94 (1971) 229.

[Wo71] P. Woolam and R. Griffiths, Phys. Lett. 37B (1971) 13.

[Wu57] C. S. Wu, E. Ambler, R. Hayward, D. Hoppes and R. Hudson, Phys. Rev. 107 (1957) 641.

[Wu66] C. S. Wu and S. A. Moszkowski, Beta Decay, Interscience Publishers, New York (1966).

Y

[Ya73] F. Y. Yap, R. R. Todd, W. H. Kelly, Wm. C. McHarris, and R. A. Warner, Phys. Rev. C. to be published.

Z

[Zw54] P. F. Zweifel, Phys. Rev. 96 (1954) 1572.

[Zw57] P. F. Zweifel, Phys. Rev. 107 (1957) 329.

[Zy68] L. N. Zyranova and Yu. P. Suslov, Proceedings of the Conference on the Electron Capture and Higher Order Processes in Nuclear Decays, Debrecen, Hungary, 15-18 July 1968, p. 234.